Final Report

Management of Rotations, Soil Structure and Water
(Rotations Research Partnership)

Work Package 2 (WP2):
Using New Technologies to Enhance Rotations

Ref: 9114000102

Reporting Period: 1 April 2016 – 30 June 2021

Report Authors: Rothamsted Research, Lancaster University, James Hutton Institute and NIAB

Date report submitted: March 2022

Additional copies of this report and other publications from the AHDB are also available at ahdb.org.uk, or can be obtained from:

Publications

AHDB

Stoneleigh Park   Tel: 02476 692051

Kenilworth   E-mail: Levy.Publications@ahdb.org.uk

Warwickshire

CV8 2TL

CONTENTS

1. PROGRAMME DELIVERY TEAM FOR WORK PACKAGE 2

Co-ordination	Marc Allison NIAB
Zoning of Yield Potential	Kirsty Hassall (Rothamsted Research) Andy Whitmore (Rothamsted Research) Alice Milne (Rothamsted Research)
Using Geophysical Scans	Andy Binley (Lancaster University) Marc Allison (NIAB)
Plough Draft	Andy Whitmore (Rothamsted Research) Marc Allison (NIAB) Mark Stalham (NIAB)
FTIR Analysis of Soil Organic Matter	Jean Robertson (JHI) Tracy Valentine (JHI) Blair McKenzie (JHI)
Using flatbed scanners to understand rooting	Tracy Valentine (JHI) Jean Robertson (JHI) Blair McKenzie (JHI)
Trafficking in potato fields	Mark Stalham (NIAB) Marc Allison (NIAB)

2.   REPORTING OF WORK PACKAGE 2

The main objective of work package 2 (WP 2) was to investigate the use of spatial information (e.g. maps of cereal and potato yields or of soil properties) to define higher and lower yield zones within fields, which may then be used to improve crop management practices. In addition, this work package investigates novel scanning technologies to better understand the dynamics of soil organic matter. For simplicity, the key findings of WP2 will be discussed in this report. Similarly, background literature, conclusions, appendices will also be reported here. However, practical recommendations from the whole project will be synthesised and reported in the summary report for the entire project.

2.1. Areas of work

This work package comprised six areas of work:

1. Zoning of yield potential (Rothamsted Research)
2. Using Electro-Magnetic Induction (EMI) scans to better understand soil variability (Lancaster University)
3. Harvesters and plough draft (Rothamsted Research and NIAB)
4. Fourier Transform InfraRed (FTIR) scanning of soil to quantify organic matter content (James Hutton Institute)
5. Use of flatbed scanner to understand rooting in soils (James Hutton Institute)
6. Plant root elongation assays using platform soils (James Hutton Institute)
7. Trafficking in arable fields (NIAB)

3. ZONING OF YIELD POTENTIAL

3.1. Introduction

Yield monitor data are now collected as standard on many farms. In addition to this, processed satellite data, which are available at increasingly fine resolution, can be used to see how crop response varies within a field throughout the growing season. These sources of data offer a means to understand and predict the variation in crop response within fields. The aim of this work was to investigate how farmers could make best use of the information captured by yield monitor data and satellite data, and to apply this knowledge within the context of precision management in potato crops.

It is a well-recognised aim of many on-farm management strategies to divide fields into zones, to ensure efficient and effective management where each zone may be treated differently. Defining such zones has been a topic of research for at least 40 years (see e.g. Webster and Burrough,1972). The process of defining zones depends upon both the variables used to inform the zones, but also the approach used to ensure the zones are spatially coherent. It is of limited practical use to farm management if resulting zones are small and disjointed (Milne *et al*, 2012).

Data used to inform zones most commonly include yield data or soil characteristics which can be measured either directly or more recently via remote sensing (Boydell & McBratney (2002); Guastaferro *et al*. (2010); Hedley et al. (2004); Song *et al*. (2009))

Yield monitor data has been accessible in cereal systems for the last 20 years or more and with the relatively short rotation cycle, data can be collected relatively easily on the same crop in the same field over multiple seasons. Such information enables the use of current zoning methodologies to define coherent areas in a field. By collecting temporal patterns in yield, zones may not simply be areas of high or low yield but may also include zones at risk to particular events. For example, areas can be identified that perform well in most years but show particularly bad yield in certain years which could, for instance, be due to a susceptibility to drought.

With the ever-increasing availability of data, there is also an increase in data sparsity. Data sparsity can impact a dataset in different ways, be it through variable sparsity, spatial sparsity or colocation sparsity. Variable sparsity refers to a lack of information in the set of measured variables. Yield data often exhibit a high level of variation across time and space. Thus, to be able to definitively identify distinct clusters, several years' worth of data needs to be collected in order to define zones within which yield varies similarly from year-to-year. However, if the yield data are variable sparse and contain too little information, i.e. that the signal is too weak compared to the variability, clusters will be difficult to identify and distinguish regardless of how many years' data are available.

Spatial sparsity occurs when data are not collected uniformly across a field, this is the case for many infield measurements. Such spatial sparsity generates holes in the coverage of data over a field and can either result in a large loss of resolution in the resulting field zones or in some cases, a failure in the convergence of the smoothing algorithms (See Section 3.2.3.3).

Measuring multiple variables across the field will rarely result in the same field locations being measured at each time point, which will result in, what is termed colocation data sparsity. Current zoning methods require each location to have a complete set of observations. Thus, colocation sparsity can result in a large loss of data, since any location for which only a subset of measurements was observed are omitted from the analysis, compounding the issue of spatial sparsity. Previous applications went some way to address this problem by aligning data to a

common grid, however, complete coverage of all variables is rare without a prohibitive level of aggregation.

As part of the project, data sparsity was addressed by adapting current methods for forming spatially coherent zones (Hassall *et al*, 2019).

This project focussed on the ability of yield monitor data to inform potato management on-farm, through the identification of distinct yield zones and the benchmarking of yield performance across farms and seasons. There are many tools available to farmers for such benchmarking purposes (e.g. Farmbench, and others at https://ahdb.org.uk/tools) and these are routinely used by growers. However, these tools are generally focussed on coarse spatial resolution and are difficult to align to precision management techniques. This work looked at combining both the yield zoning approach with yield benchmarking to provide more personalised information.

A key aspect of this project was the availability of potato yield data across multiple seasons. In contrast to cereal systems, temporal datasets are unavailable for potatoes given the long rotation cycle. Hence, other remote sensed data was also evaluated for its ability to inform potato management and to predict yield zones. In addition, the expert knowledge of growers was sought to inform future directions of methodological advancements in yield zoning methodologies.

Thus, in this project the following questions were addressed:

- Do potato yield monitor data demonstrate expected patterns of variability in yield?
- Can improvements be made to computational methods in order to mitigate the issues of data sparsity?
- Can yield monitor data be used to inform zones for potato management?
- Can these data be useful for benchmarking performance?
- Can we predict useful management zones from other remote and proximal sensed data?
- Can we incorporate growers' expert knowledge into the definition of management zones?

3.2. Materials and Methods

Potato yield monitor data were extracted directly from potato harvesters and supplied by the project team (see Table 1). These data were then processed through the ROTH-YE yield cleaning software (Muhammed et al., 2015) to remove outlying data points, typically achieved by specifying a minimum and maximum yield threshold. In addition, the potato yield data often exhibited flow delays where consecutive passes were misaligned. To adjust for this, edits to the software were made to first identify the start and end of each pass and to impose a shift delay, typically of around 15-20 seconds.

Table 1 below, details the number of fields for which there was data and the number that were deemed to have sufficient data quality after the ROTH-YE cleaning steps to be used in downstream analysis.

Table 1. A summary of the number of fields for which potato yield monitor data were available and were carried through to the different downstream analyses.

Year	Number of Fields	Number of fields with sufficient data quality	Number of fields zoned	Number of fields with sufficient NDVI data
2017	32	20	17	17
2018	40	33	32	25

In particular, some fields were immediately filtered due to too few data points recorded in a field or due to large areas of missing monitor data. Not all fields deemed to be of sufficient data quality after the cleaning step were successful in the zoning usually due to strong striations (potentially due to varietal differences in planting) in the yield maps.

Not all fields deemed to be of sufficient data quality after the cleaning step were successful in the zoning usually due to strong striations in the yield maps. Typically, about 10% of fields were filtered out at this step. In addition, cereal yield monitor data was made available for a small number of fields. These cereal data were also processed through ROTH-YE. In particular, four fields of winter wheat (1 field with 1 year and 3 fields with 2 years) of yield monitor data were processed.

3.2.1.   Field Alignment

Field boundaries were obtained through Digimap Ordnance Survey. Using ArcGIS software, satellite data were extracted for each field by masking these field boundaries and converting the raster images to point feature sets. Given some misalignment between the yield monitor GPS and the OS field boundaries, shape files were produced for the yield set and shifted to maximise the intersection between the OS field boundary and the yield monitor shape file.

3.2.2.   Variogram of linear features

To determine whether potato yield monitor data were likely to be sensitive enough to pick up spatial patterning in yield, the data was first analysed to see if known features of variation could be detected, such as those associated with tramlines. For this, geostatistics was employed which specifically characterised the yield variation by fitting variograms. The variogram is a function that relates variance to separation in space, $\boldsymbol{h}$, in distance and direction. The quantity $\boldsymbol{h}$ is known as the lag, which is a vector describing both distance and direction. For any particular $\boldsymbol{h}$, the variogram is given by

$$\gamma(\boldsymbol{h}) = \frac{1}{2}\,\mathrm{E}\left[\left(\mathrm{Z}(\mathbf{x}) - \mathrm{Z}(\mathbf{x} + \boldsymbol{h})\right)^2\right]$$

where $\mathrm{Z}(\mathbf{x})$ and $\mathrm{Z}(\mathbf{x} + \boldsymbol{h})$ are the values of the random variable Z at places $\mathbf{x}$ and $\mathbf{x} + \boldsymbol{h}$. The values of $\gamma(\mathbf{h})$ were estimated by the method of moments (Webster and Oliver, 2007),

$$\hat{\gamma}(\mathbf{h}) = \frac{1}{2m}\sum_{i=1}^{m}[\mathrm{z}(\xi + \mathbf{h}) - \mathrm{z}(\xi)]^2$$

where $\mathrm{z}(\xi)$ and $\mathrm{z}(\xi + \mathbf{h})$ are the observed values at positions ξ and $\xi + \boldsymbol{h}$ separated by $\boldsymbol{h}$, and of which there are m paired comparisons at that lag. Typically, as observations of the processes

become further apart they become less correlated, until there is no relationship between observations. This is characterized by the variogram. To see if the likely spatial patterning associated with compaction around tramlines could be detected, the variogram was calculated with lag distances constrained to 90 degrees to the direction of harvest and looked to see if any periodicity was detectable. This direction was found by,

$$\theta = \tan^{-1}\frac{\Delta x}{\Delta y} + 90$$

Where $\Delta x, \Delta y$ are the change in Eastings and Northings, respectively, of the sequentially measured harvest data. The variogram of the field was calculated in the direction of θ with a tolerance of 10 degrees.

3.2.3. Zoning

Following Hassall *et al.* (2019), the formation of spatially coherent zones consists of three steps: data pre-processing, clustering and smoothing.

3.2.3.1. *Data pre-processing*

Each yield (or NDVI) variable is first standardised to have unit variance. Since measurements from different variables will rarely co-locate within a field, data are aligned to a regular grid. Where multiple measurements of the same variable align to the same grid location, these are then averaged.

The grid size should be chosen carefully. Previous implementations recommended a grid size of 10m, which produces a reasonable resolution for practical field management. However, the choice of grid size does not only affect the zone resolution but also the zone coherence.

3.2.3.2. *Clustering*

Non-hierarchical methods of clustering have been found to outperform the hierarchical methods on field-based measurements due, perhaps in part, to the lack of a hierarchical structure in soil (Milne et a, 2012). Furthermore, fuzzy clustering methods enable a good assessment of cluster entropy and allows one to identify points that lie between clusters, as well as those that are easily classified.

Let z_{iv} be the standardised observation for variable $v = 1, \dots, p$ at location $i = 1, \dots, n$. The aim of the classification algorithms is to group the n objects into k classes. Each class $q = 1, \dots, k$ is characterised by a centroid vector $\overline{z_q} = \{\overline{z_{1q}}, \dots, \overline{z_{pq}}\}$. A fuzzy c-means classification is obtained by minimizing,

$$\sum_{q=1}^{k}\sum_{i=1}^{n} u_{iq}^{\omega}\delta_{iq}^{2}$$

11

where u_{iq} is the membership probability of location i to class q such that $\sum_{q=1}^{k} u_{iq} = 1$, $\omega > 1$ is the fuzzification parameter with values close to 1 resulting in a less fuzzy classification ($\omega = 1$, returns the non-hierarchical k-means algorithm). As recommended in Milne *et al.* (2012), $\omega = 1.25$. The variable δ_{iq} is the vector norm used to measure how well location i resembles class q. Here, the Euclidean norm is used.

Observations are clustered using the optimal completion strategy of Hathaway and Bezdek (2001) which allows for partial missingness in the vectors z. Choosing the appropriate number of clusters remains a subjective decision. Here, the normalized classification entropy is used $\xi(k)$, Dunn (1977), to identify the most appropriate number of clusters k,

$$\xi(k) = \frac{-1}{\log k} \sum_{q=1}^{k} \sum_{i=1}^{n} \frac{1}{n} u_{iq} \log u_{iq}$$

Where u_{iq} is the membership probability of location i to cluster q.

Following Roubens *et al.* (1982), point k is identified, that falls below the overall trend, such as a local minimum, or the point at which the entropy changes gradient. Note, in the following, graphs of $1 - \xi$ are presented, as this scale typically enabled an easier identification of the change points in ξ.

3.2.3.3. *Spatial smoothing*

In this work, recommendation that smoothing should occur after the classification or clustering step is maintained. Two reasons to do so are, firstly, classifying after spatial smoothing or kriging does not guarantee the spatial coherence of the resulting clusters. Specifically, with a view to on-farm management strategies, the aim was to force spatial coherence since the identification of many disjointed zones would be of little practical use in field. Secondly, to smooth the data first, would be to interpolate across the field with the potential effect of artificially increasing the number of completely observed locations. By smoothing in the final step of the zoning process, the need to propagate imputed data is avoided (and its associated uncertainty) through the cluster algorithms.

Following Lark (1998), spatial coherence is imposed over the clusters by recalculating the class memberships at each location as a weighted average of the neighbourhood of class memberships. Since membership probabilities form a composition (constrained to sum to 1), this weighted average is calculated after a symmetric log-transformation of the membership probabilities Aitchison (1982),

$$\widetilde{u_{Iq}^{*}} = \sum_{j \in R} w(i,j) \widetilde{u_{Jq}}$$

where $\widetilde{u_{Iq}}$ is the transformed membership probability for location i, class q, R defines the radius of a circular neighbourhood of location i and w is a weight defined by the dependence between locations i and j.

The weights $w(i,j)$ are formed so that points close to location i are given higher weight than locations further away and are derived from the variogram function Webster and Oliver (2007),

$$\gamma(h) = c_0 + cf(h)$$

12

where γ, termed the semi-variance, is a function of the expected mean squared difference between random variables at locations separated by a distance h. The variogram therefore characterises the spatial dependence between points and is incorporated into the weighted smoothing through the following (Lark, 1998),

$$w(i,j) = \frac{1 - f(h_{ij})}{\sum_{l \in R} 1 - f(h_{il})}$$

where h_{ij} is the distance between points i and j.

An example variogram is shown in Figure 1(C) and illustrates i) the nugget variance, c_0, which is the spatially independent contribution to the variance, ii) a period of increasing γ, characterising the property that points separated by a small distance h, are more similar than points separated by a large distance h and iii) a sill, $c_0 + c_1$, indicating points separated by large distances are spatially independent.

The inclusion of the variogram function in the definition of the weights provides a rational measure of spatial dependence between points. Specifically, the variogram is calculated from the transformed class membership probabilities. Although there will be k possible variograms, one for each class membership, in practice it is found that, except for the nugget, very little difference can be seen in the variograms of the different class memberships. Thus, the empirical variogram is obtained from the transformed membership probabilities of the most commonly occurring class, to which the model variogram is fitted. Since there will be a class membership for every location, including those with incomplete measurements (when implementing the revised cluster algorithm), all locations are included in the calculation of the spatial dependence and moreover the variogram will explicitly capture the spatial dependence of the classification.

Not only is the choice of weights important, but also the choice of R, the radius of smoothing. If R is too small, clusters remain fragmented, whereas for large R, clusters are oversmoothed. Hassall et al (2019), defined a coherence index, I_c^*, which when maximised, defines a radius that balances out the need to reduce spatial fragmentation and to ensure the resulting smoothed clusters are consistent with the original variables,

$$I_c^* = \frac{\eta_a^*}{\sum_{q=1}^{k} \psi_q^2}$$

Here η_a is the proportion of pairs of points within a distance a*, that belong to the same class and ψ_q is the proportion of units that belong to class q. a* is defined by the 25th percentile of the square root of the Voronoi cell area, where the Voronoi grid is defined by the Delaunay triangulation of the locations within the field. Defining a neighbourhood based on the observed Voronoi grid ensures a reasonable coverage and a consistent coherence index. Such a coherence index maximises the probability that two individuals separated by a distance a* are in the same class, normalized by the probability that two randomly selected individuals from the dataset belong to the same class.

Figure 1. **A) Locations of the set of complete observations for a single field on a grid size of 5m. B) Locations are coloured according to the transformed membership probabilities for the most commonly occurring class resulting from a fuzzy c-means clustering with 4 clusters and C) shows the associated variogram. D) An illustration of the neighbourhood under spatial sparsity. E) The Voronoi grid of observed spatial locations. F) Histogram of the "length" of Voronoi cell size, calculated as the square root of the Voronoi cell area. G) The numerator of the coherence index calculated based on a grid neighbourhood (red) and a Voronoi neighbourhood (black). H) The coherence index calculated based on a grid neighbourhood (red) and a Voronoi neighbourhood (black).**
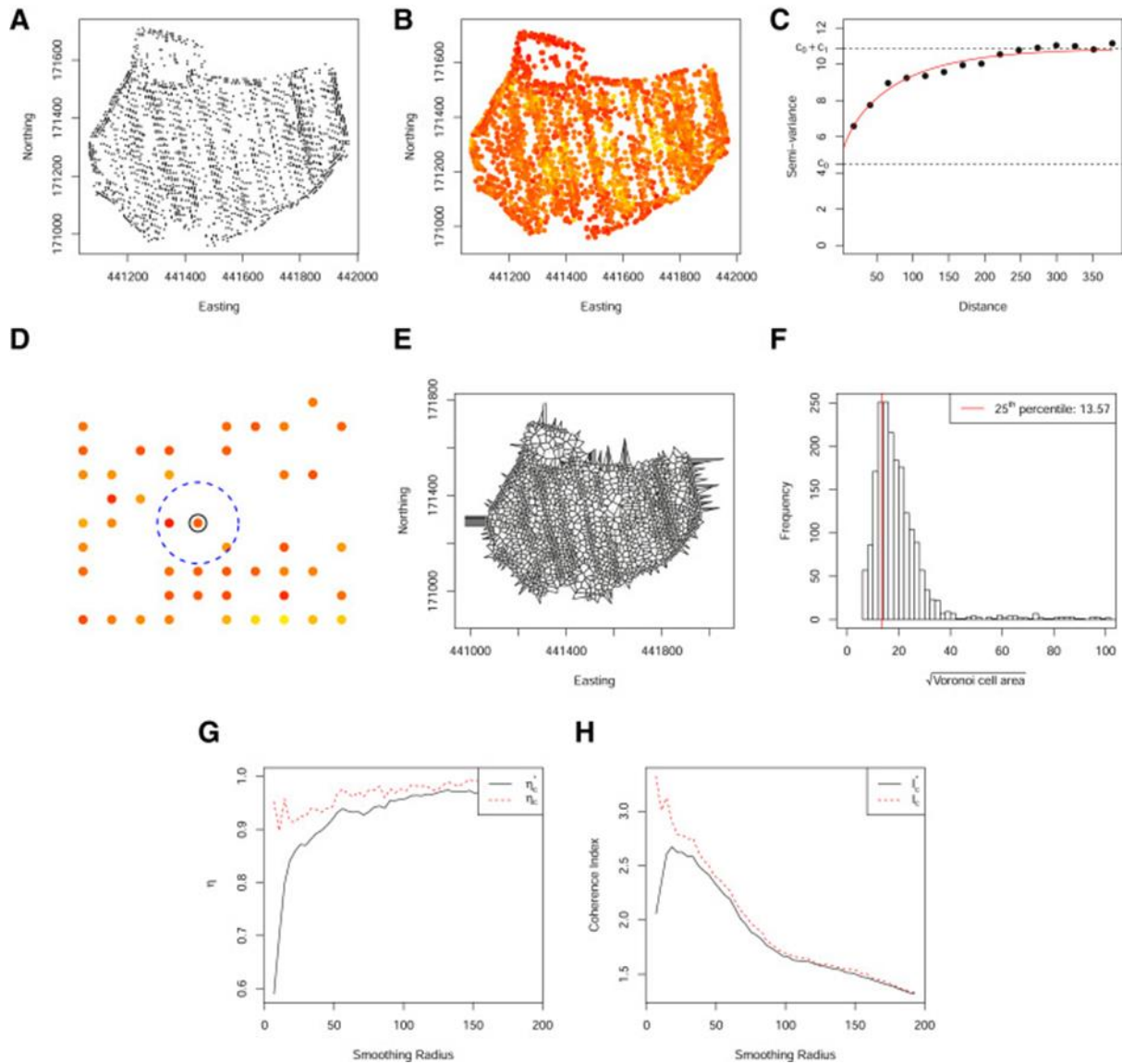
3.2.4. Benchmarking

A prototype yield benchmarking tool was developed with the primary aim of engaging growers in the interpretation of management zones. The tool was developed as an R shiny application and allows users to see how individual fields compare in terms of average yield to the whole set of 49 fields from 2017 and 2018. The average yield was calculated based on the 10-m gridded yield monitor data.

For an individual field, the yield zones as determined from that single years' worth of potato harvest data were identified. These were shown along with boxplots of the measured yield (aggregated to 10 m x 10 m squares) per zone.

A final option showed how these within field zones compared across different fields within the region. To calculate the zones across different fields, the fuzzy clustering algorithm was run on the gridded 10m yield data of all fields simultaneously. Thus, the clusters identified cut across all fields. The spatial smoothing was done on each field independently, whereby the variogram of the fuzzy membership was identified per field and smoothed as per the methods detailed above. Thus, the smoothing index may have been optimised at different distances for each field.

3.2.5. Satellite data

Satellite data from Sentinel-2 were extracted and processed via Pixalytics Ltd. Sentinel-2 carries a wide swath (290 km) high-resolution multispectral imager with 13 spectral bands, and a dynamic range of 12-bits. Spatial resolution is dependent on wavelength, with Visible (VIS) and NIR at 10 m, Vegetation Red Edge and Short-wave Infrared (SWIR) at 20 m, and Coastal Aerosol, Water Vapour and Cirrus bands at 60 m.

A selective time series of data was chosen for the target area based off image availability and cloud cover. A summary of Sentinel-2 data found most appropriate for developing NDVI products is listed below (Table 2). For consistency, only Level-1C (Top-of-atmosphere reflectance in cartographic geometry) data were used.

Table 2. Dates of extracted Sentinel-2 data for the region of interest. Dates were chosen within particular ranges (May - June and September - October) such that cloud cover was minimised

Year	Month	Day
2018	May	7th
2017	June	21st
2017	June	18th
2017	September	24th
2016	June	6th
2016	September	14th

3.2.5.1. Pre-Processing

To convert Sentinel-2 values from Top-of-Atmosphere to At-Surface reflectance, the *Atmospheric and Radiometric Correction of Satellite Imagery1* (ARCSI) tool was used. Level-1C Sentinel-2 data has been atmospherically corrected using Dark Object Subtraction techniques, cancelling out haze caused by scattering from remotely sensed data. The empirical method searches each band for the darkest pixel value and subtracts this from every pixel in the band to remove the effects of additive scattering.

Due to the atmospheric correction technique, Sentinel-2's three 60-m spatial resolution bands (Coastal Aerosol, Water Vapour, Cirrus) have been removed from the product. This will not impact the calculation of any future thematic indices using the Visible, NIR and SWIR bands.

3.2.5.2. NDVI

The Normalised Difference Vegetation Index (NDVI) algorithm was used to exploit the vitality of vegetation using Near Infrared (NIR) and Red visible light. Vegetation presents an abrupt rise in spectral signature reflection at 700 nm, whereas spectral signatures of non-vegetated land cover will remain linear. The more active the chlorophyll within the vegetation, the more pronounced this rise in spectral reflectance will be. This allows not only the determination of vegetated/non-vegetated areas, but also acts as a proxy for vegetation vitality.

NDVI is a result of the following equation:

$$\frac{NIR - Red}{NIR + Red}$$

This equation returns a value between -1 and +1, with numbers closer to +1 representing the increased presence of chlorophyll, and thus as a proxy, the increased strength of vegetation. NDVI products have also been used to derive other biophysical properties of vegetation such as Leaf Area Index, biomass, chlorophyll concentration, plant productivity and fractional vegetation cover. Using the atmospherically corrected data, NDVI has been calculated for each individual image using the above formula.

3.2.6. Farmer participation

To date, field zoning techniques have focussed on the data analytics. However, it is well-recognised that farmers and growers have inherent knowledge about their fields and how to manage them. Thus, incorporating this knowledge into the zoning algorithms is a desirable outcome. This knowledge may be quantitative such as the size, shape and number of zones for which it is practical to divide a field into or it may be qualitative such as "area X never seems to do as well as area Y." It was the aim of this project to run facilitated workshops to identify such information and to integrate this into the mathematical algorithms for forming zones. Due to the COVID-19 pandemic, it was not possible to hold elicitation workshops to integrate farmer knowledge with the above zoning methodologies, and further develop the decision support tools. Instead, an online workshop was run as part of the 31st Annual Conference of the Cambridge University Potato Growers Association (CUPGRA). Around 70 participants actively engaged in the workshop. The workshop consisted of an initial introductory presentation of the motivation and zoning outputs along with a short video demonstration of the benchmarking tool. Input from participants was sought using an interactive questionnaire. This was done using the Mentimeter software (https://www.mentimeter.com) and consisted of the following questions:

1. I would consider variable field management of potatoes because… [Rate from strongly disagree to strongly agree]

   - It will increase my yield
   - It will increase my profit
   - It will reduce the impact on the environment
   - It will save me time
   - Because it will support negotiations for a new contract

2. I would like to vary [please rank]

   - Nutrient application
   - Irrigation
   - Seed rate (including leaving some areas unsown)
   - Pesticide sprays
   - Harvest time

3. Other information I need to help me manage zones differentially [please select]

   - Maps of within field soil variation (e.g. EMI)
   - Yield maps from other crops
   - My expert knowledge of the field in question
   - Topography

4. Is it useful to benchmark zones of the field… [Rate from strongly disagree to strongly agree]

   - It is useful to compare zones across fields
   - It is useful to compare zones within a field

5. What are the main hurdles to data sharing [Please rank]

   - Disclosing yield information
   - I don't routinely collect yield data
   - Disclosing the location of the field
   - I don't know how to share my yield monitor data
   - I don't have time to download the data

6. What should be included in a benchmarking tool? [free text]

3.3. Results

3.3.1. Summary of potato yields

Figure 2A shows the distribution of yields over the surveyed fields through 2017 and 2018. Yields ranged from approximately 25 tonnes per hectare to more than 90 tonnes per hectare with lower yields generally seen in 2018, an exceptionally dry year. There was also a range in the size of fields considered as shown in below Figure 2B). Fields varied from approximately 6 to 11 ha and a small number of larger fields exceeding 20 ha.

Figure 2.   (A) Boxplots of the average yield per field. Field yields were estimated after aggregating the yield monitor data to 10 m grid squares. (B) Boxplot of the areas of the 49 potato fields.
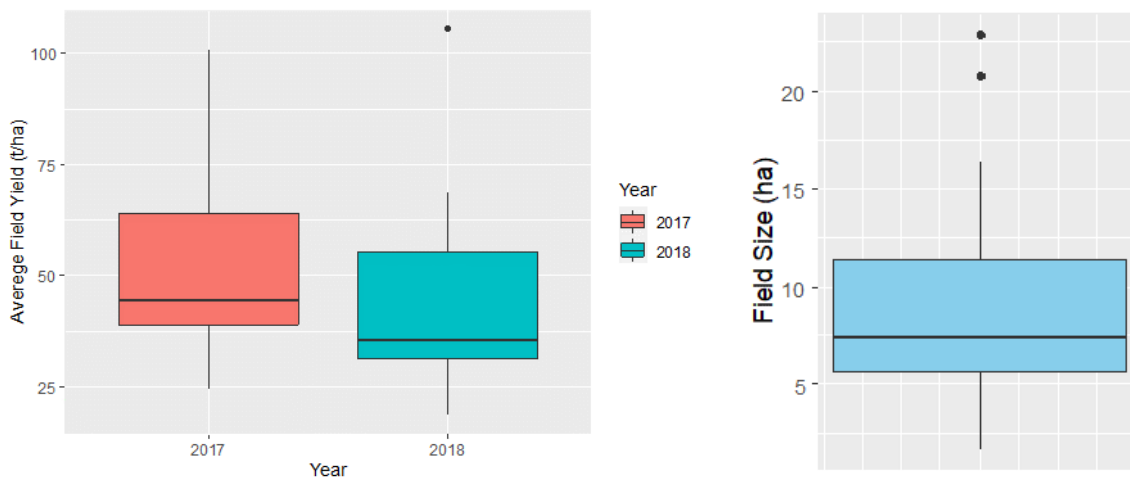
Figure 3 shows that as the average productivity in a field increased, so did the variation. This relationship appears quite linear with the standard deviation approximately one third of the average yield. Thus, in-field variation of potato yield is substantial.

Figure 3.   Scatterplot showing the average yield per field and the associated variability (standard deviation) in yield across the field.
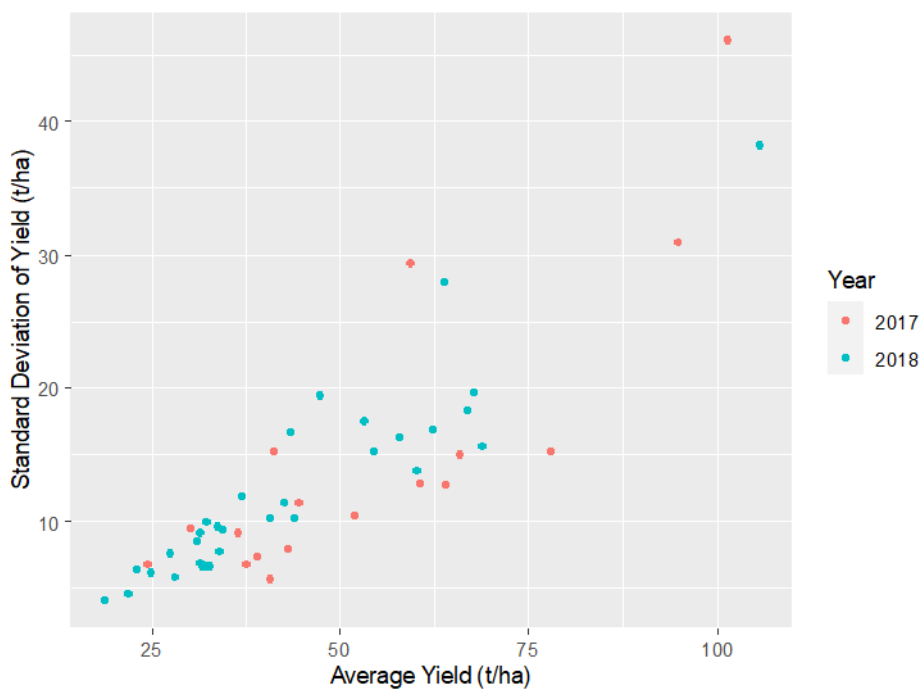
3.3.2.   Potato yield monitor data demonstrate expected patterns of variability

Management of potato crops can be quite extensive with heavy use of machinery through the field. It is therefore expected that tramlines will have a significant impact on the yield of crops. Such an effect is indeed visible from yield monitor data (Figure 4), whereby the directional variogram picks up dips in the semi-variance at intervals consistent with the width of tramlines. This was evident in approximately 70% of observed fields.

Figure 4.   (A) and (B) show the yield monitor data for two different fields of potato harvests. (C) and (D) show the associated empirical variogram calculated in the direction perpendicular to harvest. The dashed red lines show the tramline intervals in the field which look to correspond with observable dips in the semi-variance.
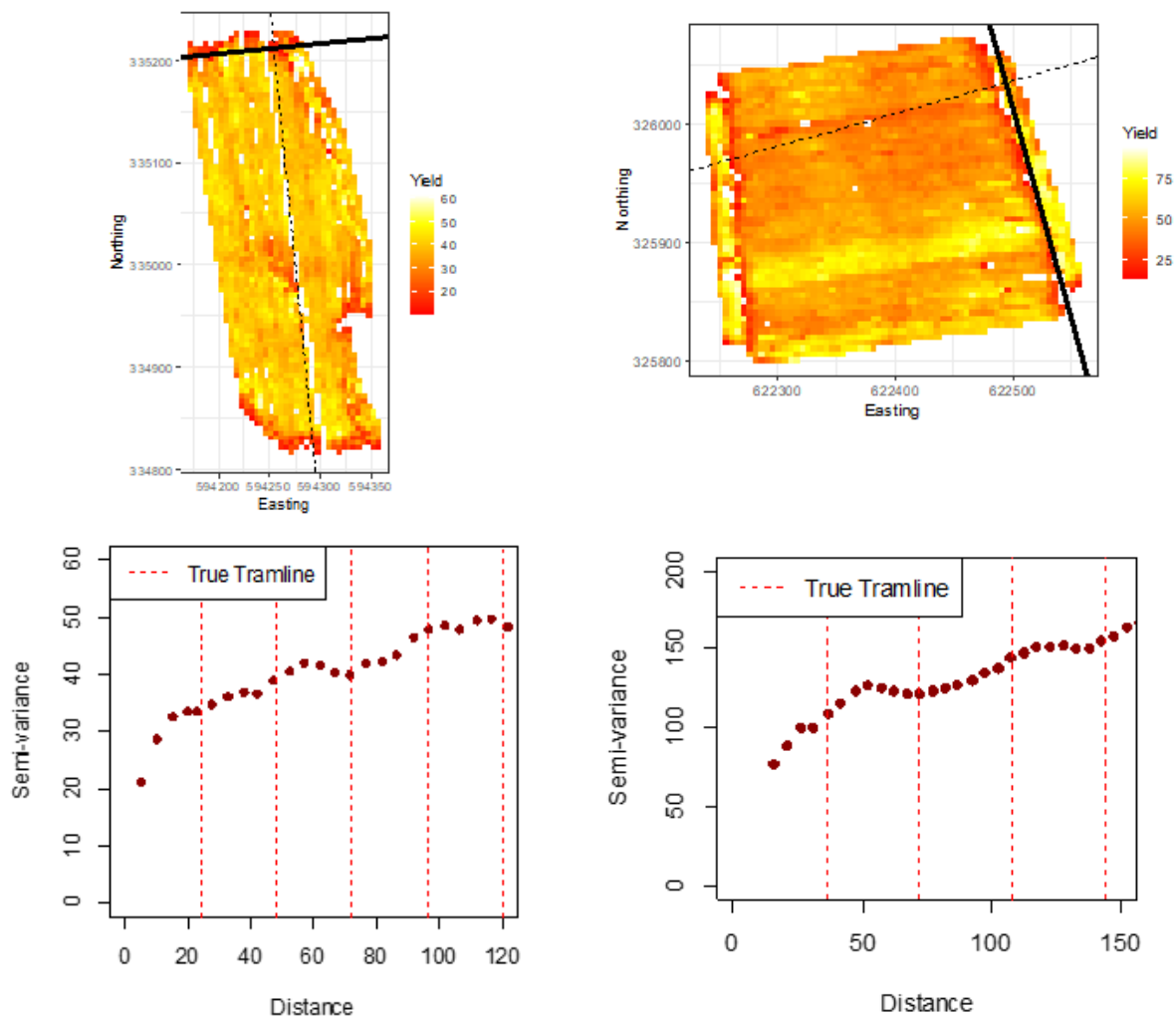
3.3.3.   Mitigating the issues due to data sparsity

As detailed in Hassall *et al.* (2019), guidance has been issued on the formation of spatially coherent zones under data sparsity as summarised in Figure 5. The methodological advancements we've made, as detailed in Section 3.2.3, are demonstrated through an extensive empirical study of wheat yield monitor data collected from multiple fields at different temporal and spatial resolutions in Hassall *et al* (2019) and are included in Appendix at the end of this document.

Figure 5. A flow diagram describing the process by which spatially coherent zones are calculated. Boxes highlighted in grey indicate the implementation of our methodological advancements specifically addressing the issues of data sparsity. Boxes highlighted in black indicate additional options one can iterate through to refine the formation of zones under high levels of sparsity.
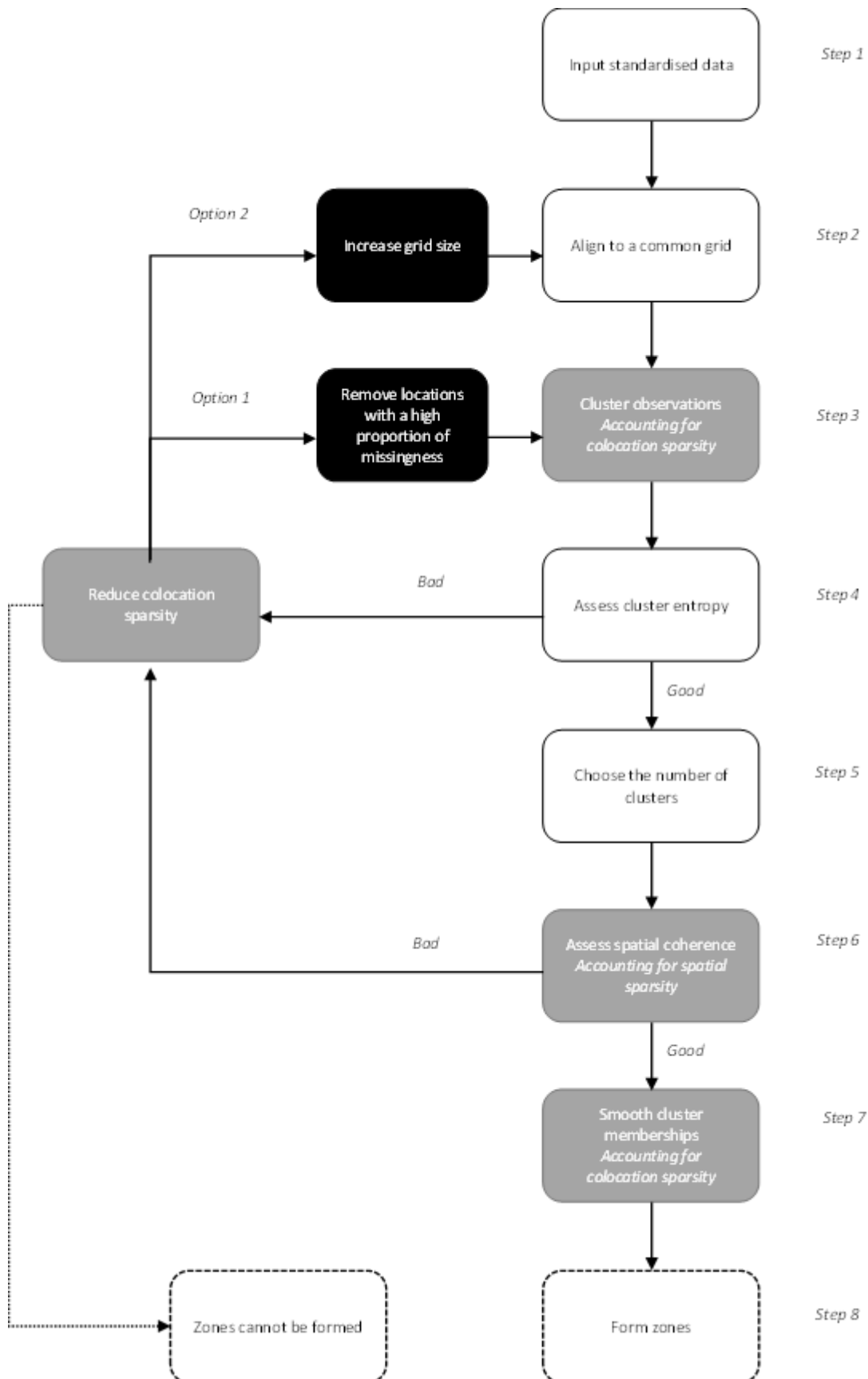
3.3.4. Identifying variable sparsity

Results shown in Hassall et al (2019) and Appendix 8 indicated that cluster identification often improves with the inclusion of more variables. However, distinct zones and clusters can still be formed from just two years' worth of data. Furthermore, the inclusion of more variables does not guarantee cluster formation.

Thus, before proceeding with the formation of coherent spatial zones, the raw clustering output should be evaluated through an assessment of the cluster entropy (Step 4 in Figure 5). The minimum number of years required to result in a reasonable clustering, as identified from the entropy (Muhammed *et al.* 2015), depends on both on the field and the particular subset of years considered. Thus, although there exist recommendations in the literature, (see for example. Boydell *et al.* (2002) for assessment of cotton yields), a case-by-case evaluation of the clustering is recommended to determine whether resulting zones will be distinct enough to be of use.

3.3.5. Spatial sparsity impacts coherence and smoothing

It is common to have 5 years or more of cereal yield data for a single field. When these data are aligned to a 5-m grid, there are relatively few locations for which there are a complete set of observations. Despite so few locations with a complete set of observations, clusters can be well-identified. However, due to the spatial sparsity, they cannot be made spatially coherent with the coherence index of Lark. Moreover, although the revised coherence index based on the Voronoi cell size is an improvement, it does not identify an optimal smoothing range (at Step 6 of Figure 5). In this scenario, data are too sparse to form coherent zones.

Spatial sparsity can be mitigated by retaining the partially observed locations. This can be done through the revised clustering algorithm outlined in Section 3.2.3.2 (Step 3 of Figure 5). When implementing the revised clustering algorithms to allow for partially observed locations, a much finer grid of spatially dense data can be used. The consequence of such is to provide a much improved (smooth and well-defined) coherence index. The use of partial data in the clustering algorithms did require more computational effort to ensure the algorithms converged. In rare cases where a high proportion of locations were partially observed, the algorithms sometimes failed to converge. In practice, one may need to consider a combination of variable-wise and unit-wise deletion of observations to reduce the colocation sparsity.

An alternative solution is to increase the grid size. As the grid size increases, the spatial sparsity decreases, and the coherence index is better identified. However, for larger grid sizes, the coherence index is less smooth reflecting the higher level of discretization in the grid alignment.

3.3.6. Mitigating data loss from colocation sparsity

Figure 6 demonstrates one of the key advantages to the methodological extensions outlined in Section 3.2.3. Specifically, this is a field for which many data are available. In particular cereal yield measurements have been collected for seven fields. However, with an increase in the number of years measured, the co-location sparsity increases, resulting in fewer locations having a complete set of observations. The subsequent zones, obtained from the original approach of Lark, although identified, are at a relatively low spatial resolution (Figure 6K). Allowing for partial observations, increases the spatial resolution of the resulting zones but not at the cost of zone coherency (Figure 6N).

Figure 6. **Figure 6 A)-G) Standardised wheat yield measurements over 7 years, aligned to a 10m grid. H) The spatial locations of both complete (black) and partial (grey) observations on a grid of 10m. I) The normalized classification entropy of the fuzzy c-means. J) The associated coherence index based on the underlying grid of 10m (red) and Voronoi cell length (black) and K) the associated smoothed clusters. L) The normalized classification entropy of the OCS fuzzy c-means. M) The associated coherence index based on the underlying grid of 10m (red) and Voronoi cell length (black) and N) the associated smoothed clusters.**
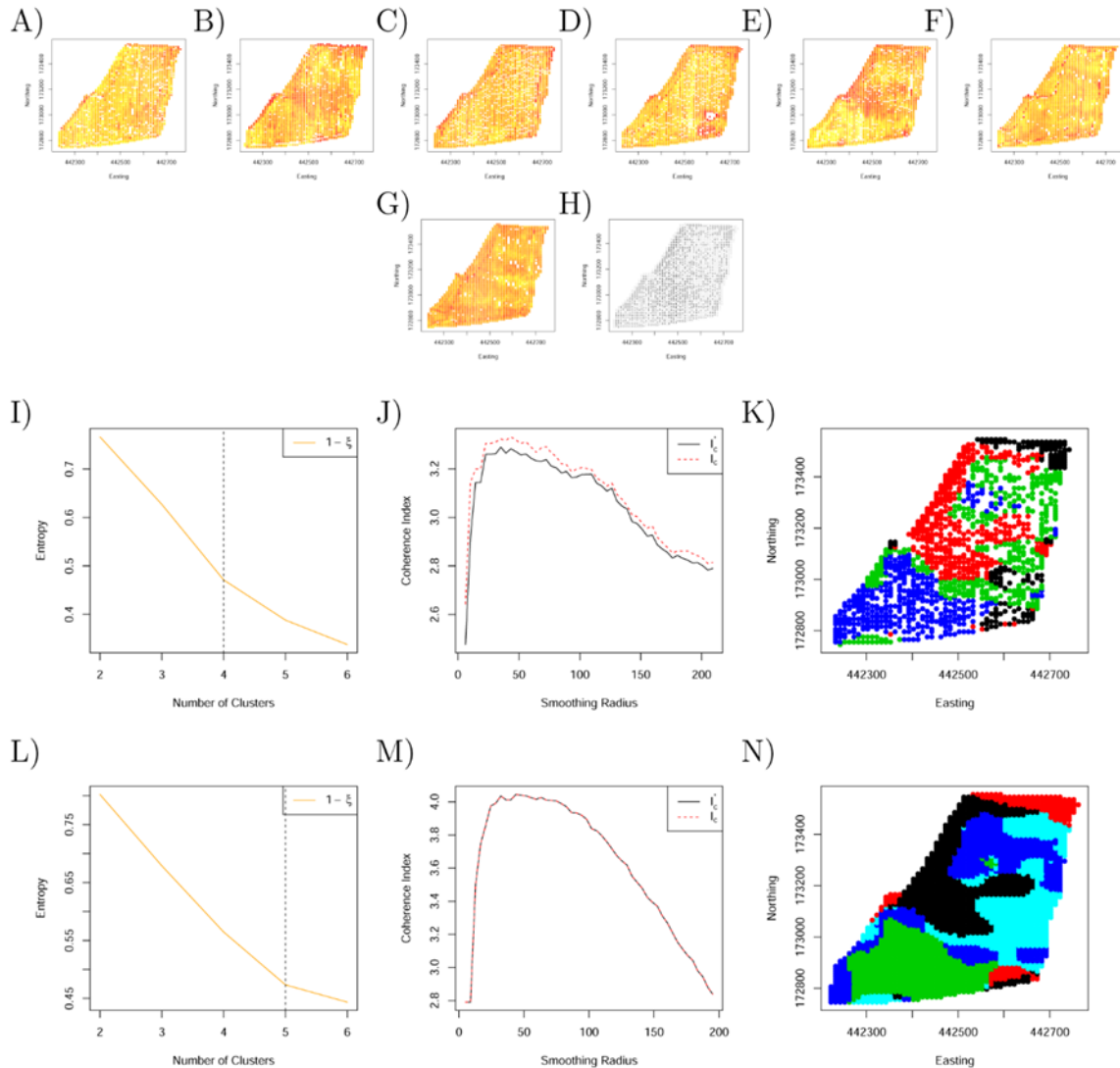
3.3.7. Zoning of potato yields

Table 3, shows the number of zones found per field for the year of potato yields, typically, this was of the order of 3 to 4 zones per field. The corresponding yield of each zone (per field) is shown in Figure 7. There is considerable variation both between fields and between zones withing the same field.

Table 3.   Frequency table showing the how many fields exhibited 3, 4, 5, or 6 distinct zones

Number of Zones (within a field)	Total number of fields
3	18
4	18
5	10
6	3

Figure 7.   Boxplots of the yield (tonnes per hectare) for every 10m2 grid cell within each zone per field.
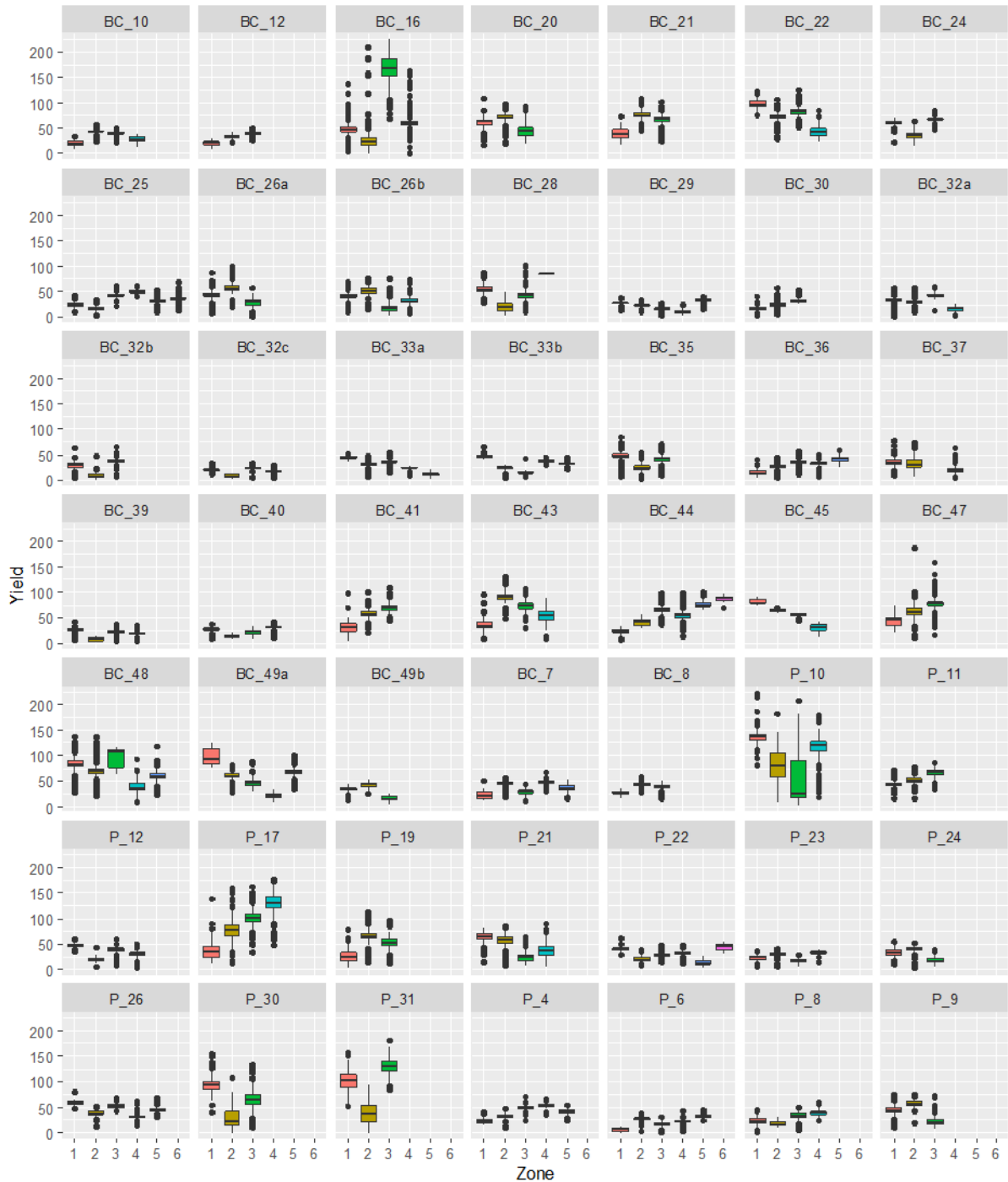
As can be seen in Figure 8, the between-zone variation can be quite substantial, with the average yield in the blue zone of 66.3 tonnes per hectare and the average yield in the green zone of 76.6 tonnes per hectare. For the field shown in Figure 8, yield variation shows clear zonal demarcation. However, there were more homogeneous fields, for which the yield variation was more clearly associated with striations in the field, potentially due to headlands, differing varieties grown in different sections of the field etc. Some examples of these are shown in Figure 9.

Figure 8.   Field map indicating the delineation of zones along with the corresponding boxplots of yields within each zone.
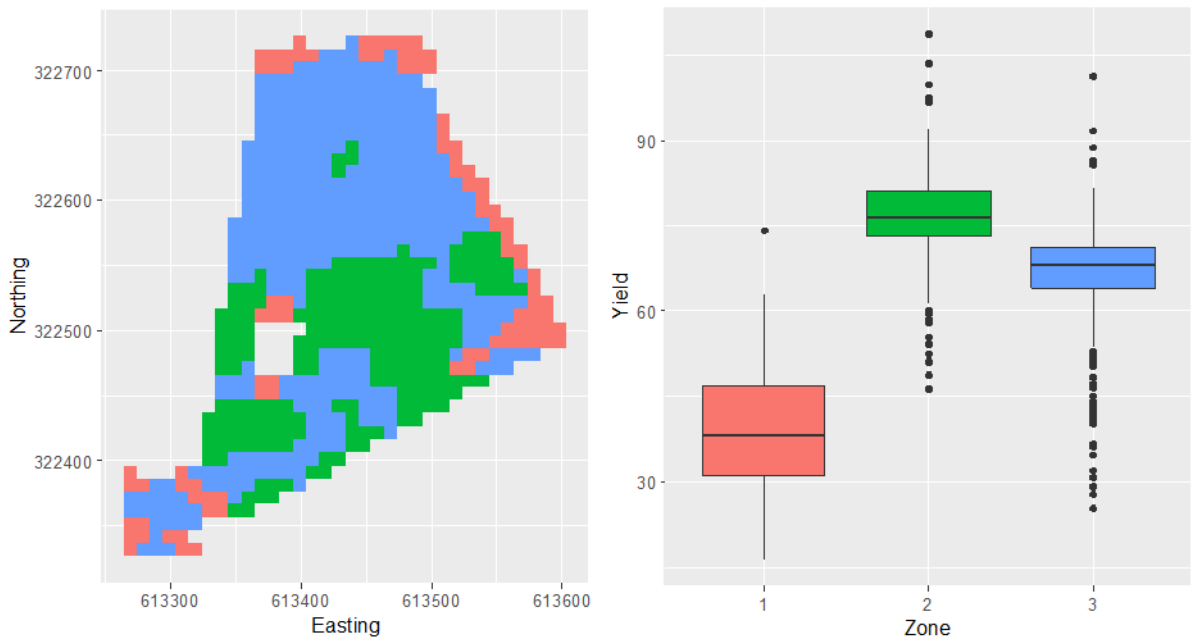
Figure 9. Example fields highlighting strong striations in the raw yield monitor data and the subsequent identified yield zones.
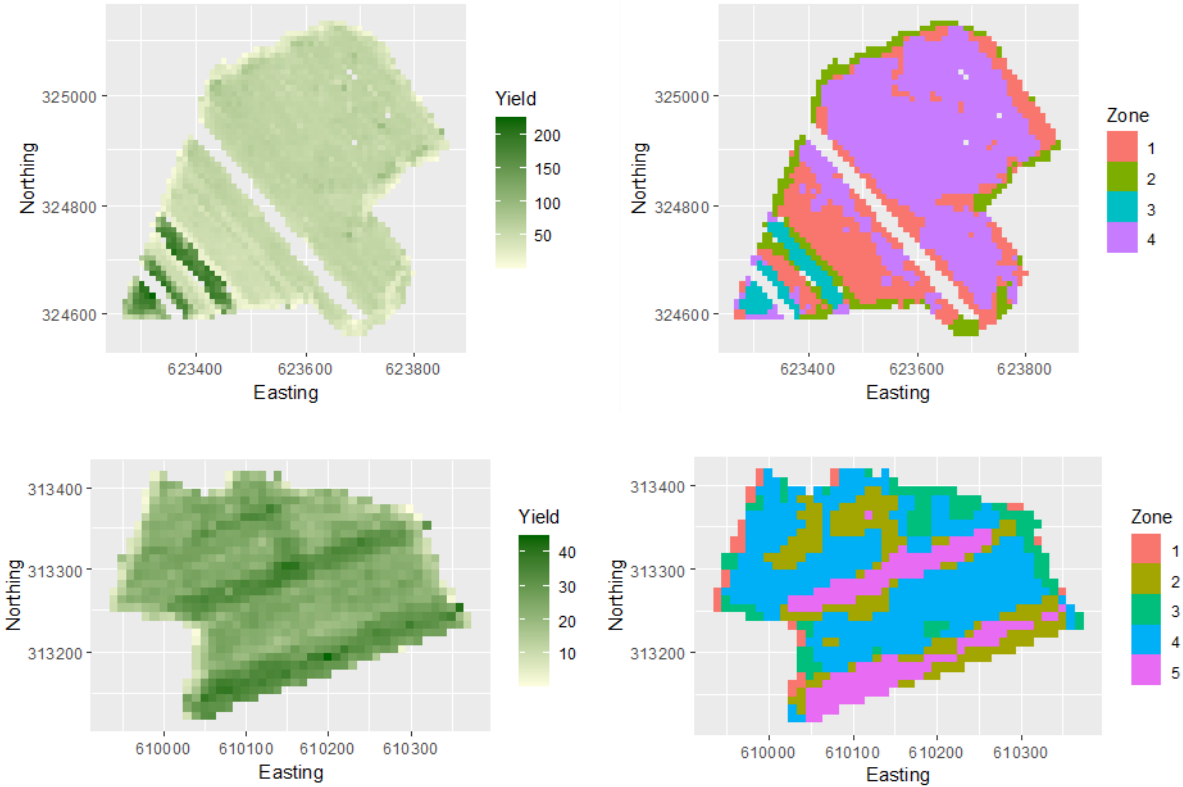
3.3.8. Benchmarking via zones provides additional information

The data and analyses shown in sections (ref appropriately) were incorporated into an R-Shiny software application for benchmarking. Screenshots are shown in Figure 10.

Figure 10. Screenshots of the yield zoning benchmarking tool
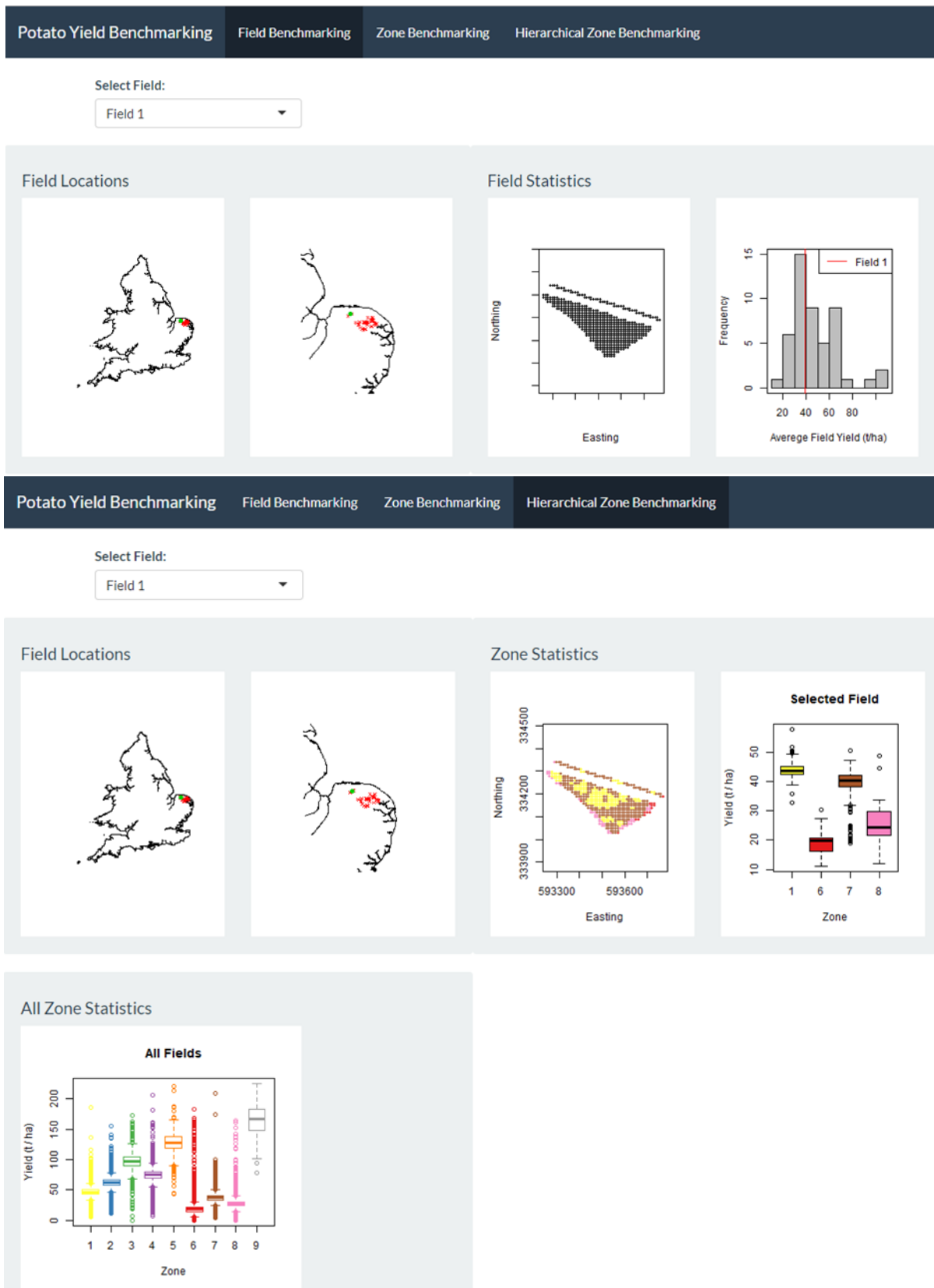
Not only were general statistics incorporated about the yield per field relative to all fields included in the sampling along with how that field was zone. But coherent measures were investigated for comparing zones across different fields. This was achieved by forming clusters of similar yield from across all fields simultaneously. Naturally, more zones were needed to represent this behaviour, 9 in total. The resulting clusters were then smoothed on a field-by-field basis. Thus, one can see if the zones identified in their field correspond to high or low yielding zones across the whole set of sampled fields.

3.3.9. Zoning via proximal data

Section 3.3.7 has focussed on the potato yield data. Although variational zones are apparent in in potato crops, the above analyses do not help to aid management practice in advance of harvest. To do so, would require an approach that predicts such zonal variation in potato crops that can be used by growers to manage different areas of a field in such a way as to optimise productivity both through costs and profit. The following subsections discuss approaches such as using proximal sensed remote satellite data and cereal yield information of other crops in the rotation.

3.3.10. Zoning via satellite imagery

Figure 11 shows the resulting zones based on NDVI measurements only. It is clear that for some fields variation in NDVI over the seasons has been detected. However, it is also clear that for some fields the NDVI does not show enough variation in order to pick out individual zones. In the majority of fields, a strong "edge effect" can be seen. This is due to the artefact in extracting satellite data based on field boundaries. The resolution of the imagery means the field boundary will be apparent in the NDVI. Figure 12 shows how the potato yield is associated with the NDVI defined zones. Some fields show a better correspondence than others but in general, the difference in yield between zones appears less than when zones are defined on actual yield measurement. This could be due to several reasons; the NDVI is picking up variation in different years that are not necessarily representative of the particular potato season, the resolution of the NDVI is not fine enough to pick up yield variation, the NDVI would be more accurate if taken at more time points spread through the growing season.

Figure 11. Resulting zones from clustering NDVI data for 42 fields that grew potatoes in 2017 and 2018
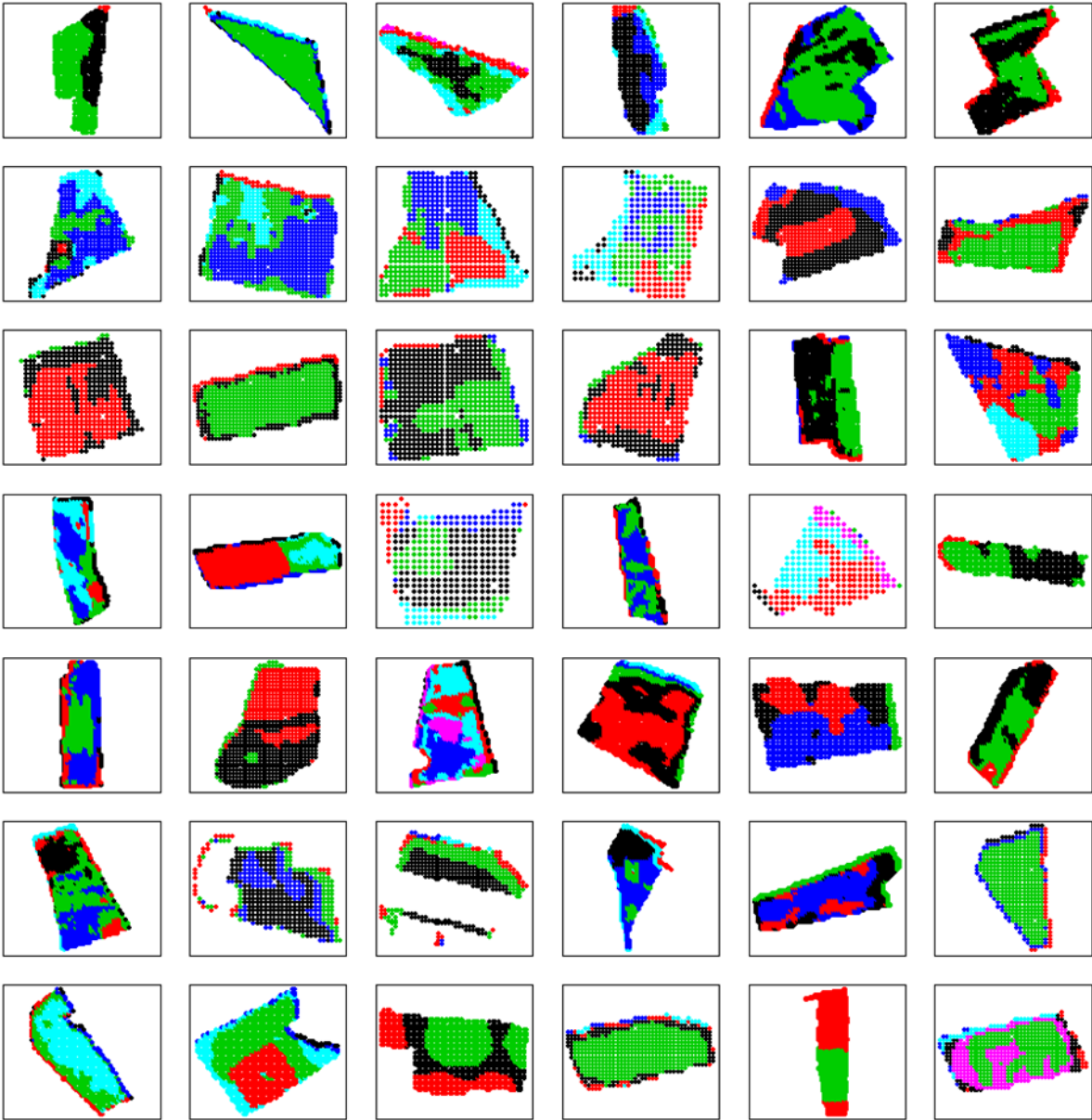
Figure 12. Figure 12 Boxplots of the 10m² average yield falling within each NDVI zone
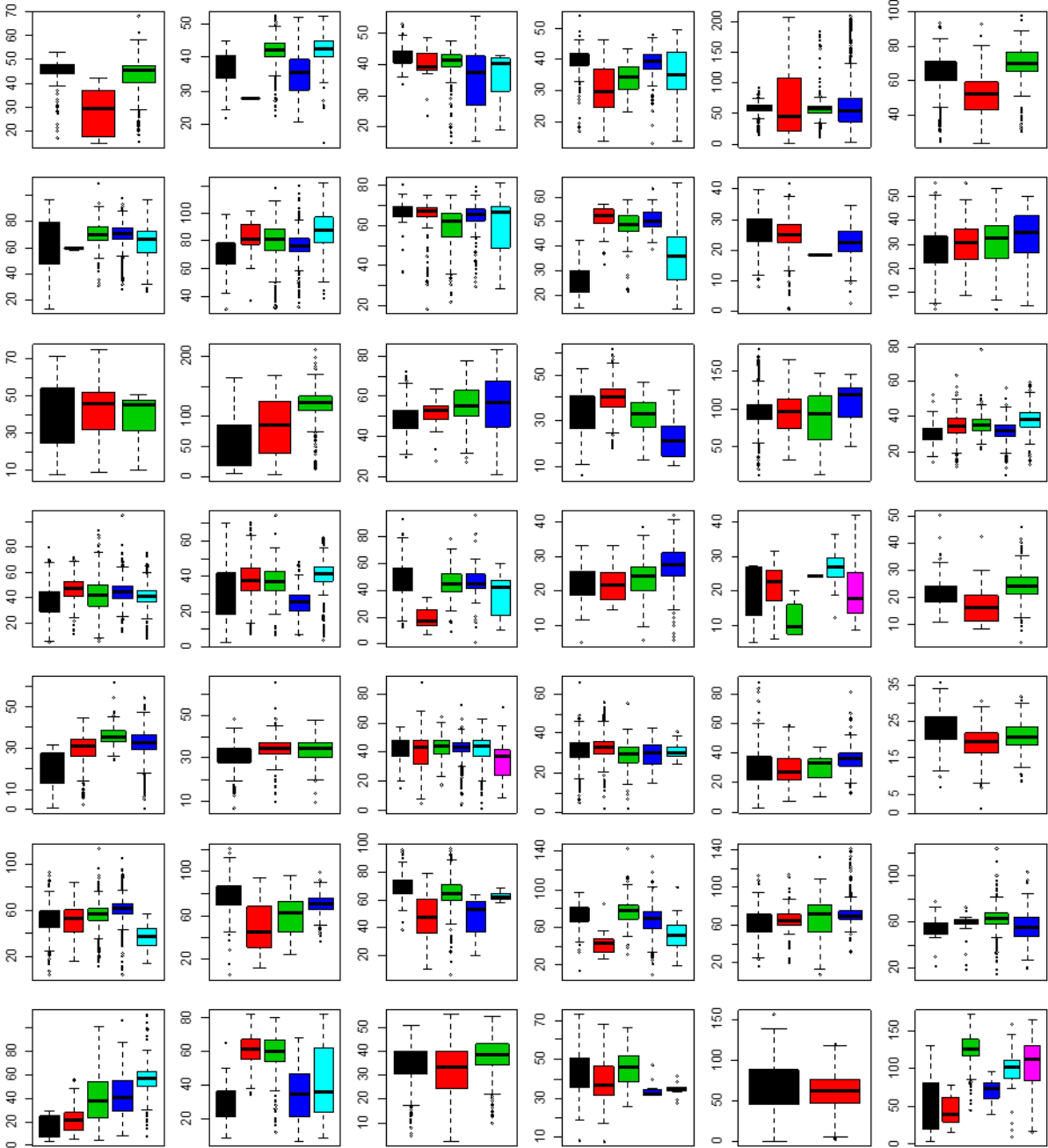
3.3.11. Zoning via cereal yield data

Figure 13 shows the resulting zones of 5 fields that grew potatoes in either 2017 or 2018 based purely on the respective cereal data. Clear zonal variation can be detected in all 5 fields. Boxplots in Figure 14 show how these zones are related to associated potato yields.

Figure 13. Resulting zones from clustering cereal yield data for 4 fields. The top left fields are zoned from a single year's worth of winter wheat yields, whilst the remaining 3 fields had two years of cereal data available.
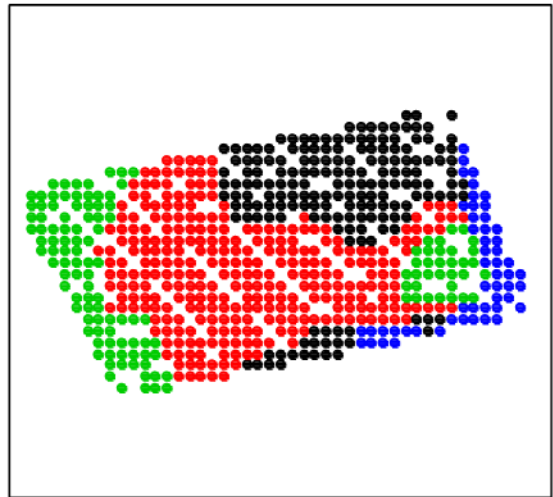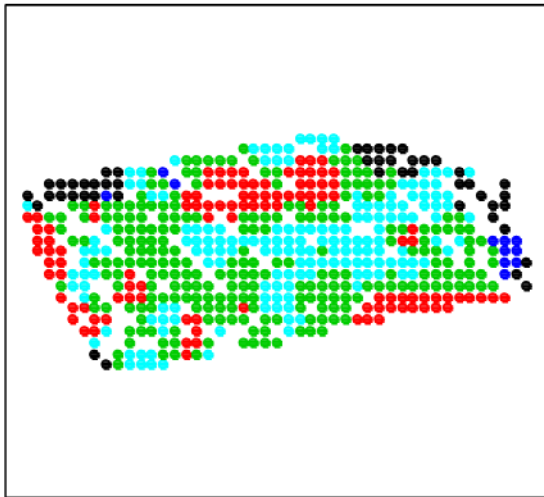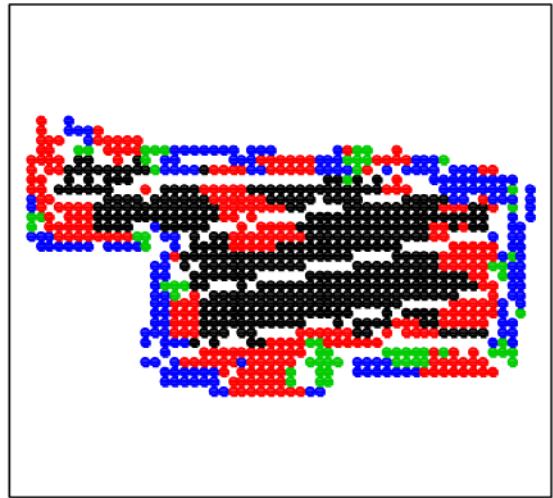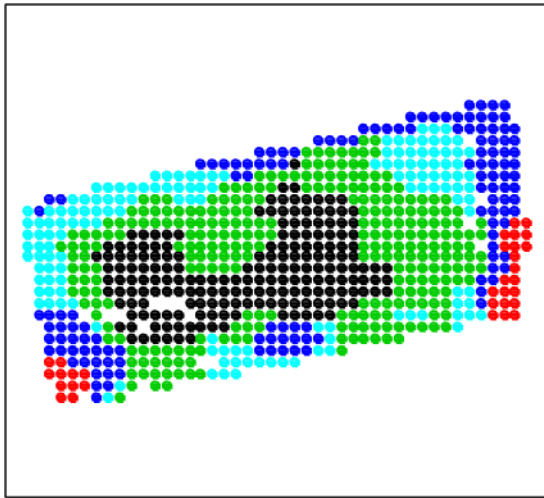
Figure 14. Boxplots of the 10m^2 average yield falling within each cereal zone.
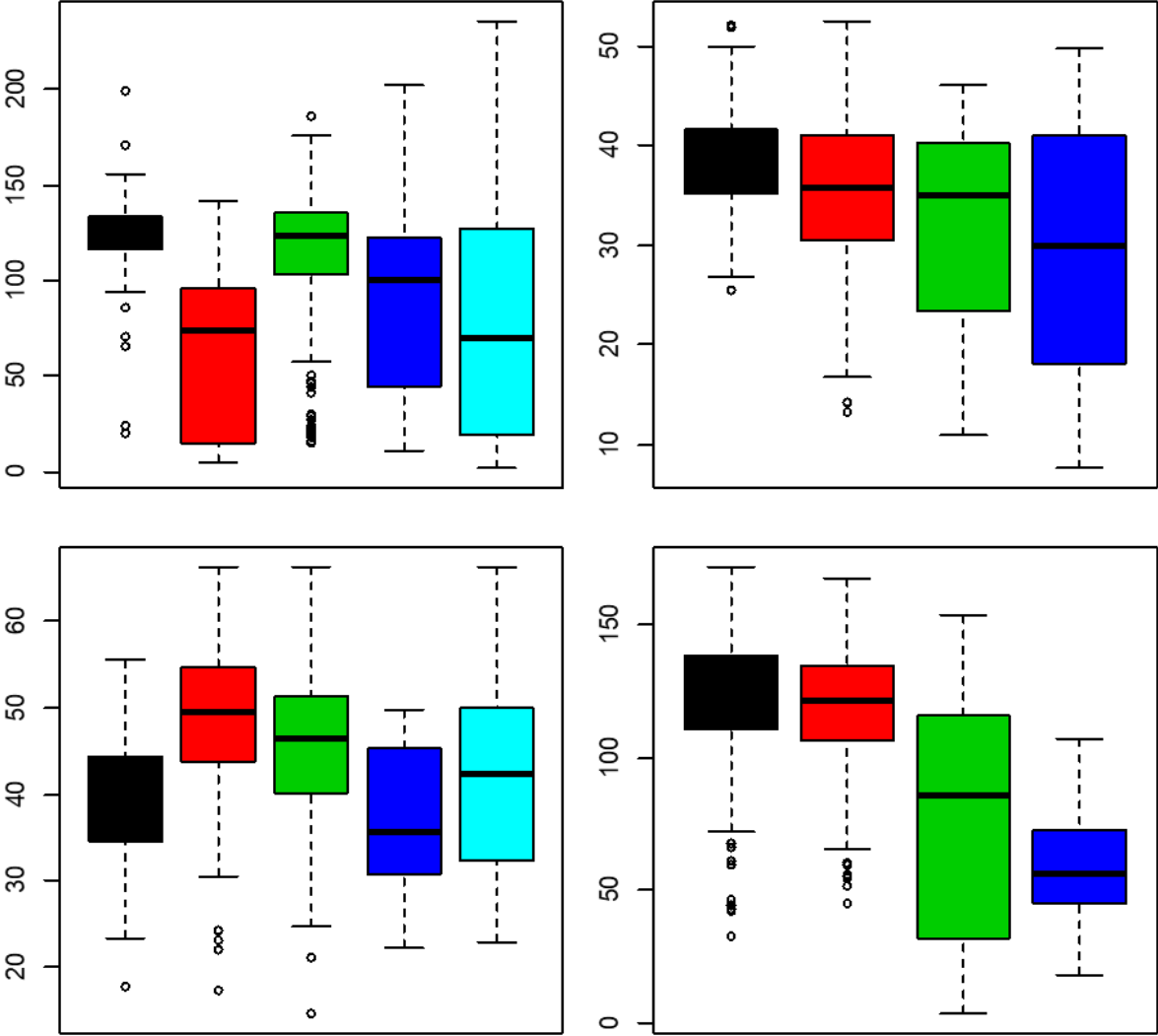
3.3.12. Incorporation of expert knowledge

The CUPGRA workshop focussed on extracting a holistic overview of what the main requirements and obstacles there are to variable rate field management of potatoes. Around 90 participants attended the workshop with approximately 65 engaging in the interactive survey. Participants varied in their expertise and included growers, agronomists, and industry representatives, among others. The survey itself, run through Mentimeter, showed visualisations of the questions as respondents inputted their answers. These are shown along with the full data below.

Q1: I would consider variable field management of potatoes because...						
Choices	Weighted average	1	2	3	4	5
It will increase my yield	3.43	4	9	13	25	9
It will increase my profit	3.75	4	3	16	18	19
It will reduce the impact on the environment	3.68	2	3	19	27	11
It will save me time	2.38	18	15	19	5	4
Because it will support negotiations for a new contract	2.46	13	18	17	10	1

Q2: I would like to vary (please rank)…					
Items	1	2	3	4	5
Nutrient application	33	12	10	3	3
Seed rate (including leaving some areas unsown)	15	11	16	10	6
Irrigation	10	20	15	12	3
Pesticide sprays	4	14	12	13	10
Harvest time	1	2	6	16	27

Q3: Other information I need to help me manage zones differentially...	
Choices	Votes
My expert knowledge of the field in question	59
Maps of within field soil variation (e.g. EMI)	56
Topography	42
Yield maps from other crops	40

Q4: Is it useful to benchmark zones of the field?						
Choices	Weighted average	1	2	3	4	5
It is useful to compare zones across fields	3.68	3	7	13	19	17
It is useful to compare zones within a field	4.44	1	3	5	10	40

Responses from the questionnaire suggested that the main motivation for potato farmers to adopt variable rate management was to increase profit, closely followed by reducing impacts to the environment. The respondents believed that variable-rate management was most appropriate for fertilizer application, but irrigation and adjusting seed rate also ranked highly in the list of operations that should be managed differently. With respect to the use of management zones formed from sensed data, most respondents suggested interpretation would be best enhanced through their own expert knowledge of the field and additional maps of soil variation. Comparing yield metrics through a Benchmarking tool was also seen as a helpful way to interpret and use management zones.

A key requirement for the further development of the analytical tools described in this report is the access to yield data both of the potato crop but also other crops in the rotation. When asked in the online survey what the main hurdles are for data sharing, it is not only issues with data privacy, namely disclosing the yield information itself but also a constraint that such data is still not routinely collected within the potato growing industry.

Q5: What are the main hurdles to data sharing? (please rank)					
Items	1	2	3	4	5
Disclosing the location of the field (Data privacy)	6	14	5	9	13
Disclosing yield information (Data privacy)	20	14	4	9	3
I don't have time to download the data	4	5	13	11	10
I don't know how to share my yield monitor data	5	9	13	6	9
I don't routinely collect yield data	20	9	8	5	5

3.4. Discussion

As detailed in the introduction, this project aimed to answer the following questions,

- Do potato yield monitor data demonstrate expected patterns of variability in yield?
- Can improvements be made to computational methods in order to mitigate the issues of data sparsity?
- Can yield monitor data be used to inform zones for potato management?
- Can yield monitor data be useful for benchmarking performance?
- Can we predict useful zones from other remote and proximal sensed data?
- Can we incorporate growers' expert knowledge into the definition of management zones?

3.4.1. Do potato yield monitor data demonstrate expected patterns of variability in yield?

Potato yield monitor data show reasonably high levels of in-field variability with the standard deviation approximately one third of the average yield per field. Furthermore, expected patterns of variation were identified corresponding to management practice such as tramlines and changes in variety. This suggests that should potato yield monitor data become more widely gathered it has the potential to inform on management of subsequent potato crops.

3.4.2. Can improvements be made to computational methods in order to mitigate the issues of data sparsity?

The methodological advances described in Section 3.2.3 enable a more efficient use of data by discarding less information in the formation of spatially coherent zones. In particular, it has been

demonstrated that by extending the clustering methods to cope with partially observed locations, more data are available as input to the coherence index and resulting variogram smoothing. Furthermore, by obtaining a variogram of the transformed class memberships, a complete set of data is available to determine any spatial dependence. However, the membership at each location will not be equally reliable as some will be based on incomplete data. Although this uncertainty is not accounted for explicitly, to a great extent, it will be captured through the class membership probabilities. For example, a location with only a single observation is likely to have a flatter distribution of membership probabilities as it is less clearly associated with a particular cluster profile.

As with almost all statistical analysis a certain level of manual assessment is prudent and remains a key component. As shown in Figure 5**Error! Reference source not found.**, an assessment of cluster entropy is required to identify the presence, and associated number, of distinct clusters. Clusters may not be identifiable in the presence of high levels of colocation sparsity (equivalently, in scenarios with a high proportion of locations with an incomplete set of observations). This may be addressed i) by removing locations with a high proportion of missingness or ii) by aligning data to a coarser grid. If neither option enables the identification of clusters, more variables are needed to inform the clustering. It is a topic of ongoing work to include alternative data sources, including subjective information, into the methodology to better define zones for farm management.

Once clusters have been identified, a second manual assessment can be made of the associated neighbourhood coherence index. This coherence index identifies the range over which to smooth the cluster zones. By implementing a Voronoi neighbourhood definition, this coherence index can be more reliably defined under spatial sparsity. However, a manual assessment of the index may still identify a "jagged" behaviour indicative of data that are too spatially sparse. To address this issue, aligning data to a coarser grid may be considered, to reduce spatial sparsity at a cost of lower data resolution.

In summary, data sparsity will always be present in one form or another. As described in this report and in Hassall *et al.* (2019), the effects of different types of sparsity have been investigated: variable, spatial and colocation sparsity, as well as how these can be mitigated. Guidance has been provided both on the steps to forming spatially coherent zones and how the use of manual assessments can be used to identify data scenarios that are too sparse to reliably form coherent field zones. This extends previously developed methods in the literature (Lark *et al.* 1998; Milne *et al.* 2012) and is an approach already being implemented in a CENTA PhD project at Cranfield investigating site-season effects on crop productivity to support sustainable intensification.

3.4.3. Can yield monitor data be used to inform zones for potato management?

The potato yield monitor data available in this project clearly demonstrate the capacity to detect in-field variation. Furthermore, this variation can be partitioned into distinct zones of size suitable for management. Since there was only potato data for a single year in any one field, it was not possible to assess its power to predict across seasons, but our analysis suggests that this source of information holds promise, and indeed, stakeholders responded positively to idea of comparing zones within a field.

3.4.4. Can these yield monitor data be useful for benchmarking performance?

The project had access to yield monitor data from a reasonable number of different fields and this allowed the comparison not only of the average yield per hectare across fields, but also how the zones compared across all fields within the study. This adds a new dimension to yield benchmarking tools and potentially aids interpretation for farmer-led decisions. Upon surveying stakeholders on the potential use of such information, the response was generally positive although not as useful as understanding zonation within a field.

3.4.5. Can we predict useful zones from other remote and proximal sensed data?

Remotely sensed data give the opportunity to overcome the limited cross-seasonal yield monitor data. As seen in Section 3.3.9, some fields show a good correspondence between the predicted zones based on remote data whilst others do not. This could be for many different reasons, but ultimately results will become more robust as more years' worth of data are available and at higher resolution (Song *et al. 2009*) to identify the longer-term trends apparent within individual fields.

3.4.6. Can we incorporate growers' expert knowledge into the definition of management zones?

It remains of interest to incorporate growers' knowledge into the definition of management zones. Although this hasn't been investigated in depth during this project, the stakeholder workshop generated useful findings. For instance, knowing which management practices a grower is willing to vary may influence the target size of the resulting zones. It is also clear that growers' expert knowledge of their fields should be incorporated, and this could be done, for instance, by the inclusion of an additional data layer in the clustering algorithms where a grower identifies differential areas of the field.

3.5. Conclusions

There are three key findings from this project. The first of which is that the quantitative methodology developed within the project is sufficient to deal with the ever-increasing availability and arguably the associated inevitability of an increase in sparsity of said data.

The second key finding is that potato yields exhibit somewhat coherent variation which can result in the formation of meaningful zones. It has been demonstrated how this can be useful for benchmarking and for informing management practice. However, such zones are hard to predict given the current levels of available data. Further work in this area using i) yield monitor data from the rest of the rotation ii) higher resolution (both temporally and spatially) of satellite imagery and iii) other sources of data such as soil maps is needed to improve the robustness of identified zones. To do this, a change in data management practice is needed to overcome issues associated with data sharing, for example GPS location, farm performance and with data ownership, for example collection of data from fields on rented land. These data privacy issues can become large barriers to the development of robust methods but also in the wider implementation of such methods through e.g. decision support tools.

The third key finding is that expert knowledge remains a valuable resource to be incorporated, whether this is the downstream practical input on how management can be adapted based on

zonal information or whether it is a direct input into how the zones are derived based on extensive knowledge of particular field features. It remains a key interest of the authors to continue this line of research and with the relaxation of Covid restrictions, farmer engagement on such topics can be achieved.

3.6. Acknowledgements

4. USING GEOPHYSICAL TECHNIQUES TO BETTER UNDERSTAND SOIL AND CROP VARIABILITY

4.1. Introduction

It has been demonstrated that electrical geophysical methods can be used for assessing spatial variation in soil textural properties and temporal variation in soil moisture. These methods include electrical resistivity tomography (ERT) and electromagnetic induction (EMI). ERT uses an array of electrodes in contact with the soil to produce a 2D or 3D image of the subsurface electrical resistivity (the inverse of electrical conductivity). EMI is a non-contact method that uses rapid electromagnetic sensors to measure the soil electrical conductivity. This method is now widely available commercially for 'soil scanning' of entire fields. ERT is more ideally suited for surveys of smaller plots because of the need for deployment of cables and electrodes coupled to the soil. Blanchy *et al.*(2020) provide more information on the two methods.

4.2. Materials & Methods

Scans of ERT and or EMI were measured in a series of experiments summarised in Table 4. For the ERT scans, an ERT array (Syscal Pro, Iris Instruments, France) comprising 24 electrodes (0.25 m electrode spacing) was used to collect resistivity transects on all plots of block 3 by putting the electrodes in the furrows between the ridges. A typical ERT layout is shown in Figure 15 (images from 2019 experiments). After inverting each ERT survey, the difference in resistivity from early and late surveys ($\Delta\rho$) is computed and divided by the resistivity of the early ($\rho0$) to obtain a relative difference between the two sampling dates. Electromagnetic Induction scans were done in 2019, 2020 and 2021. The instrument used was a CMD Mini Explorer (GF Instruments, Czech Republic). Scans were typically done in six EMI orientations (vertical and horizontal coplanar, VCP and HCP, respectively) and coil spacings of 0.32. 0.71 and 1.18 m. An example of EMI scan in progress is shown in Figure 16.

Please note that the work completed in autumn 2020 and spring 2021 were not performed on Rotations Research Partnership Project experiments but were conducted to fulfil obligations that had to be delayed due to COVID related travel restrictions.

Table 4.   Details of electromagnetic induction scans

Year	Location, (experimental code) and scan type.	Details of experiment
2018	NIAB F37 (2018-31)	Factorial combination of compost application rate, compaction and irrigation. Full details in Report for WP1. ERT scans on 12 June 2018 and 3 August 2018
2019	NIAB F30 (2019-49)	Factorial combination of compost application rate, compaction and irrigation. Full details in Report for WP1. ERT and EMI scans on 23 May and 24 July 2019
2020	NIAB F38/39T	EMI scans on 15 October 2020 of two similar experiments in 'light' and 'heavy' parts of the same field.
2021	NIAB F37	EMI scans on 23 March 2021. Whole experimental area scanned at a "low" resolution and a specific experiment scanned at high resolution

Figure 15. A typical electrical resistivity tomography array as used in 2019

Figure 16. Illustration of EMI scanner in use on 23 March 2021

4.3. Results and discussion

4.3.1. Electrical Resistance Tomography Scans 2018

Figure 17 shows the relative difference in inverted resistivity ($\Delta\rho/\rho_0$ expressed as percentage) sections with yellow area associated with an increase in resistivity (drying) and blue area associated with a decrease in resistivity (wetting). All sections show a larger positive change, probably associated with soil drying close to the surface, extending no deeper than 0.7 m. The compacted wet treatment shows the shallowest drying by the crop, while the non-compacted treatments exhibit deeper drying. Figure 17a and 17c also clearly show the depth of drying is limited, probably by the compaction, compared to non-compacted treatments (Figure 17b and 17d). No treatments showed any major differences in resistivity deeper than approximately 1.5 m depth

Figure 17. Relative change in inverted resistivity ($\Delta\rho/\rho_0$) section between 12 June 2018 and 3 August 2018 showing the different treatments: (a) compacted wet, (b) non-compacted wet, (c) compacted dry and (d) non-compacted dry. Note that the resistivity is the inverse of the conductivity. The semi-transparent white overlay shows the sensitivity of the survey.

41
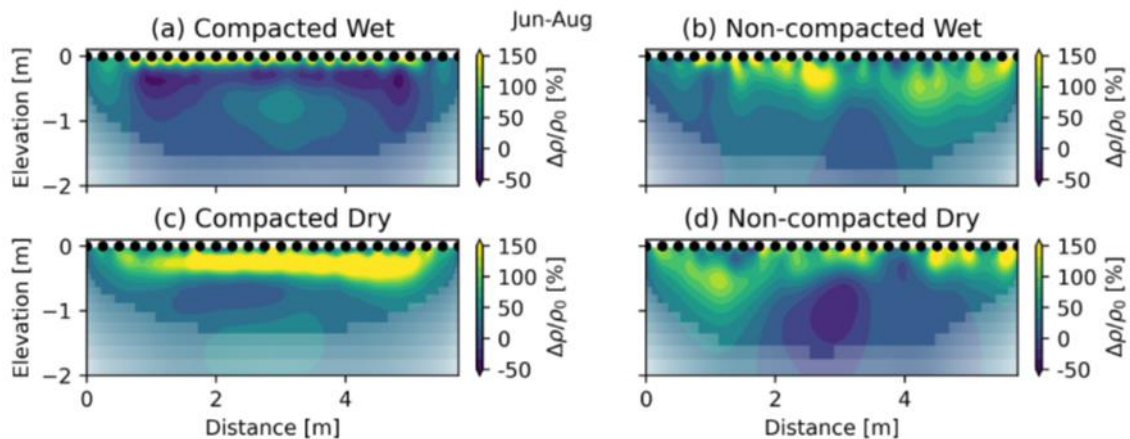
4.3.2. Electrical Resistance Tomography and Electromagnetic Induction Scans 2019

Further (repeat) ERT surveys were conducted in 2019 allied to Lancaster PhD student Katharina Huntenburg's AHDB funded research. Figure 18 illustrates greater depth of high electrical resistivity in the uncompacted plots.

Figure 18. Resistivity images obtained July 2019 showing the effect of compaction on soil drying.
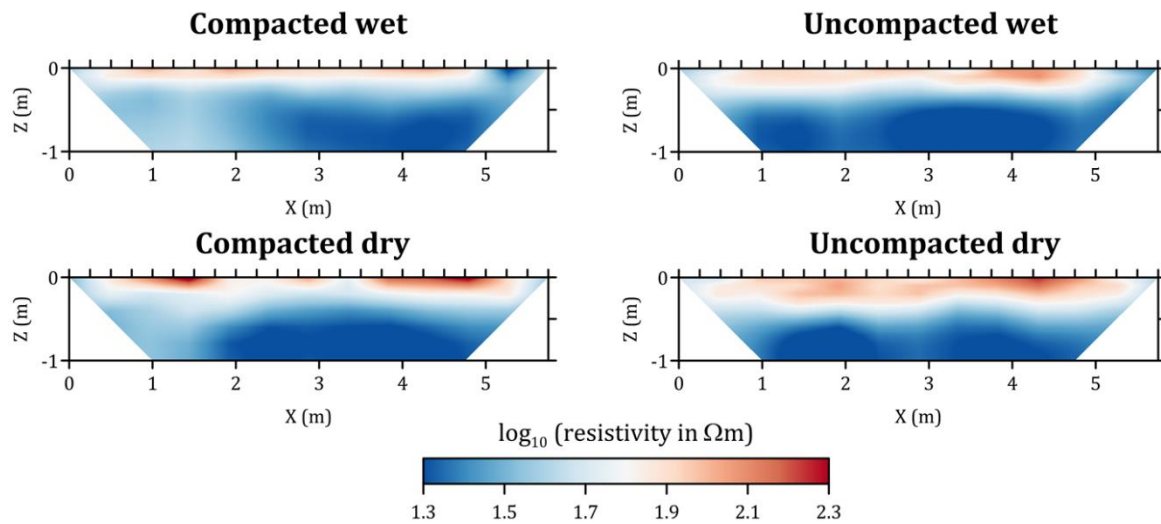
Figure 19 shows observed changes in soil conductivity for irrigated and non-irrigated cases. However, the effects of compost addition and compaction are more subtle (Figure 20 and Figure 21, respectively).

Figure 19. Effect of irrigation on soil electrical conductivity. The figure shows the change in electrical conductivity between 23 May 2019 and 24 July 2019 from the six EMI coil spacing/orientation. VCP is vertical coplanar, HPC is horizontal coplanar. The coil spacing used was 0.32m, 0.71m ad 1.18m. The value in brackets is the approximate depth of investigation
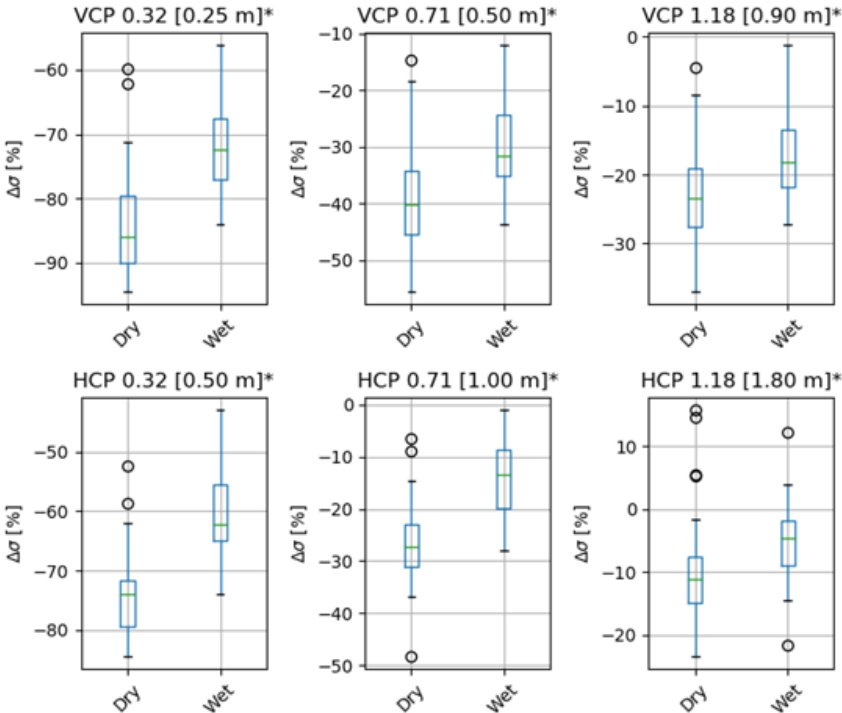
Figure 20 Effect of compost application on soil electrical conductivity. The figure shows the change in electrical conductivity between 23 May 2019 and 24 July 2019 from the six EMI coil spacing/orientation. VCP is vertical coplanar, HPC is horizontal coplanar. The coil spacing used was 0.32m, 0.71m ad 1.18m. The value in brackets is the approximate depth of investigation
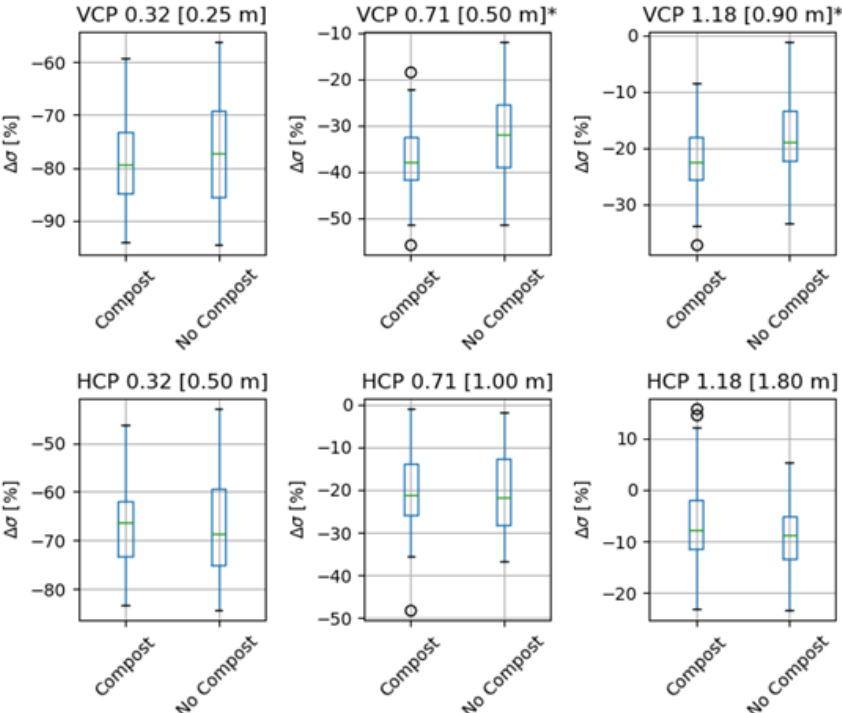
Figure 21. Effect of soil compaction on soil electrical conductivity. The figure shows the change in electrical conductivity between 23 May 2019 and 24 July 2019 from the six EMI coil spacing/orientation. VCP is vertical coplanar, HPC is horizontal coplanar. The coil spacing used was 0.32m, 0.71m ad 1.18m. The value in brackets is the approximate depth of investigation.
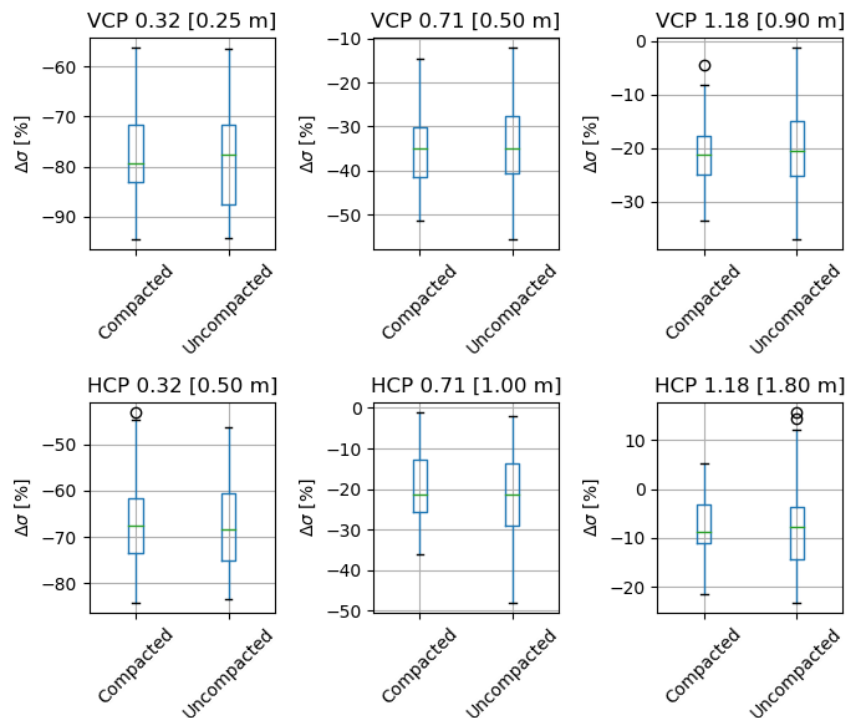
4.3.3.   Electromagnetic Induction Scans of contrasting soil textures 2020

An example of mapped EMI scan data is shown in Figure 22. In the Light area, there is a distinctive arc-shaped feature with higher conductivity (indicating an increased water content and heavier texture). This feature does not coincide with any known man-made structures (e.g. a field-drainage system) and may be the remnants of a silted up stream. In the Heavy area, there was a noticeable increase in conductivity from relatively low conductivity in the north-east corner of the experiment to higher conductivity in the West and South West (Figure 22).

Figure 22. Map of electromagnetic induction scans in the Heavy and Light areas on 15 October 2020. Each area is 21 m wide and 55 m long.
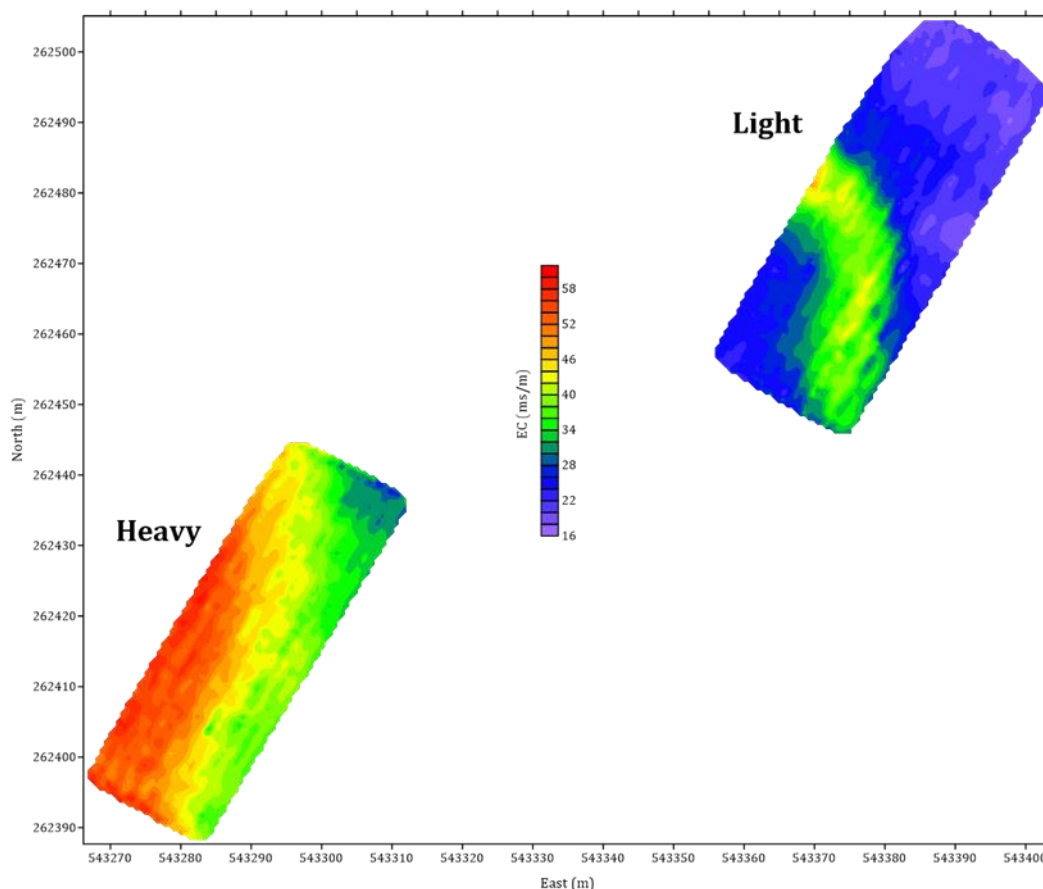
Simple linear regression showed that there was a statistically significant relationship between Julian date of 50 % plant emergence and soil conductivity. The regression explained over 50 % of the variation in emergence date (Figure 23). For all treatment combinations, the range in soil conductivities (28.1 to 53.4 mS/m) corresponded to an 8-day range in emergence date (Julian dates 137 to 145). This range in emergence date was seen in individual treatment combinations. For example, Russet Burbank (210 kg N/ha), grown in Block 1, had an electrical conductivity of 28.6 mS/m and achieved 50 % emergence on Julian day 137. However, in Block 4, the conductivity was 50.1 mS/m, and the 50 % emergence date was a Julian date of 144.

Electrical conductivity indirectly measures soil water content which, in turn, is a proxy for clay content. It is probable that the delayed emergence in the heavier parts of the experiment was due to a cloddy seedbed reducing water availability to the emerging potato plants. Weather data indicated that April and May were warmer and drier than average and this would have exacerbated the problem.

Figure 23. Relationship between Julian date of 50 % plant emergence and soil electrical conductance in the Heavy Experiment. Estima, □; Innovator, ■; Royal, △ and Russet Burbank, ▲. The fitted regression line for all treatments is y = 127.5 (± 1.77)+0.330 (± 0.0433)x, R^2 = 0.53; P < 0.001.
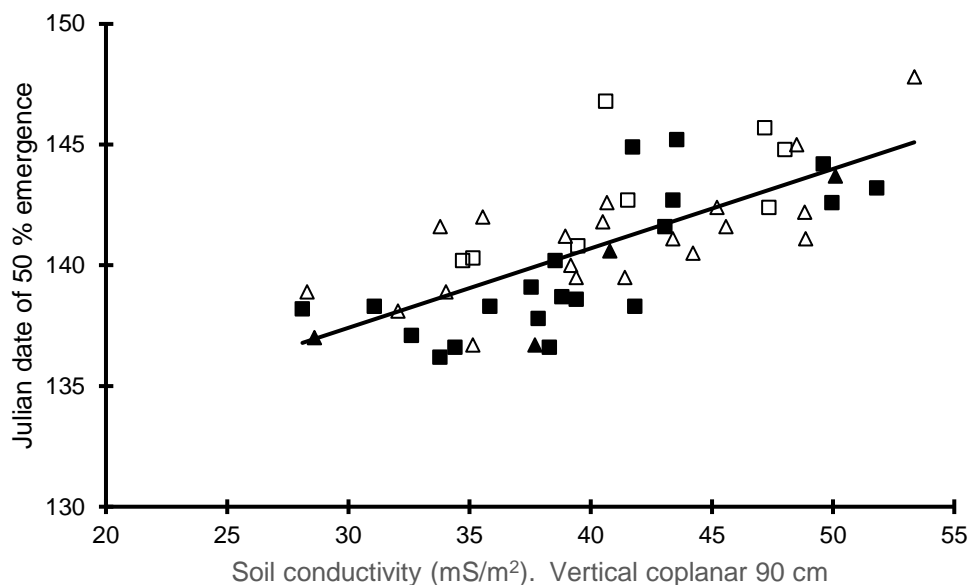
The effect of including electrical conductivity (vertical coplanar to 90 cm) as a covariate in the analysis of variance of key crop performance variates are summarised in Table 5. In general, the effect of including electrical conductivity data was of little benefit in the Light experiment. However, the covariate was statistically significant in the Heavy experiment for the interpretation of emergence and yield data from the early sampling. The absence of significance in the Light experiment, may be a consequence of the Light area being more uniform or the variation in soil texture was below a threshold that affected crop performance. It is also possible, that the block structure in the Light area was effective at removing the "error" due to variation in soil texture but this was not the case in the Heavy area. In hindsight, the direction of blocking may have been better at right angles to the direction used. The absence of any significant effect in the second sampling of the Heavy experiment may reflect that performance of an established crop is less dictated by soil texture.

Originally it was planned to take the EMI measurements at the start of the season shortly after the experiments were planted, but due to travel restrictions this was delayed for several months. The mid-October measurements were made in non-ideal conditions after the plots had been sampled and trafficked. Despite this, the initial analysis has demonstrated the potential usefulness of using high resolution EC scans to aid agronomic research. In particular, use of EC scans may help reduce residual error when experiments are analysed and scans done at the start of the season may help with designing effective blocking.

Table 5. Effect on statistical significance (*P* value) of treatments of including EC90 as a covariate (CV) and the statistical significance the covariate in the analysis of key variates in each treatment

	Light			Heavy		
	No CV	With CV	CV	No CV	With CV	CV
Julian date of emergence	< 0.001	< 0.001	0.584	0.115	0.034	< 0.001
Total tuber population at H1	< 0.001	< 0.001	0.154	< 0.001	< 0.001	0.259
Total tuber yield at H1	< 0.001	< 0.001	0.451	0.004	< 0.001	< 0.001
Tuber DM concentration at H1	< 0.001	< 0.001	0.646	< 0.001	< 0.001	< 0.001
Total N uptake at H1	< 0.001	< 0.001	0.266	< 0.001	< 0.001	< 0.001
Total tuber population at H2	< 0.001	< 0.001	0.004	< 0.001	< 0.001	0.687
Total tuber yield at H2	< 0.001	< 0.001	0.295	< 0.001	< 0.001	0.921
Tuber DM concentration at H2	< 0.001	< 0.001	0.208	< 0.001	< 0.001	0.232
Total N uptake at H2	< 0.001	< 0.001	0.326	< 0.001	< 0.001	0.348

4.3.4. Electromagnetic Induction Scans of contrasting soil textures 2021

The scanned areas are shown in Figure 1. The areas of increased conductivities (lighter colour) are associated with increased soil water contents which, in turn, are associated with larger clay contents. When compared with the scans from the 2020 Reference Crops, there was less variation in conductivity in 2021. However, Figure 1a shows areas of low and high conductivity in proximity c. half-way down the field. Ground truthing by digging soil pits showed that the heavy (darker) areas were nearly pure clay at depth, whilst the lighter areas had a very high stone content. The soils in the Reference Crop appeared relatively uniform in the upper soil horizons but adjustment of the scanning coils showed some variation at depth. This information was used to redesign the experiment so that the block-structure could take more account of this variation. Using the EMI data, the block structure was changed from four rows of blocks (as used in 2021) to 2 rows within 2 columns. Analysis of the date of 50 % plant emergence showed that this revised blocking structure removed a statistically significant amount of variation from the analysis of variance and helped improve the sensitivity of the experiment. The variation of soil properties over a range of scales is also illustration in the variogram shown in Figure 25.

Figure 24. Electromagnetic Induction scans of (a) NIAB CUF experimental area (c. 48 × 220 m, low-resolution scan). The dashed line represents the location of Reference Crop, and (b) Reference Crop experimental area (c. 21 × 72 m, high-resolution scan) at three different depths. The dashed perimeter in the low-resolution scan is location of high-resolution scans shown in (b).
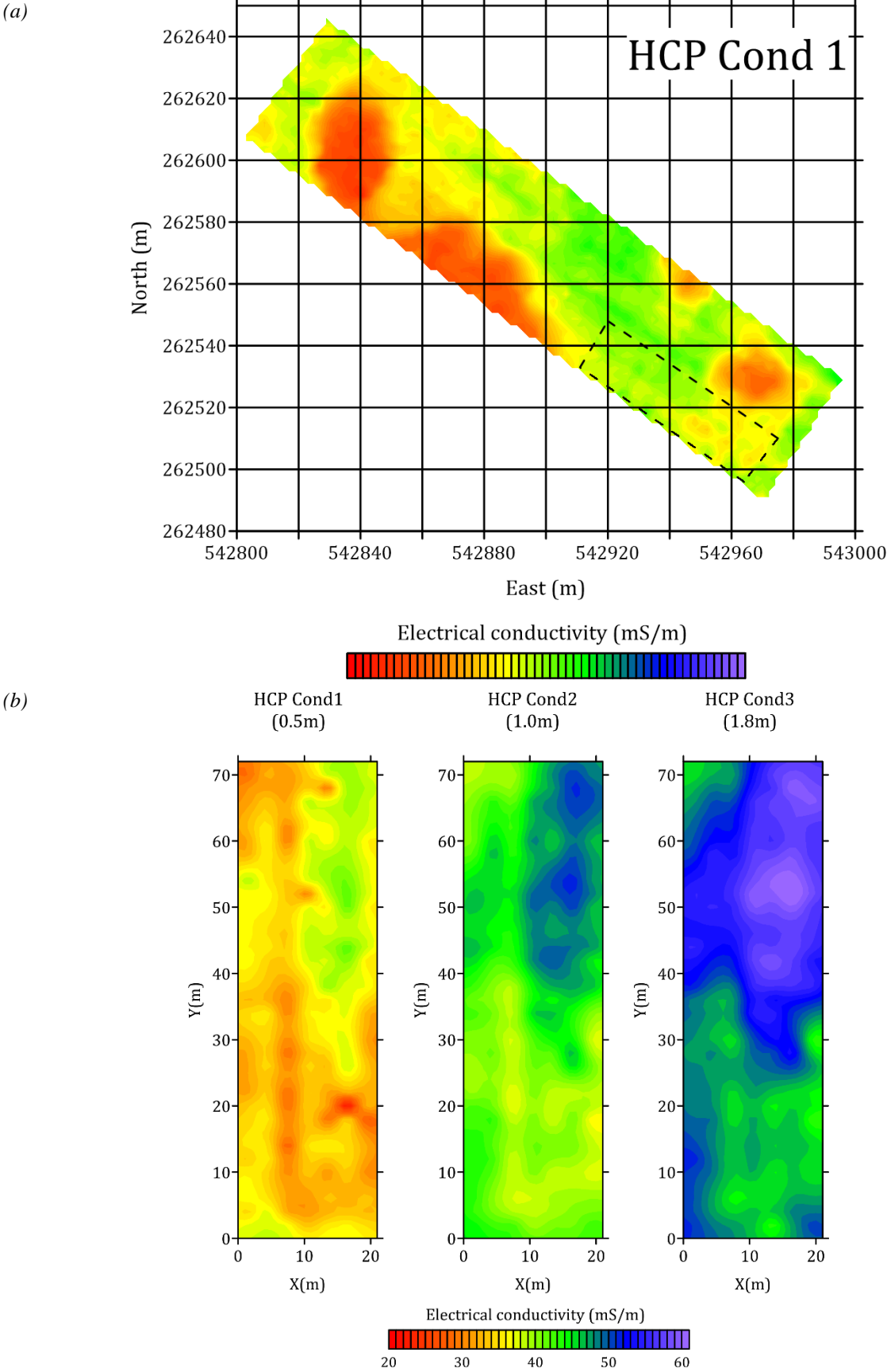
Figure 25. Variogram of electrical conductivity measurements. The measurements used are horizontal coplanar with a coil spacing of 1.15 (depth of investigation = 1.5m)
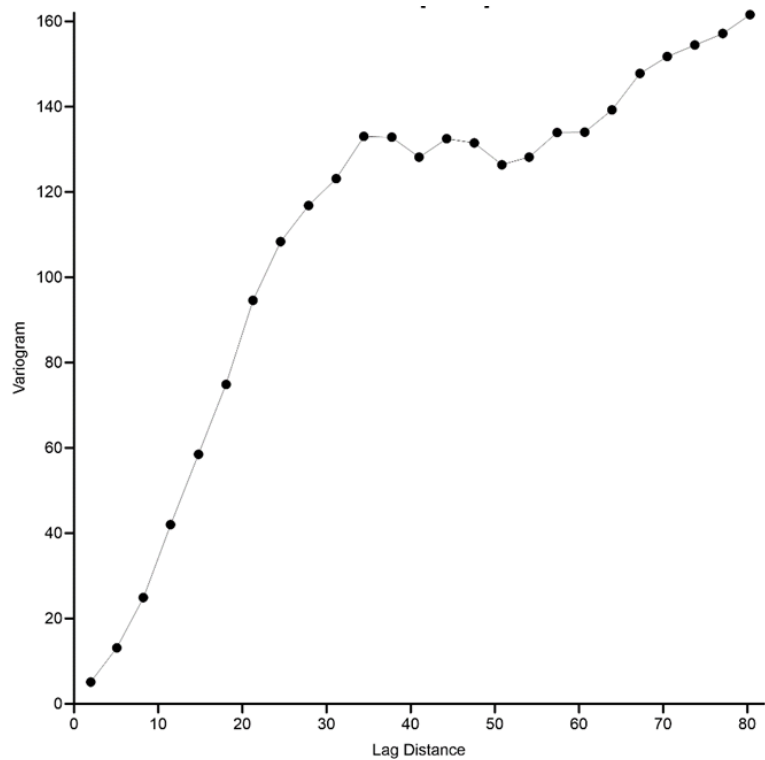
4.4. Conclusions.

Geophysical methods have demonstrated their usefulness in providing cost-effective ways of providing metrics of variation in soil texture which, in-turn, can be used to design more effective experiments. Furthermore, a better understanding of the causes of variation in potato crop emergence will be key in understanding the wider issue of spatial variation in potato crop performance and yield. This study has also provided useful insight into the effects of agronomic treatments (irrigation, organic amendments, and compaction) on water abstraction by potato crops. Apart from providing further insights into the link between soil conditions and crop performance, these techniques have wide applicability in phenotyping potato varieties to efficiently gather information on water capture.

5. PLOUGH DRAFT

Previous experimental work at Rothamsted had shown that variations in plough draft (a measure of soil strength) were inversely correlated with grain yield. It was hoped that use of the draft-sensing plough on potato fields would produce a map of the variation in soil strength which could then be correlated with spatial variation in potato yield. Unfortunately, one of the strain measuring steel pins was damaged in 2016 and was found to be beyond economic repair. Following discussions of this problem at a project review meeting on 29 March 2017 it was suggested that John Deere's GreenStar system may collect information (power-output, forward speed, wheel-slip and plough-depth) that could be combined to make a proxy for a direct measurement of plough draft. However, despite repeated attempts to access data held on Grower Platform farmers' tractors this idea also had to be abandoned.

6. FOURIER TRANSFORM INFRARED (FTIR) SCANNING OF SOIL TO QUANTIFY ORGANIC MATTER CONTENT

6.1. Introduction

Soil management strategies have significant effects on soil structure, soil chemistry and thus soil sustainability. It is therefore necessary to be able to track changes in soil status within rotations. While assessing soil physical status of soils in rotations through measurement of water release curves and penetrometer resistance, the work also aimed to assess the use of alternative methods that could be used to track soil status (i.e. FTIR and image analysis of soil images for soil structure). Fourier Transform Infrared (FTIR) Spectroscopy is a technique which uses infrared (IR) radiation to analyse samples and provide an overall chemical profile, or IR spectrum, of the sample (see example in Figure 26). The IR radiation is absorbed by the sample at specific frequencies depending on the chemical composition of the sample. It is an ideal method for characterisation of soil as, importantly, it can simultaneously provide information on both the organic and mineral components of the soil. Qualitative analysis, through interpretation of the IR spectrum of a soil sample, allows an instant insight into the mineralogy of the soil, including nature and relative proportion of clay minerals present. In addition, the IR spectrum provides a rapid assessment of the relative amount and nature of the organic matter present.

Figure 26. Example of an infra-red spectrum of a mineral soil.
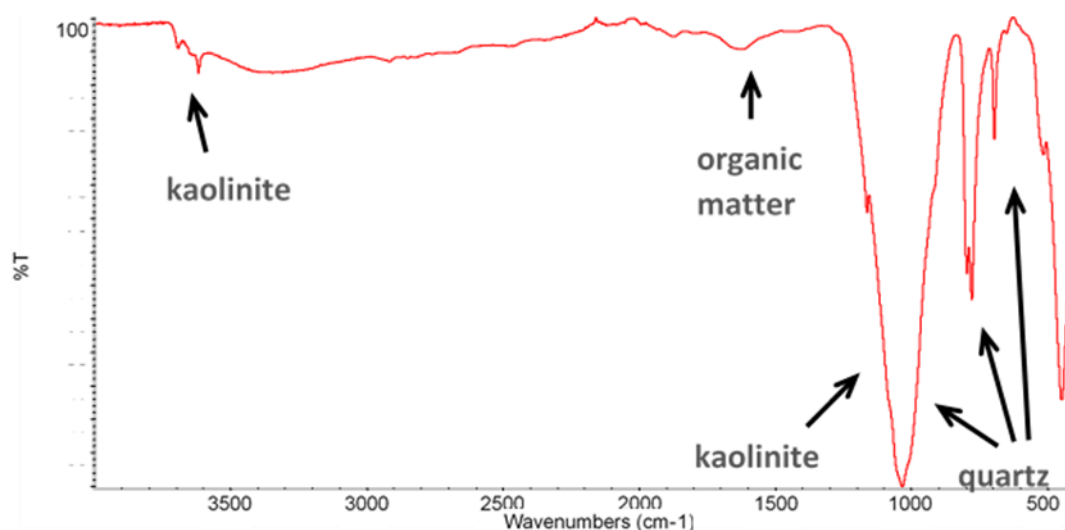
For highly organic soils, patterns are seen in the IR spectrum which relate to the undecomposed vegetation, differing due to plant population, and degree of decomposition. The chemical functional groups present in the soil and the degree of humification of the organic matter can be determined. For arable soils with lower organic matter content the patterns due to the soil organic matter (SOM) are generally weaker and less distinct in the bulk soil but can still provide useful information. In addition to qualitative analysis, quantitative analysis of soil using FTIR spectroscopy is possible. Statistical correlations between the FTIR spectra and measured soil properties create calibration models which can then be used to predict multiple parameters for a soil sample from a single spectrum (e.g. %C, %N, pH, and bulk density). FTIR analysis provides a means for accurate prediction of soil organic carbon (SOC) as has been illustrated for a national dataset of Scottish soils (Haghi *et al.* 2021).

6.2. Material and Methods

6.2.1.   Datasets

All the datasets used in the FTIR analysis were existing or historical trial plots from the James Hutton Institute, Rothamsted and NIAB farms, some of which were being used for other studies within this project.

6.2.1.1.   *Cover Crops (Binns Field, Balruddery farm, The James Hutton Institute)*

For the study of the variation in SOM through a rotation, soils were analysed as part of a study to investigate whether cover crops could be established and to quantify the effects of such crops on soil conditions at the Balruddery farm of the James Hutton Institute (Holland *et al.* 2021). Details of this experiment may also be found in the report for the 'Grower Platform,' Project 9114000101. There are several possible effects that cover crops could have on soil conditions that are of interest to farmers. These include changes to the soil water status, the resistance of the soil to erosion, and changes to the soil biology and chemistry, and the consequences and benefits for subsequent cereal crops. The FTIR analysis was conducted to assess any changes in SOM over the rotation and between the different treatments.

A replicated trial was designed with a control of stubble from the previous barley crop remaining on the soil surface and 7 treatments. The treatments were different cover crops as follows:

- 1 Control,
- 2 Jupiter Turnip rape sown at 12 kg/ ha
- 3 Kings Structure mix sown at 25 kg/ha
- 4 Defender Oil Radish at 20 kg/ha
- 5 Radish Mix 15 at 20 kg/ha
- 6 Vitality Mix at 25 kg/ha
- 7 Vetch and Rye at 40 kg/ha
- 8 EFA Mix 1 at 20 kg/ha

The Control and treatments were all replicated 3 times in a randomised block design i.e., there are 3 blocks. Sowing was in strip 6 m wide and approximately 200 m long. FTIR analysis was conducted for 2 growing seasons - 2017 and 2018. In total, 72 soil samples were analysed for each year (3 replicates x 8 treatments x upper, middle, and lower field)

6.2.1.2.   *Rothamsted Long term historical plots*

Characterisation of soil, including the nature of organic matter (SOM), on selected plots of the Broadbalk and Hoosfield long-term experiments at Rothamsted was conducted. Variation in two different series of soils which have undergone long-term addition of FYM over time was compared with corresponding soils which have had long term N, P, K and Mg addition, and an unfertilised control. For each experimental plot, 8 time points over ~150 years were selected for the FYM, N,P,K and Mg and control treatments (48 samples in total). The Broadbalk plot was under continuous wheat and the plots selected for analysis were Section 1 -FYM addition (Plot 2.2), N,P,K and Mg addition (Plot 8) and Nil addition (Plot 3). Samples were taken from years 1865, 1893, 1904, 1914, 1944, 1987, 2000, 2015. The Hoosfield plot was under continuous

barley and the plots selected for analysis were Series A, FYM (Plot 72), N,P,K and Mg (Plot 42) and Nil addition (Plot 11). Samples were taken from years 1889, 1904, 1913, 1946, 1975, 1998, 2008, 2018.

6.2.1.3. Broom's Barn medium term trial plot, NIAB

Full details of this experiment may also be found in the report for WP1 Grower Platform (9114000101). In summary, the experiment was started in the mid 1960's and assessed a three-course rotation of two cereals and then sugar beet, with FYM addition every 3 years prior to the beet crop. FYM was added to plots S & T immediately before the beet crop, but plots N & P received none. The last FYM application was in 2012, after which the experiment reverted to standard cropping. The plots were relocated in autumn 2016, and fresh FYM applied to either the E or W half of the original trial plots. Potatoes were grown in 2017, spring barley in 2018, winter wheat in 2019 and winter wheat in 2020. The plots were sampled for this study in 2020. FTIR spectra were recorded of 48 samples after drying, sieving, and milling and the samples selected are highlighted in the Broom's Barn plot plan (Figure 27).

Figure 27. Broom's Barn plot plan - The letters N, P, S, T denote historical treatment of the plot

Treat	N	P	K	Na	FYM
N	1	1	1	1	0
P	1	2	2	1	0
S	1	1	1	1	FYM
T	1	2	2	1	FYM

6.2.1.4. Elveden medium term trial plot, from the Lodge Warren Organic Manure Trial, NIAB

This trial started in 1999 and a comparison was made in this study between the no muck and the treatment in which 35t/ha of FYM had been added for 13 of the last 20 years (10 years continuously) at the Shakers Road end. The plan of the experimental plot is shown in Figure 28. Again, this was a medium-term study in which there was variation by treatment, but no time points. FTIR analysis was conducted of 20 samples comprising 10 replicates from the 2 treatments, taken over 200m.

Figure 28. Plot plan for the Lodge Warren Organic Manure Trial, Elveden

6.2.1.5. Grieves house tillage trial, Balruddery farm, James Hutton Institute

This plot comprises two types of tillage x winter or spring rotations i.e., 4 main management treatments, fully replicated (4 times) across the field (16 main blocks). Each Tillage x Rotation contains 4 strips so that each block has 4 years of cropping (forming the within treatment rotations – totalling 64 strips). Over the past 3 years each of the 64 strips have been sampled once or twice a year. FTIR analysis was conducted of 64 samples from the latest sampling date in 2020. Ideally comparison would have been made with a set of samples from an earlier date but, largely due to the COVID-19 situation, there was insufficient time available to complete this.

6.2.2. FTIR Spectroscopic Analysis

Samples for FTIR analysis were dried, sieved and finely milled, using a Retsch mill, prior to analysis to ensure representative and reproducible spectra were obtained. Where possible, they were subsequently milled using a McCrone mill and reanalysed. This milling method is more time consuming but has been shown to give the best quality spectra (Robertson *et al.*, 2013).

FTIR spectra were recorded on a Bruker Vertex 70 FTIR spectrometer (Bruker, Ettlingen, Germany) fitted with a potassium bromide beam splitter and a deutroglycine sulphate detector. A Diamond Attenuated Total Reflectance (DATR) sampling accessory, with a single reflectance system, was used to produce "transmission-like" spectra. Samples were placed directly on a DATR/KRS-5 crystal, and a flat tip powder press was used to achieve even distribution and contact. Spectra were acquired by averaging 64 scans at 4 cm-1 resolution over the range 4000 – 370 cm-1. A correction was made to the ATR spectra to allow for differences in depth of beam penetration at different wavelengths, using OPUS software (Bruker, Ettlingen, Germany, version 7.0). The spectra were also baseline corrected, using the OPUS software Automatic Baseline Correction and a rubber band correction method on 64 baseline points. No correction was required for water vapour and CO_2 as the spectrometer is continuously flushed with dry air.

Following FTIR analysis it was evident that some of the samples contained calcium carbonate, which was obscuring part of the spectrum relevant to the SOM. It was decided to try removal of the carbonate in a proportion of the affected samples, and then re-recording the spectra to allow the SOM region of the spectra to be more clearly seen. The procedure to remove the carbonate involved sodium acetate dissolution, using a 1M sodium acetate solution, buffered to pH 5. A small portion of each sample was placed in an individual beaker with 200 ml of the acetate solution and heated on a hotplate at 100 °C for 6 hours, after which time the bubbling of CO_2 had ceased. Fresh solution was added to the beakers at this point, but there appeared to be little additional reaction. Each sample was then warm water washed, two or three times, to remove the acetate and the samples were then dried prior to recording of the FTIR spectra.

Statistical analysis of the FTIR data was conducted using Unscrambler X software (CAMO, Norway).

6.3. Results

6.3.1. FTIR Analysis of Cover Crop Soils at Binns Field, Balruddery farm, The James Hutton Institute)

FTIR spectral analysis of the cover crop samples for the 2017 growing season showed the control samples (no cover crops), and some of the species' treatments, have very consistent spectra with some but not a lot of SOM evident (it is a soil with some kaolinite clearly visible). However, for some species/mixtures there were spectra which show greater proportions of SOM in some samples. An example of the set of FTIR spectra for the Jupiter Turnip Rape is shown in Figure 29.

Figure 29. FTIR Spectra of Species 2 Jupiter Turnip Rape.
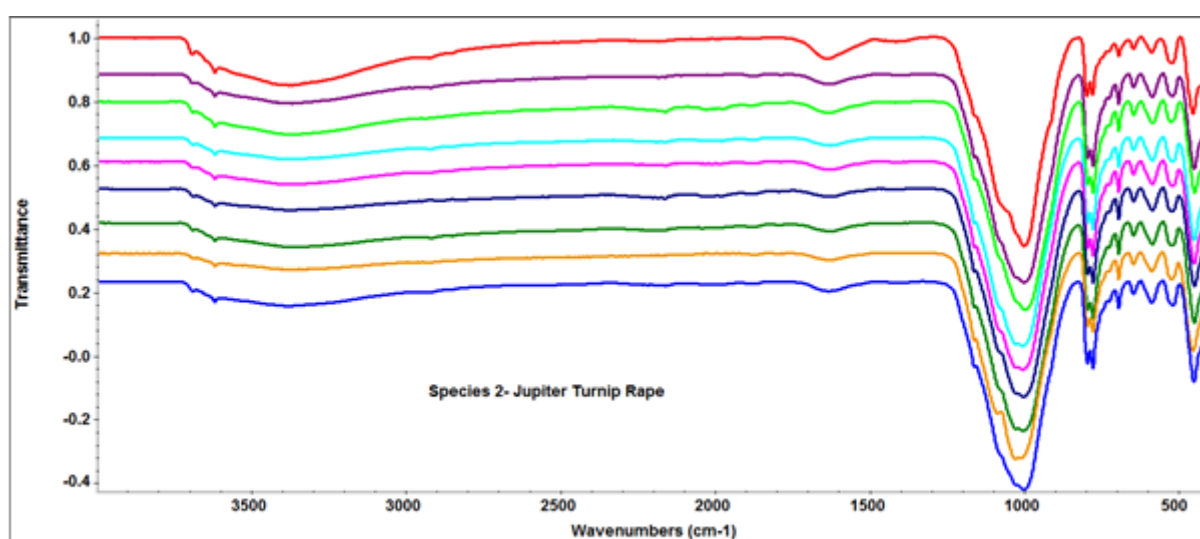
Figure FTIR_3 - FTIR Spectra of Species 2 Jupiter Turnip Rape

The top IR spectrum (in red) has a more intense band close to 1600 cm-1 than the others in the group indicating the presence of a higher proportion of SOM. This was confirmed by the lab analysis of the %C for this sample, which was 5.1%. The results for the %C analysis of the samples showed that the %C value for most of the samples was between 3-4% and the %N s ~0.3%. Overall, the Average %C (averaged over all the samples for a particular species) is lowest, at 3.40%, for the control samples and highest, at 3.73%, for species 8 (EFA mix). However, this high value for species 8 is skewed by a large value of 6.69% for the Upper 3 sample (Figure 30). It does appear that the Upper 3 samples generally have high %C values for the cover crops, despite the control value being relatively low (3.2%). Species 2, the Jupiter Turnip Rape had the second highest average % C value (3.67), and values for each sample appear more consistently high than for species 8, although there is still the value already mentioned (Upper 3) at 5.1% which may slightly skew the result. This is of interest as it was one of the treatments which showed an increased yield (Holland *et al.* 2021) in barley.

Figure 30. Percentage C Results for the 2017 samples for each treatment 1 Control, 2 Jupiter Turnip rape, 3 Kings Structure mix, 4 Defender Oil Radish, 5 Radish Mix, 6 Vitality Mix, 7 Vetch and Rye, and 8 EFA Mix 1.
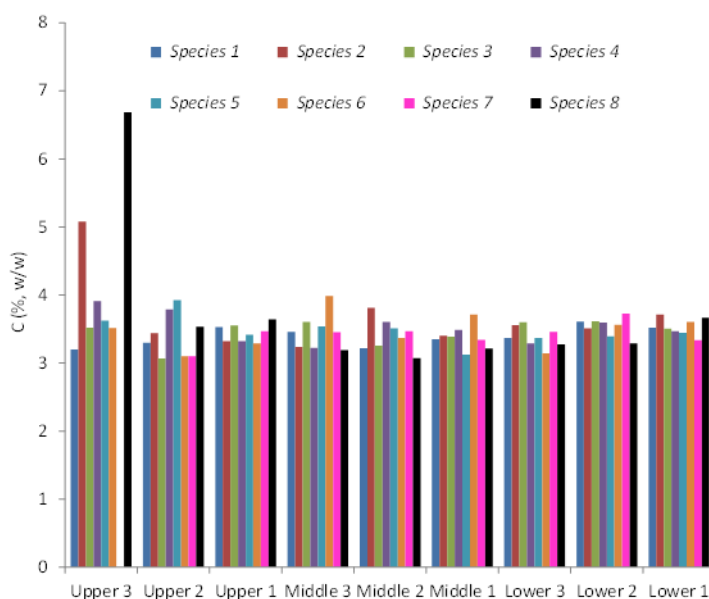
Although any differences in %C observed between treatments were not necessarily statistically significant, good correlations between the IR spectra and the %C values were obtained, as summarised in Table 6 and illustrated in Figure 31.

Table 6.   Results for Carbon

Constituent	RMSECV (%, w/w)	R^2	Bias (%,w/w)	RPD
%C	0.61	0.83	0.003	1.61

Figure 31. Measured vs. predicted C% for the 2017 calibration set
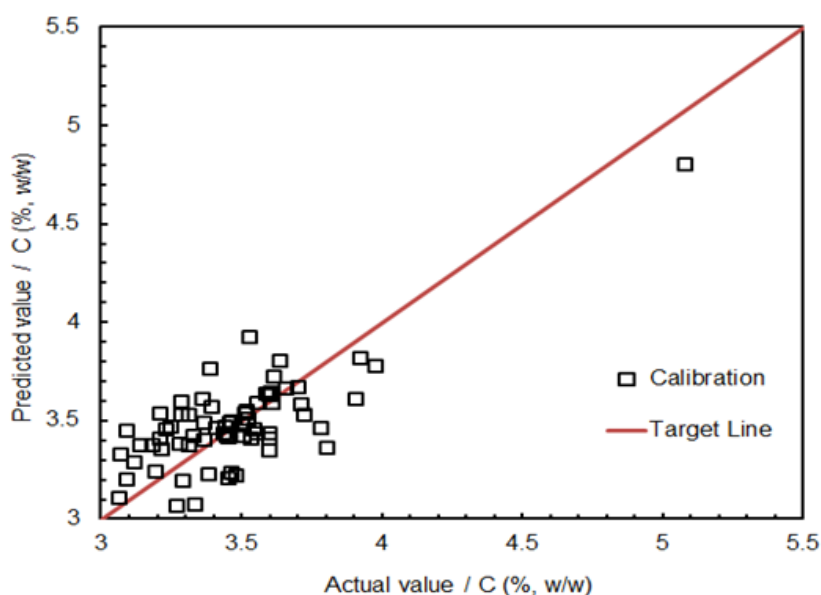
FTIR spectral analysis of the 2018 samples showed the spectra, and % C values, to be broadly similar to those of 2017. However, none of the 2018 samples showed the significantly higher SOM (%C >5) seen in a few 2017 samples and this is likely to be due to very different growing seasons, with the cover crops not establishing nearly as well in the 2018 growing season. The SOM bands in the FTIR spectra also closely correlate to the %C results (predominantly between 3 - 4% C) for the 2018 samples.

6.3.2. FTIR spectroscopic characterisation of Rothamsted long term historical plots, Hoosfield (continuous barley) and Broadbalk (continuous wheat)

FTIR analysis was conducted on three versions of these samples, the Retsch milled, McCrone milled and McCrone milled after carbonate removal. The IR spectra of samples from both the Hoosfield plot and the Broadbalk plot showed subtle but evident differences between treatments and for the same treatment on different sampling dates. Figure FTIR_6 shows that, for the 1889 sampling of the Hoosfield plot, there was carbonate present in samples from each of the treatments, with the most evident in the spectrum of the nil treatment and the least (only just detectable) in that of the NPKMg treatment. However, by the 2008 sampling, no carbonate was detectable in the spectra of any of the treatments but the IR spectrum of the FYM addition showed the presence of a greater proportion of SOM.

Figure 32. Hoosfield Barley – IR Spectra for the three treatments in 1889 and 2008
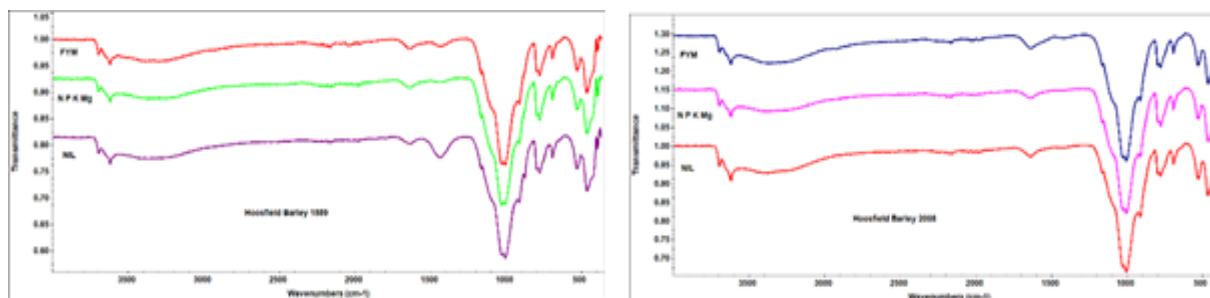
Figure 33 *shows that, for the 1893 sampling of the Broadbalk plot, there was also carbonate present in samples* from each of the treatments, but in this case proportions in the spectra of the nil treatment and that of the FYM addition was very similar, and more than in the "corresponding" Hoosfield spectra, with less in that of the N, P, K and Mg treatment.

Figure 33. Hoosfield Barley – IR Spectra for the three treatments in 1893 and 2000.
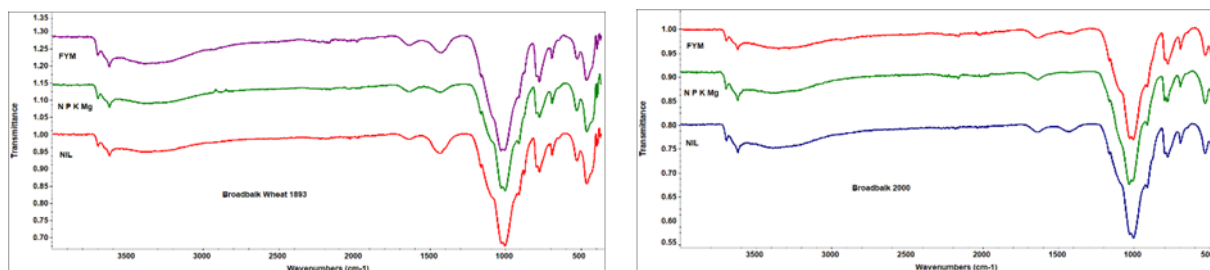
By the 2000 sampling, the proportions of carbonate in the IR spectra of all treatments had reduced but was only not detectable in the IR spectrum of the NPKMg treatment. It did appear that there was a greater proportion of SOM in the spectrum of the FYM addition.

A range of statistical analysis was conducted on the spectra from this trial. Good correlations were found between the spectral data and %C values, especially given the small numbers in the dataset and the lack of certainty as to how closely the soil samples analysed by FTIR related to those analysed by wet chemistry, and the potential lab measurement errors. The best results appeared to be for the McCrone milled Hoosfield data and Broadbalk data, individually, using the full spectral range (Figure 34).

Figure 34. Predicted versus Reference %C for Hoosfield (Top) and Broadbalk (Bottom)
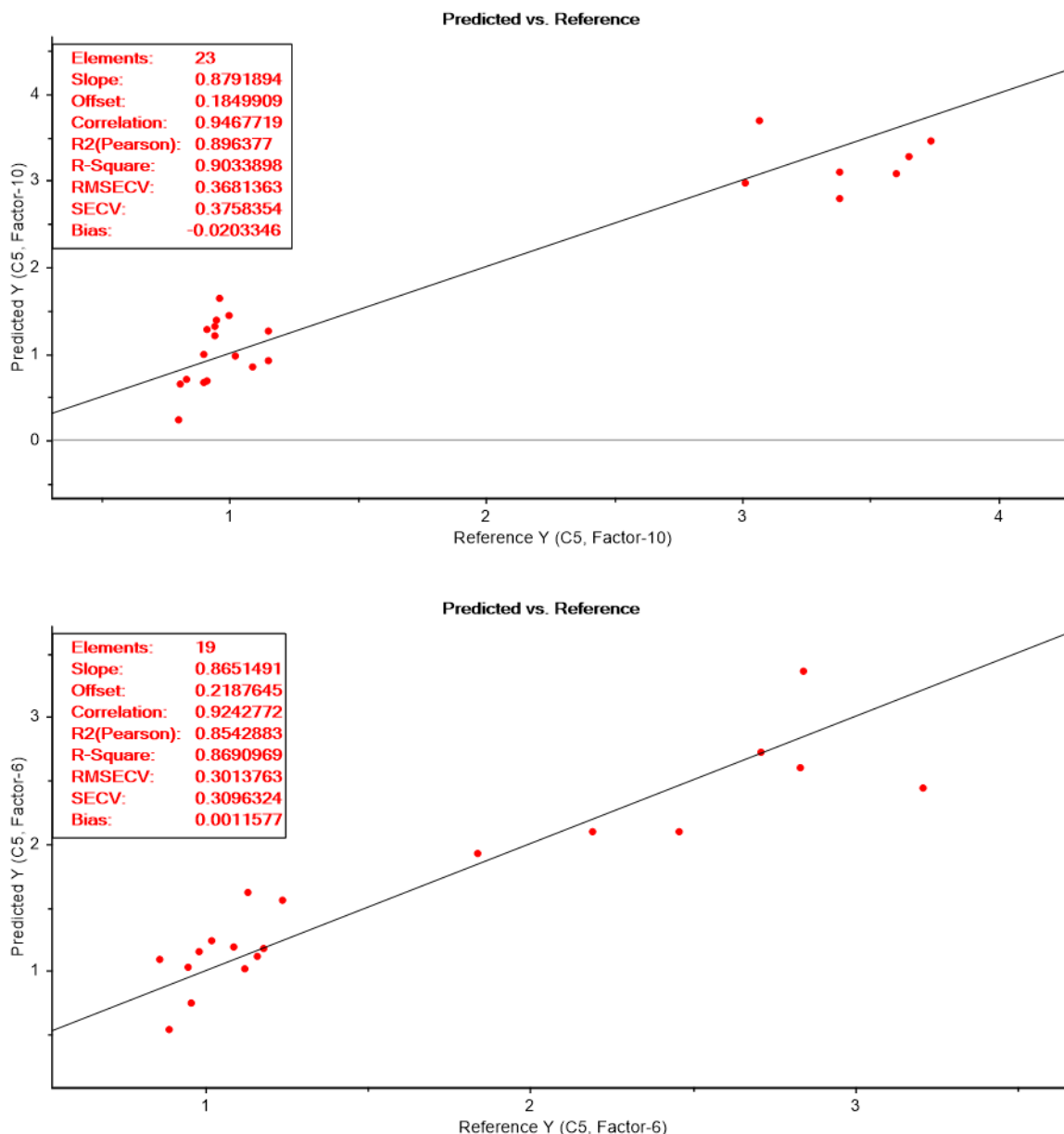
Other statistical analysis looked at correlating the soil spectra to yields of grain and barley. Although the correlations using the IR spectra of the McCrone milled samples were poor, those using the Retsch milled samples were much more promising and suggest this is worth pursuing with bigger datasets. In addition, PCA analysis of various groups of the spectra were completed.

For example, using the range between 1750-1500 cm-1 (which relates to the SOM components present), for the McCrone milled Hoosfield samples, see Figure 35.

Figure 35. PCA Analysis for the Hoosfield Samples, using the spectral range between 1750-1500 cm-1 with treatment 1 – nil, treatment 4 - N,P,K,Mg, treatment 7 – FYM.
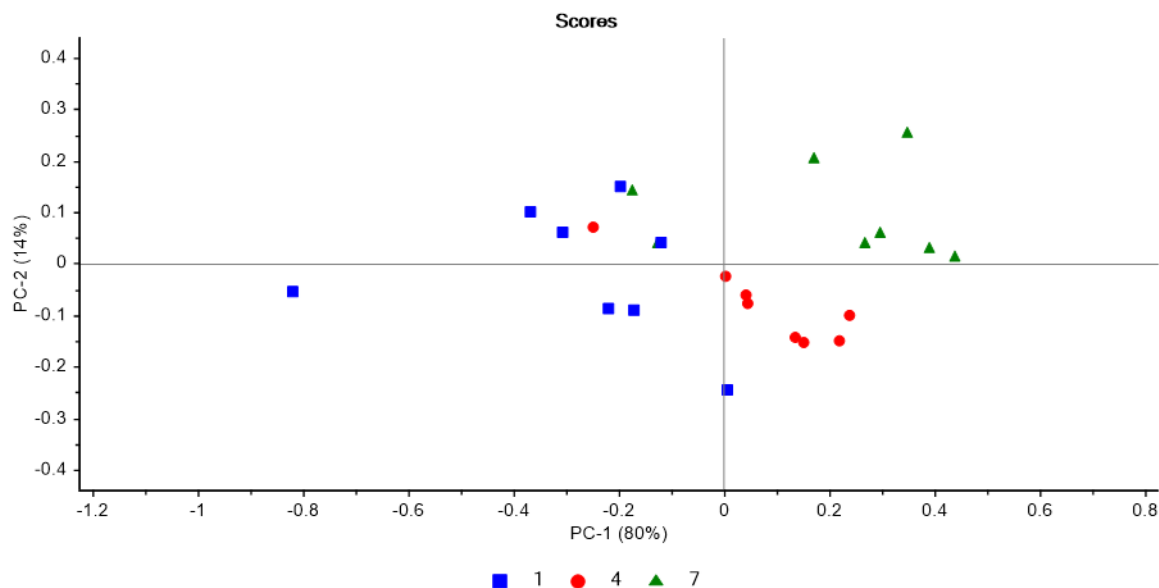
Using the full spectral range, for the Hoosfield McCrone milled samples, the FYM addition (7) and Nil addition (1) groups could be largely separated out, but did overlap to some extent with the N,P,K and Mg group (4). It seems that N,P,K and Mg group lies more with the FYM addition but does overlap both other treatments. However, when the more limited range of 1750 -1500 cm-1 is used (Figure 35), the FYM addition group can be almost completely separated from the other two, and there is also limited overlap between them.

6.3.3.   FTIR Analysis of Broom's Barn Soil Samples

Visually the differences in the IR spectra of this set of samples appeared very small, with spectra being mineral soils with relatively small amounts of SOM and no detectable carbonate present. A PCA statistical analysis was used to explore whether the spectra from the different treatments, over the whole spectral range, could be discriminated. It is shown in Figure 36, below. The patterns in the PCA are complex but there are some groupings evident, indicating the treatments were influencing the overall chemical profile of the soil. Further investigation would be required to understand the changes more fully.

Figure 36. PCA Analysis of the Broom's Barn Samples.
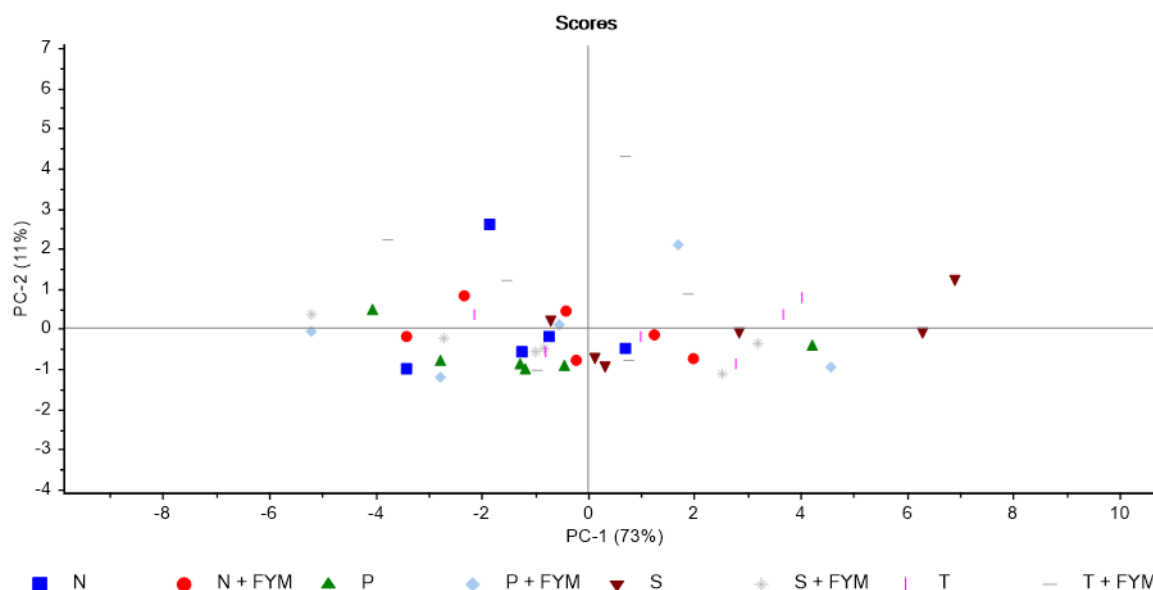
6.3.3.1.   *FTIR Analysis of the Lodge Warren Organic Manure Trial Samples*

The IR spectra in the control group show that all have appreciable carbonate present, in addition to the silicate minerals, with the proportion of carbonate varying considerably between the replicates taken over the 200m. The carbonate present appears to be essentially calcite (calcium carbonate) with evidence in a few samples for the presence of trace amounts of dolomite (calcium magnesium carbonate). Organic matter can be detected but some of the bands are obscured by those of the carbonate – particularly in the CH region.

The IR spectra in the organic trial group also show a high proportion of carbonate present with the proportion again variable but appearing to be higher on average than in the control samples (in one sample the bands from the carbonate are stronger than that of the silicate minerals). As variability in carbonate between replicates, along the field, is detected it cannot be excluded that there is a natural variation in the carbonate concentration of the soil across the field, between the two treatment strips. However, the variation could also be related to the FYM additions, either directly through addition of carbonate or indirectly by maintaining carbonate already there.

Removal of the carbonate was successfully completed for a subset of samples and bands attributable to SOM are much more clearly seen, with an appreciable amount of organic matter in the trial samples (Figure 37). The IR spectra of the samples, with the carbonate removed, allow us to detect the presence of features of the SOM including ester, protein, and lignin functional groups (1735, 1540 and 1518 cm-1). A PCA analysis, for spectra over the whole spectral range, shown in Figure 38, compares the IR spectra of the no muck and 35t/ha of FYM treatments. Although there is some overlap in the points does show that the two groups can be largely discriminated

Figure 37. Comparison of the spectra of an OM Trial sample before and after carbonate removal.
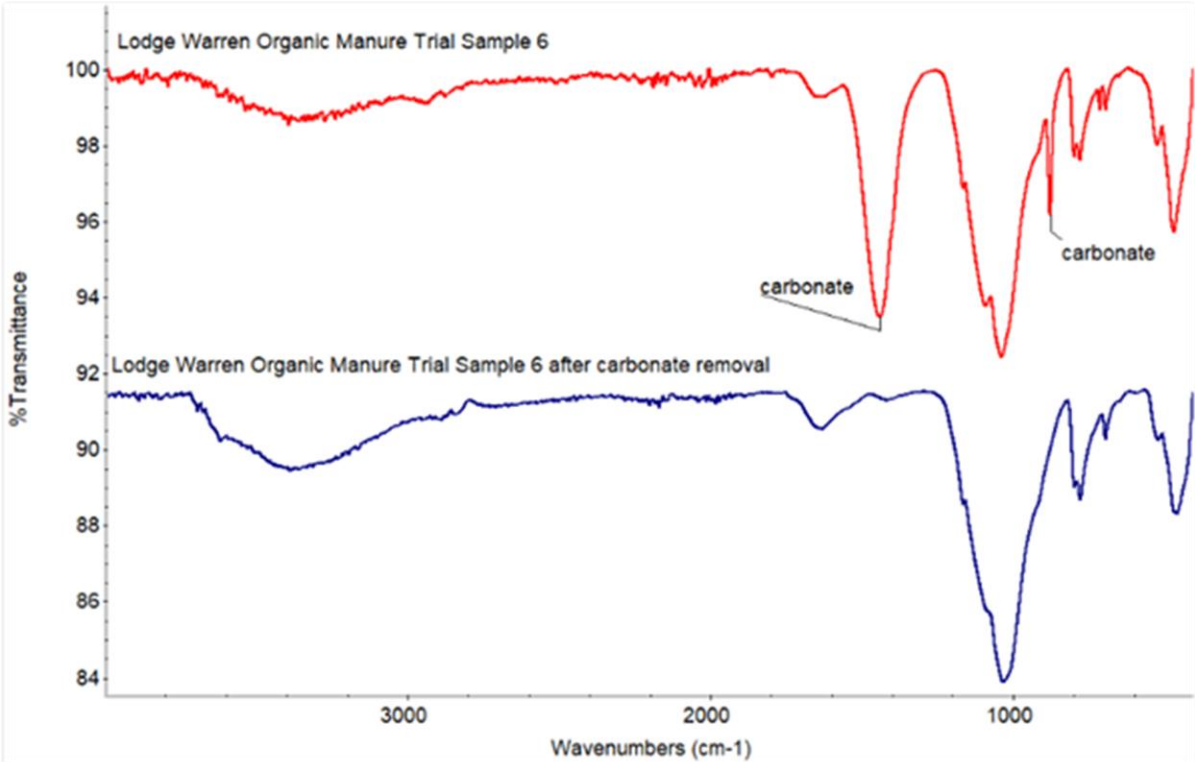
Figure 38. Analysis of the Lodge Warren Organic Manure Trial Samples
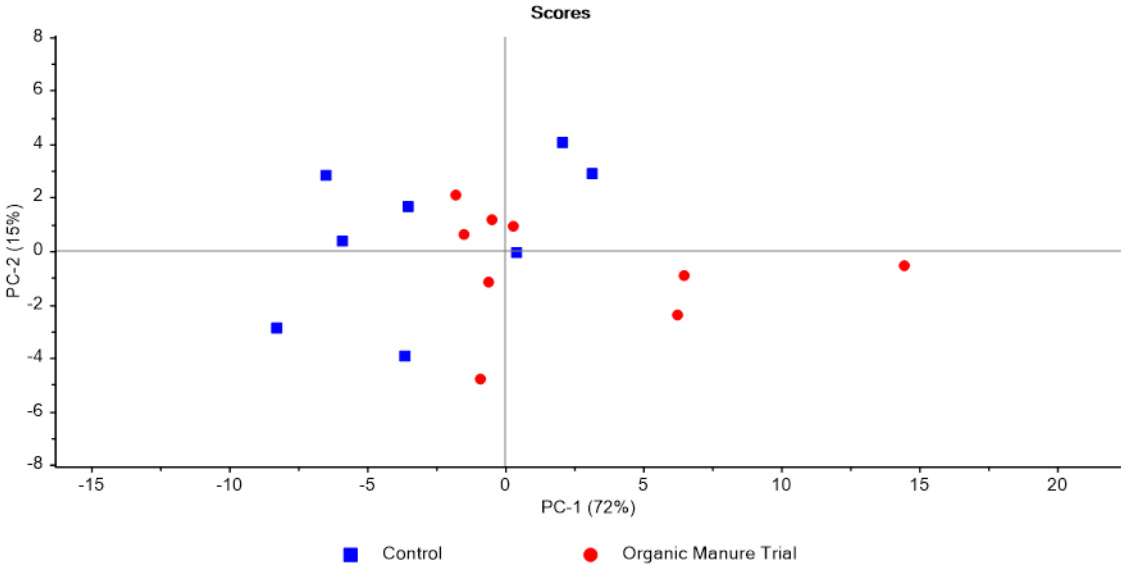
6.4. Discussion

This study set out to assess if FTIR spectroscopic analysis could be used to study variation in SOM through a rotation, including evaluating the measurement of %SOC measurement on a field scale. In the case of the cover crop trial, where there is increased SOM in the soil it can be detected using the FTIR spectroscopic analysis and the nature of it, such as whether there is increased protein present can be assessed. Calibrations developed on a field scale have been demonstrated to give accurate predictions of SOC, particularly when compared with the error for wet chemistry measurement, and overall, the FTIR spectroscopic method is a powerful tool for assessing soil C.

The influence of organic matter amendments e.g., farmyard manure (FYM) on the soil using FTIR spectroscopic analysis was also investigated. The results show that the FTIR method can provide real insight into the effect of management practices on the soil, including revealing some unexpected changes which may not have been readily picked up in any other way. The technique proved extremely useful in assessing the effect of different treatments and providing information on which components were varying. In addition, the spatial variability of soil across a field site for a single treatment could readily be assessed. This included the potential influence of variation in mineralogy as well as OM.

Preliminary investigation of correlations between the soil spectra and grain and straw yield for the Rothamsted long term historical plots gave some promising results and would be worth further study with larger and more current datasets.

6.5. Conclusions

- Interpretation of FTIR spectra of amended soil can provide valuable information on the changes in the amount and chemical composition of the SOM.

- Results show accurate prediction of %SOC are possible on a field scale using FTIR

- FTIR is a novel method for characterising soil which can rapidly assess variation in soil across a field, providing insight not otherwise available

- FTIR soil characterisation would give more accurate zoning of soil across a field and could be recommended prior to field trials being set up

- The potential for correlating crop yields directly to soil spectra has been shown

7. USE OF FLAT-BED SCANNERS TO UNDERSTAND ROOTING IN SOILS

7.1. Introduction

Soil structure plays a significant role in determining root elongation rates, in terms of inhibiting root growth due to soil strength (from a combination of dry bulk density and water status), available oxygen (linked to pore space and water content), and water availability (linked to water content and pores space distribution). Soil pore structure influences water flow through soil, and root elongation rates, though avoidance of soil compaction (by roots goring through pores), and by influencing water and oxygen availability to roots. To establish measurements of pores structure methods employed include X-ray Computed Tomography (CT), calculation of pore space bands from water release curves, and embedding fluorescent wax in soil pores followed by imaging and image analysis. Each of these methods has benefits, however they can be expensive and time consuming (e.g. X-ray CT), take several months to complete (water release curves), or are limited to larger pores space sizes. Cheap high resolution flatbed scanner can scan at a resolution of 1200 dpi (or 480 dp cm-1), and therefore have the potential to image pore sizes of 20µm in diameter or smaller with interpolation between pixels. These scanners produce a single high resolution which can be split into three images (red, green and blue), however colour variation in narrower bands can be accessed through multispectral cameras. Images from these cameras while often lower resolution can potentially as a combined dataset correlate to soil properties. Multispectral imaging has previously mainly been used in terms of remote sensing using satellite or drone imagery. However, here it is proposed that soils are evaluated at a scale relevant to the interaction of plant roots and soil. Root elongation at the early stages of crop development can be significantly impeded in soil with high bulk density, but differences in pore structure between soils of the same density can alleviate or worsen the effects of soil strength (Valentine et al., 2012). Once a crop is established, unless roots continue to elongate, the size of the root system will affect access to water depending on the relationship between soil water pools and root soil contact. The exact relationship between ability to elongate in drying hard soils and the root soil contact, will thus depend on differential root traits (e.g. root diameter) that vary significantly within and between cereals and root crops such as potato and carrot/parsnips but also on the pore structure of the soil developed due to underlying soil properties and the management used. Previously work with barley, has shown the influences of soil strength and pores size distribution on root elongation and had shown significant reduction in root elongation in soils both across the landscape scale in Scotland, and in soil cores taken from different tillage systems, within field trials across the UK (McKenzie *et al.*, 2017; Valentine et al., 2012. This project therefore aimed at assessing the initial root growth characteristics of carrot and parsnip roots, in structured soil. This required the initial assessment of root growth under controlled mono conditions, the development of a soil-based root elongation assay, followed by testing of root elongations under heterogenous structured soil conditions, all under controlled water conditions.

7.2. Materials and Method

Intact soil cores were sampled from: 1) Grieves House Tillage Platform (GHTP); 2) the Centre for Integrated Cropping (CSC); 3) Lodge Warren (LW); 4) Brooms Barn (BB); 5) and Oxnead (On). Table_SS_Methods_1 gives an overview of the field trials used in this section of the report. Usually cores consisted of two 5cm high x 5cm diameter plumbing pipe taped together with duct tape to form a 10cm high cores. For sites 3-5 two metal cores (4 cm high x 5.5 diameter) taped together forming an 8 cm x 5.5 diameter core) were used. Sites were sampled depending on the site experimental plan and treatments given in Table 7. At each individual sampling site

within a Trial, both an intact soil core and loose soil was taken. Loose soil was sieved to <2mm and repacked at a dry bulk density of 1.25gcm-3 into cores 5cm high for CSC & GH and double height cores for all NIAB site cores. Where necessary for validation or comparison soil cores, were saturated and taken through partial water release curves. Finally, the matric potential of cores was adjusted to -50kPa. If cores were double height cores, the duct-tape was removed from the outside of the cores, and the cores were broken by pulling the core apart allowing the soil to fracture according to the soil structure, without sheer movement.

Table 7.   Table SS_Methods_1 : Sites sampled for example datasets

Trial Site	Abbreviation	Brief site description
Grieves House Tillage Platform	GHTP	Four replicates of factorial combination of two tillage (inversion plough to 20 cm) and two rotations (including 4 cropping years). https://www.arablescotland.org.uk/virtual-tours
Centre for Integrated Cropping	CSC	Six split fields, half Integrated cropping (including direct drill), half conventional cropping (including inversion tillage, mineral nutrition, standard pesticide). Fields are under a six-year rotation. https://www.arablescotland.org.uk/virtual-tours https://csc.hutton.ac.uk/
Lodge Warren	LW	Organic amendments compared with control. See FTIR section
Brooms Barn	BB	Factorial comparison of historic and recent additions of FYM. See FTIR section
Oxnead	On	Organic amendment compared with control.

7.2.1.   Soil imaging

For imaging of soil samples in metal cores, the cores were covered with a ring template cut out of paper to give a "white" exposed surface, over the ring. For plumbing pipe soil cores the cores were imaged as is. For high resolution RGB images the exposed surface of the soil cores were imaged using a flatbed scanner (Cano Canoscan 9000F Mark II) turned upside down and placed so that it was approximately 5mm from the soil surface, but not touching the surface. This scanner has a depth of field focus of approximately 1cm). Images were taken at 1200dpi and stored as uncompressed TIFF. For multispectral images two Ximea cameras (https://www.ximea.com/en/usb3-vision-camera/hyperspectral-usb3-cameras-mini) VIS (400nm-600nm)nm) and a VIS-NIR (600-975 nm) were used without filters. The soil core surface was illuminated using white LED lamps from two sides of the core. The cameras produce mosaiced images, which once split into waveband channels comprise of 16 wavebands x 512 x 272 pixels images (VIS) or 25 wavebands x 409 × 217 pixels images (VIS – NIR).

7.2.2.   Image Analysis

All image analysis was performed in RStudio running R. Figure 39 illustrates the sequence of processes involved for RGB images and Figure 42 illustrates the process for multispectral images. For multispectral images, the images are initially de-mosaiced such that there are 16 or 25 separate images corresponding to each camera wavelength. RGB images were separated into the 3 wavelengths. The soil area of the image is extracted based on the position of the soil core and a contour map followed by polygonization was used to obtained areas of the soil designated as "pores/structures," edge correction was added to the analysis for multispectral dataset analysis. This corrected for areas where contour lines were connected to the edge of the soil core. For each initial set of pores/structures the area and perimeter were calculated, and then for each dataset the total, mean, standard deviation, skew and kurtosis of the distribution of the area and perimeter values was calculated.

7.2.3.   Statistical Analysis

All statistical analysis was performed in Rstudio running R. For each of the soil images the profile of the histogram of pore/features sizes was analysed to produce descriptive statistics. These were not of features in total ("Features"), the area of the image assigned to features / pores ("Total_Area"), the total length of the perimeters of the features ("Total_Perim"), the mean size ("Mean_size"), the mean length of the perimeters ("Mean_Perim"), the standard deviation of size and perimeter ("SD_size", "SD_Perim"), the skewness of the size and perimeter length histogram ("Skew_size" , "Skew_Perim") and the kurtosis of the size and perimeter histograms ("Kurt_size" , "Kurt_Perim").   For datasets of images the soil pore profile statistics were then analysed use linear mixed models (package "lmerTest") based on the experimental design of the field experiment, to determine shifts in feature profiles linked to field treatments. Normality and fit of models were assessed using mcp.fnc function, and where necessary to improve model fit, dependant variables were transformed using yeo.johnson transformation (or link functions). Models were evaluated with ANOVA (package "car"), and emmeans (package "emmeans") was used for evaluation of contrasts between specific treatments.

7.3. Results

7.3.1.   RGB high resolution analysis

High resolution structural analysis was able to parameterise structural changes in the soil cores obtained from the Grieves House platform and the CSC. Figure 39 shows example images from an example sample taken through the analysis process.

Figure 39. Visualisation of the process of extracting feature information from RGB soil images. (A) Original images from scanner, (B) extraction of soil area of image, (C) splitting image into Red, Green, and Blue channels, (D) Histogram of features and correction of the PCA direction, (E) PCA image after correction with features marked in black. (F) Shape Area vs the average brightness for extracted features (G) Features coloured by size (H) higher resolution example area showing feature edges.
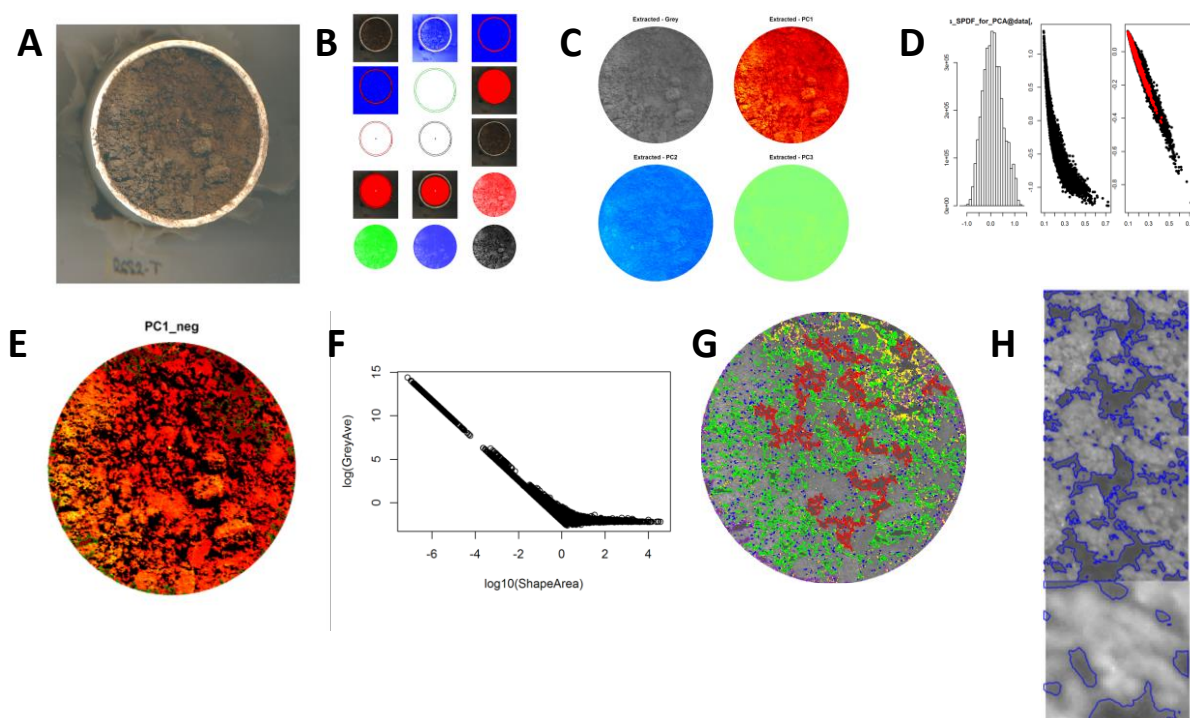
7.3.2.   RGB analysis of Grieves House tillage Trial soil

Samples from Grieves House Tillage platform were sampled from the plot rows, rather than main plots. Three soil core types (top bottom and repacked) were analysed from the two separate sampling points randomly chosen on a North South line from the top of each plot strip, totalling 384 core images. Differences in the full models were limited to differences between Core types (for Total Area, Total Perimeter, and Skew of the Size histogram) Figure 40. The reduced models however were perhaps more informative, with several significant differences showing up for Tillage. Within the reduce models, differences in tillage were found in the Total area (p = 0.011), Mean size (p = 0.001), mean perimeter length (p = 0.017). There were also significant interactions between Tillage and the Core type (Total Area p = 0.033, Mean size p =0.021, SD size p = 0.020, SD Perimeter p = 0.039). The direct drill plots therefore had a similar number of features, but these covered a smaller area of the sampled soil (573k vs 612k (pixels)), because they were on average smaller (24.2 vs 28.9), however the interaction with core type, showed that repacking the cores changed this relationship. The mean perimeter values were also slightly lower for the DD vs the IP plots also (10.0 vs 10.8).

Figure 40. Variation in features parameters extracted from soil images from Grieve's House Tillage Trial. (i) No of features, (ii) Total area of features (pixels), (iii) mean perimeter of the features extracted, (iv) Mean length of feature perimeters.
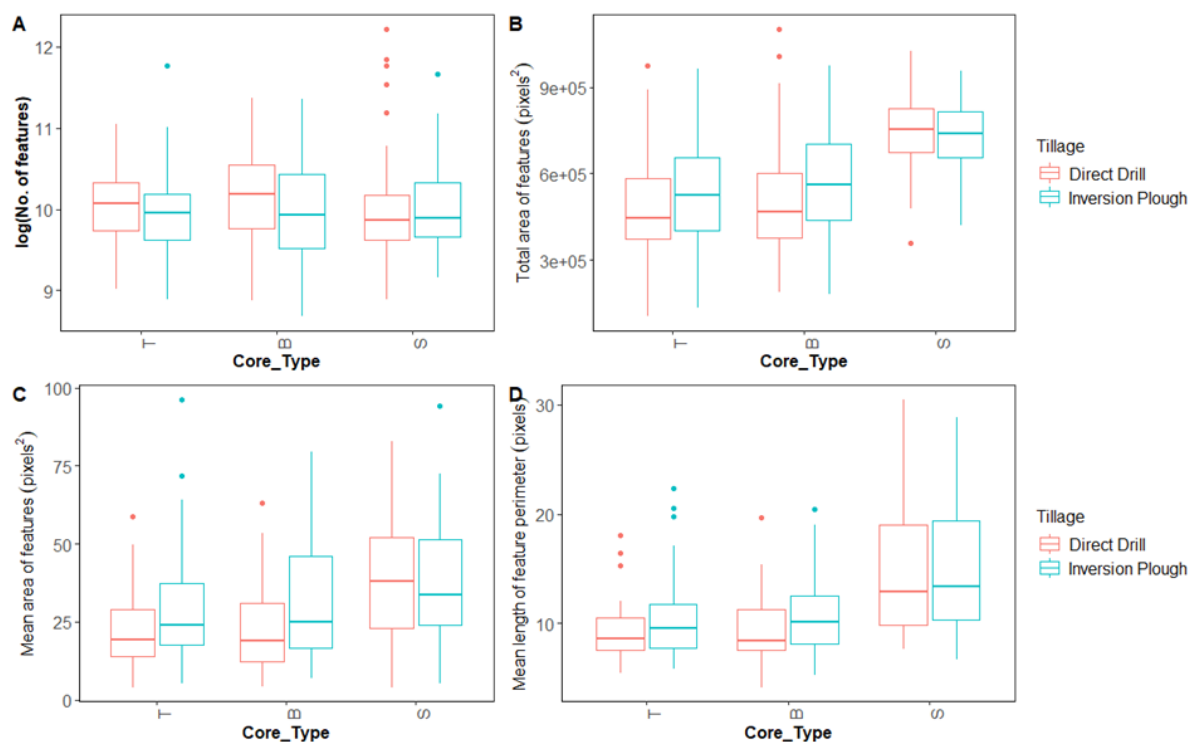
7.3.3.   RGB analysis of Centre for Sustainable Cropping (CSC) soil

Samples were obtained from the Centre for integrated cropping, including the furrows and rows of the potato field. A total of 420 cores were analysed 3 core types (top, bottom, repacked), from the two treatments (integrated and conventional) from each of the six fields, and in each of the two "cultivar rows" in each management half. In the potato fields, samples were taken from the top of the ridges and the bottom of the furrows. Each field strip was sampled at five sampling intervals, totalling 20 sample points per half field, giving the total of 420 core images. Analysis comes with the caveat that the samples are taken from one time point, and the fields are split fields, so true replication is not achieved as the treatments are split fields and are not true replications. However, analysis of the shape parameters of the histograms of feature sizes, revealed differences in the structures between field halves/tillage systems within individual fields. Specifically, differences were found between the field halves/tillage treatments in the potato fields and the WOSR fields (Table 8), Figure 41(A)), but not in the other crops/fields. Samples from the integrated side of the fields in the potatoes, had a higher number of features (No. of features $p = 0.043$), that were larger than average in overall size (Mean size, $p = 0.005$). Within the WOSR, the samples from the integrated side, had a reduced number of features (No. of features $p = 0.009$), however they were on average larger (Mean size $p = 0.038$), with a longer perimeter (Mean perimeter, $p = 0.010$). Differences could also be detected between the soil sampled from the furrows and rows of the potato field (Table 9), however the effect on soil features was tillage dependent. For example, differences were found between the ridges and furrows of the conventional tillage, with a higher area of the image being designated as features in the ridge samples (Total Area $p = 0.042$), suggesting a higher pores space in the ridges compared with furrows. Although the trend was the same for the integrated side of the field, the difference was not statistically significant (Figure 41B(i) Total Area $p = 0.277$). The opposite effect occurred for the "skew of the

67

perimeter" and "Kurtosis of the perimeter" parameters, which showed significant differences in the integrated side of the fields, but not the conventional. The values of "Skew_Perim" were higher for the furrows than for the ridges, within the integrated side of the potato field (Figure 41B(ii) Perimeter skewness p = 0.016), suggesting, more complicated pores/features with increased perimeter length. The distribution of the perimeter lengths within the soil cores from the potato field was also shown to be different between the ridges and furrows in the integrated side of the fields but not the conventional (p =0.019 vs p = 0.871), suggesting the furrows of the integrated fields had a more extended range but narrower peak than the ridges. Difference between the integrated and conventional treatment in the potato field only analysis was found in the furrows only for feature numbers (p = 0.015), Total perimeter (p=0.010), mean size (p = 0.045)

Figure 41. Analysis of the CSC soil samples, showing differences in the image analysis extracted parameters. Across (A) all fields (B) Potato field 9comparing ridges and furrows. Ai Number of features Aii mean area of features, Aiii mean perimeter length of features. Bi Total area of features, Bii Skewness of the histogram of features, Biii kurtosis of the features histogram.
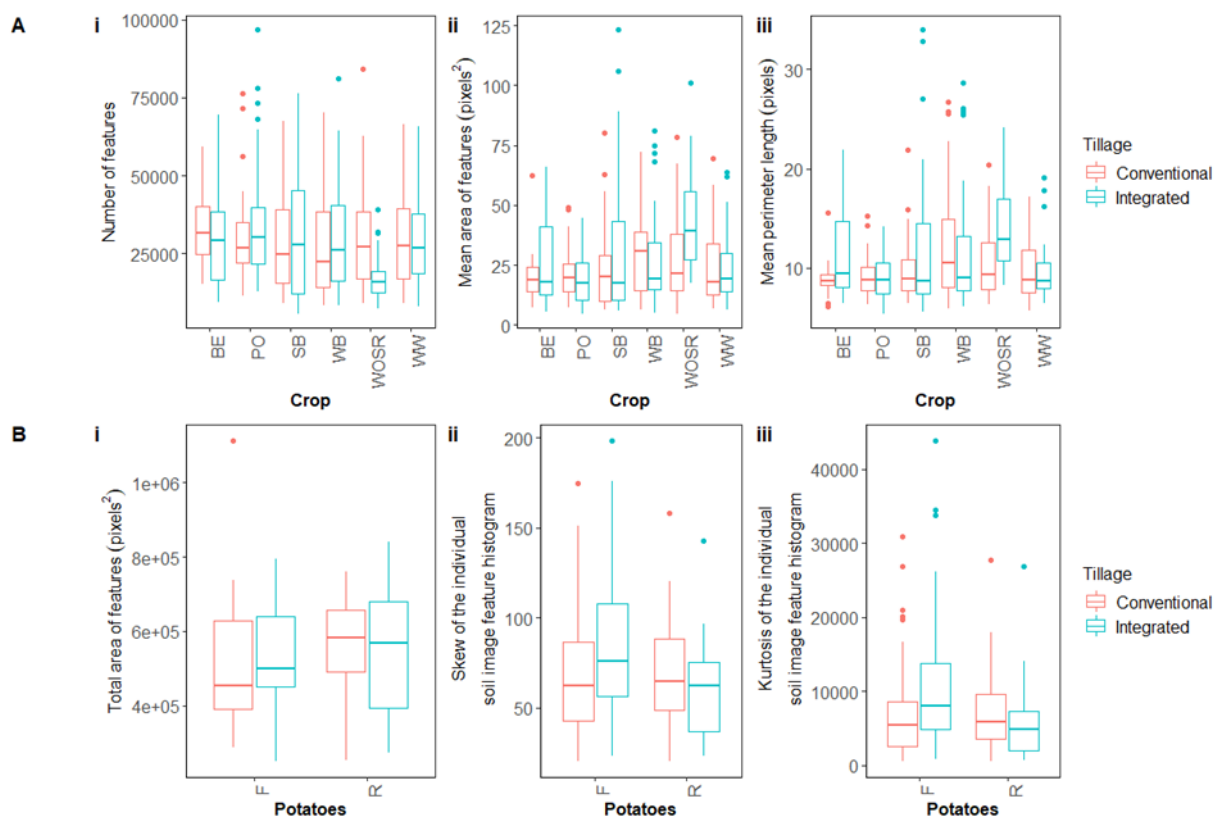
Table 8. **Analysis of soil cores descriptive statistics of the feature / pore distribution in the CSC soil cores using the high-resolution scanner image analysis method**

Parameter	(Intercept)	Crop	Tillage	Core Type	Crop Tillage	Crop Core Type	Tillage Core Type	Crop Tillage Core Type
Features	**0.000**	0.910	0.159	**0.036**	**0.027**	**0.000**	**0.005**	**0.014**
Total area	**0.000**	0.195	0.717	0.499	0.459	**0.015**	**0.011**	**0.001**
Total perimeter	**0.000**	0.557	0.414	**0.033**	0.108	**0.000**	0.132	0.176
Mean size	**0.000**	0.570	0.339	**0.024**	**0.048**	**0.000**	**0.000**	**0.000**
Mean perimeter	**0.000**	0.525	0.200	0.154	**0.036**	**0.000**	**0.007**	**0.009**
S.D. size	**0.000**	0.173	0.840	**0.000**	0.142	**0.000**	**0.004**	**0.000**
S.D. perimeter	**0.000**	0.111	0.706	**0.000**	0.376	**0.019**	0.233	**0.013**
Skew size	**0.000**	0.940	0.755	**0.005**	0.504	**0.000**	0.569	0.197
Skew perimeter	**0.000**	0.962	0.603	**0.013**	0.810	**0.000**	0.413	0.245
Kurtosis size	**0.000**	0.901	0.809	**0.010**	0.464	**0.000**	0.520	0.231
Kurtosis perimeter	**0.000**	0.954	0.648	**0.024**	0.795	**0.000**	0.335	0.265

Table 9. Analysis of soil cores descriptive statistics of the feature / pore distribution in the potato field soil cores samples from the CSC using the high-resolution scanner image analysis method, comparing the ridge and furrow.

Parameter	(Intercept)	Tillage	Core Type	Potatoes	Tillage Core Type	Tillage Potatoes	Core Type Potatoes	Tillage Core Type Potatoes
Features	**0.000**	**0.000**	**0.000**	0.053	**0.000**	**0.001**	0.301	**0.004**
Total area	**0.000**	0.151	**0.006**	**0.016**	0.050	0.359	0.306	0.791
Total perimeter	**0.000**	**0.000**	**0.000**	0.067	**0.002**	**0.003**	0.394	**0.007**
Mean size	**0.000**	**0.002**	**0.019**	0.971	**0.000**	**0.026**	0.716	0.054
Mean perimeter	**0.000**	**0.003**	**0.002**	0.374	**0.000**	**0.038**	0.611	0.245
S.D. size	**0.000**	0.862	**0.004**	0.259	**0.001**	0.591	0.433	0.786
S.D. perimeter	**0.000**	0.145	**0.017**	0.191	**0.002**	0.080	0.314	0.177
Skew size	**0.000**	**0.021**	**0.001**	0.490	0.082	**0.031**	0.122	**0.040**
Skew perimeter	**0.000**	**0.012**	**0.004**	0.302	0.084	**0.006**	0.121	**0.032**
Kurtosis size	**0.000**	**0.019**	**0.002**	0.510	0.081	**0.034**	0.124	**0.044**
Kurtosis perimeter	**0.000**	**0.013**	**0.010**	0.341	0.115	**0.007**	0.129	**0.041**

7.3.4. Multispectral

Example images demonstrating the analysis of structure using the VIS, and VIS_NIR Ximea cameras is illustrated in Figure 42. This analysis was applied to samples from Lodge Warren, Brooms Barn, Oxnead trials. The intact and repacked cores were analysed separately due to the differences in core diameter and height. If these were analysed together the differences may have resulted in differences in lighting conditions during imaging and would have resulted in non-comparable areas analysed during the image analysis process. A total of 96 intact and repacked cores were analysed. Sample "Lodge_Warren_OM_4" was removed from the Intact data analysis due to the analysis not successfully finding the core in

the image.

Figure 42. Visualisation of the multispectral soil feature analysis. (A) PCA of wavelengths with extraction area marked. (B) PCA1 wavelength image. (C) Histograms of wavelength across full extracted soil area. (D) histogram of PC1 of image at point of direction correction. (E) PCA1 image with feature overlay (alternative colour). (F) PCA1 image with area marked (in yellow) where edge correction occurred. (G) Features marked after edge correction. (H) Example output PCA and individual wavelength reflection from area of image designated inside or outside of features.
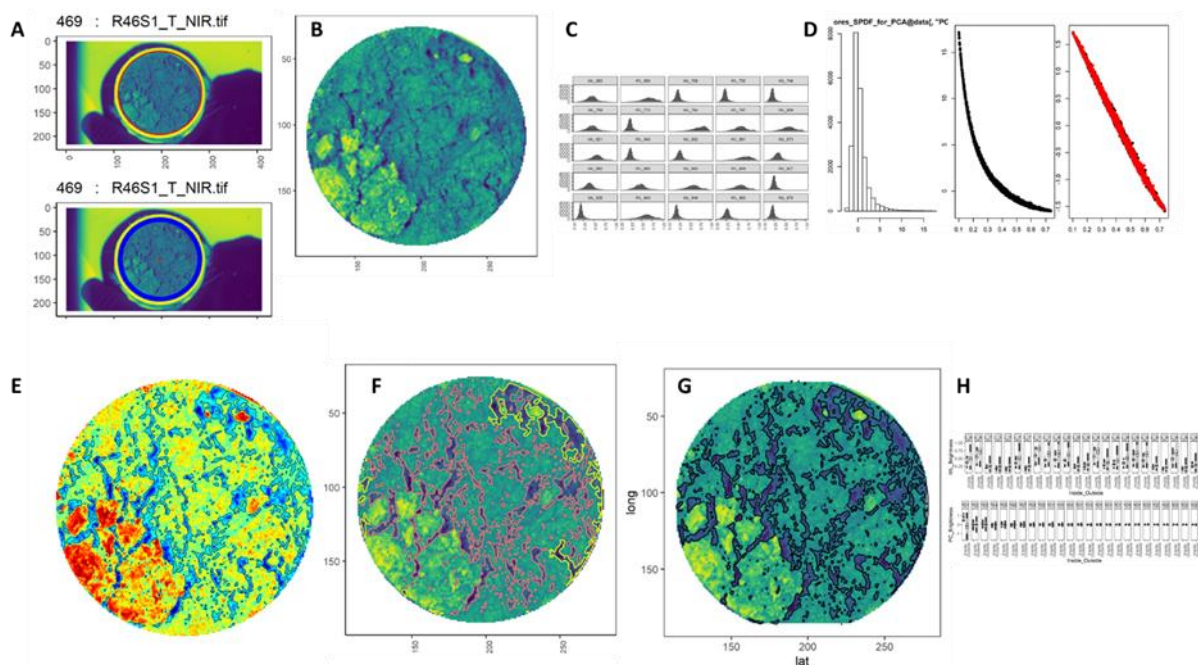
Figure 43 illustrates summary PCA of the differences in the wavelength patterns across the whole soil cores from the three Trials and the treatments. No individual wavelength was significantly different between the trials, but 13 out of 41 showed differences at the soil treatment level ($p<=0.05$). Investigations of the contrasts within each Trial between the principal components of the brightness of wavelengths across the soil cores were found between Brooms Barn – Lodge Warren (Intact cores- PC 1 ,3,4,5 & 6 (PC 1,3,4,6) repacked cores – PC 2,4,5 & 6 (PC2, 4,5,6,7), Brooms Barn - Ox2 (Intact cores- PC 3,6 & 8 (PC4,6,7, 13) repacked cores -PC 2,4 & 10 (PC2,3), and Lodge Warren - Ox2 (Intact cores- PC 5,6,8 & 13 (PC6,13) repacked cores - PC4 & 6 (PC5,7). Differences between treatments within the Trials were more limited with differences between treatment in the Brooms Barn (Intact PC21, Repacked), Lodge Warren (Intact PC6 (P1,3,4,6) Repacked – PC4, PC5 (PC3), but no significant differences were found in the treatment contrasts for Oxnead ((Intact (PC 6), Repacked). Therefore, there is evidence that the overall distribution of reflectance across the

wavebands from the different Trials and treatments was different, with the potential to track changes in land usage in terms of organic matter amendments.

Figure 43. Principal comments analysis of the reflection intensity for wavelength bands across the whole of the extracted areas (no separation between inside / outside features. (A)   (B)
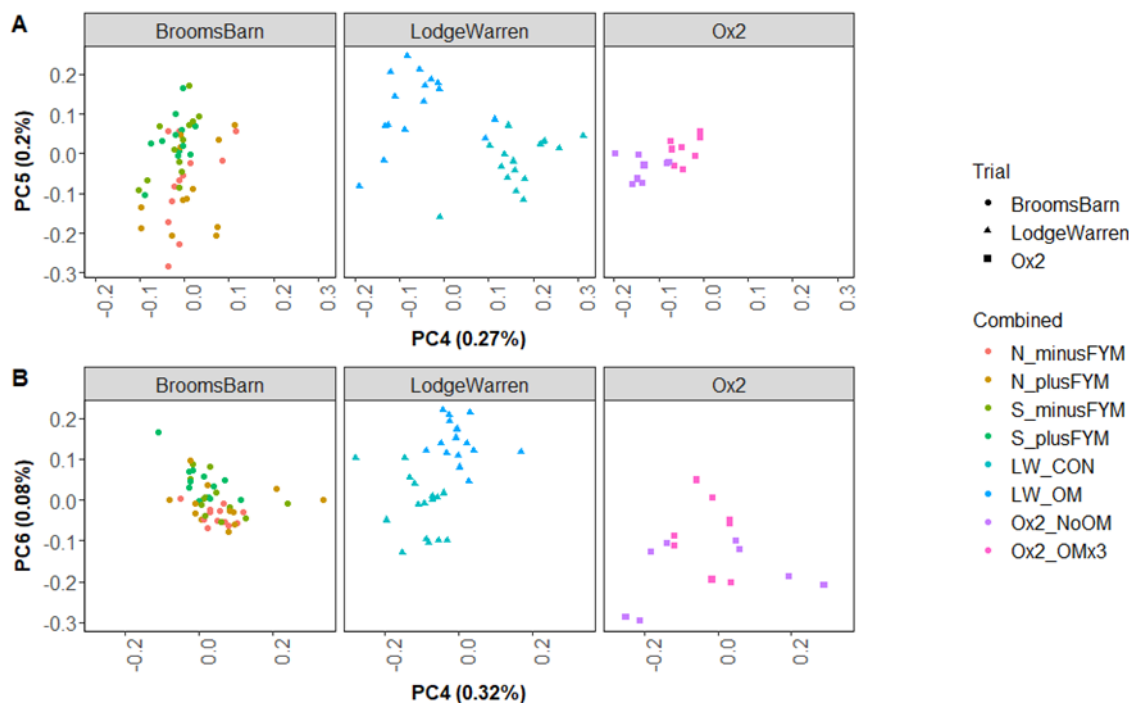
Datasets were also analysed at the features level, i.e. area, mean size and shape of the parts of the image designated as features. Differences in structural measurements were found between Trials in both repacked (Table 10) and Intact Cores (Table 11) see also Figure 44 A & B. There were also differences found at the treatment level within the individual trials (Table 10 and Table 11 and Figure 44).

Table 10. Feature level evaluation of repacked soil cores from Lodge Warren, Oxnead and Brooms Barn experiments

Parameter	Model type	(Intercept)	Trial	Trial	Parameter
VIS_Features	base	**0.000**	0.097	**0.010**	0.083
VIS_Total_Area	yj	**0.000**	0.837	0.461	0.557
VIS_Total_Perim	base	**0.000**	**0.050**	**0.024**	0.163
VIS_Mean_size	yj	**0.000**	0.168	**0.024**	0.077
VIS_Mean_Perim	bcn	**0.000**	0.168	**0.009**	**0.008**
VIS_SD_size	yj	**0.000**	**0.022**	0.168	0.300
VIS_SD_Perim	bcn	**0.000**	**0.022**	0.101	0.170
VIS_Skew_size	base	**0.000**	**0.019**	0.209	0.570
VIS_Skew_Perim	base	**0.000**	**0.005**	0.434	0.566
VIS_Kurt_size	bcn	**0.000**	**0.026**	0.199	0.459
VIS_Kurt_Perim	yj	**0.000**	**0.008**	0.382	0.495
NIR_Features	base	**0.000**	0.223	**0.000**	0.120
NIR_Total_Area	yj	**0.000**	0.177	0.526	0.281
NIR_Total_Perim	base	**0.000**	0.071	**0.015**	**0.013**
NIR_Mean_size	yj	**0.000**	0.355	0.100	0.946
NIR_Mean_Perim	yj	**0.000**	0.333	0.065	0.889
NIR_SD_size	yj	**0.000**	**0.016**	0.655	0.837
NIR_SD_Perim	yj	**0.000**	**0.001**	0.634	0.901
NIR_Skew_size	base	**0.000**	0.060	**0.004**	0.580
NIR_Skew_Perim	base	**0.000**	**0.008**	**0.006**	0.523
NIR_Kurt_size	bcn	**0.000**	0.108	**0.003**	0.631
NIR_Kurt_Perim	yj	**0.000**	**0.020**	**0.004**	0.523

Table 11. Feature level evaluation of intact soil cores from Lodge Warren, Oxnead and Brooms barn trials.

Parameter	Model_type	(Intercept)	Trial	Trial	Parameter
VIS_Features	base	**0.000**	**0.012**	0.579	**0.006**
VIS_Total_Area	yj	**0.000**	0.311	0.439	0.436
VIS_Total_Perim	base	**0.000**	0.157	0.960	0.111
VIS_Mean_size	yj	**0.000**	**0.005**	0.409	**0.000**
VIS_Mean_Perim	bcn	**0.000**	**0.000**	0.263	**0.001**
VIS_SD_size	bcn	**0.000**	0.081	0.627	0.196
VIS_SD_Perim	yj	**0.000**	0.139	0.746	0.353
VIS_Skew_size	base	**0.000**	0.768	0.618	**0.033**
VIS_Skew_Perim	base	**0.000**	0.615	0.432	0.057
VIS_Kurt_size	base	**0.000**	0.692	0.556	**0.023**
VIS_Kurt_Perim	bcn	**0.000**	0.678	0.525	**0.041**
NIR_Features	base	**0.000**	**0.009**	0.953	0.358
NIR_Total_Area	bcn	**0.000**	**0.046**	0.240	0.908
NIR_Total_Perim	base	**0.000**	0.145	0.404	0.479
NIR_Mean_size	bcn	**0.000**	**0.011**	0.815	0.507
NIR_Mean_Perim	bcn	**0.000**	**0.003**	0.500	0.589
NIR_SD_size	bcn	**0.000**	0.079	0.436	0.862
NIR_SD_Perim	bcn	**0.000**	0.153	0.330	0.540
NIR_Skew_size	base	**0.000**	0.252	0.140	0.077
NIR_Skew_Perim	base	**0.000**	0.292	0.095	0.076
NIR_Kurt_size	yj	**0.000**	0.206	0.170	0.107
NIR_Kurt_Perim	bcn	**0.000**	0.225	0.124	0.132

In post-hoc analysis for significant contrast differences between treatment within trials differences were found within the Brooms barn trials for NIR Features (N plusFYM - S plusFYM $p = 0.042$ in the repacked soil cores. For the intact soil cores, differences were found between treatments at Lodge Warren site (VIS_Features $p=0.0250$).

Figure 44. Selected feature characteristics of Repacked (A) and Intact (B) soil cores extracted using the multispectral feature analysis.
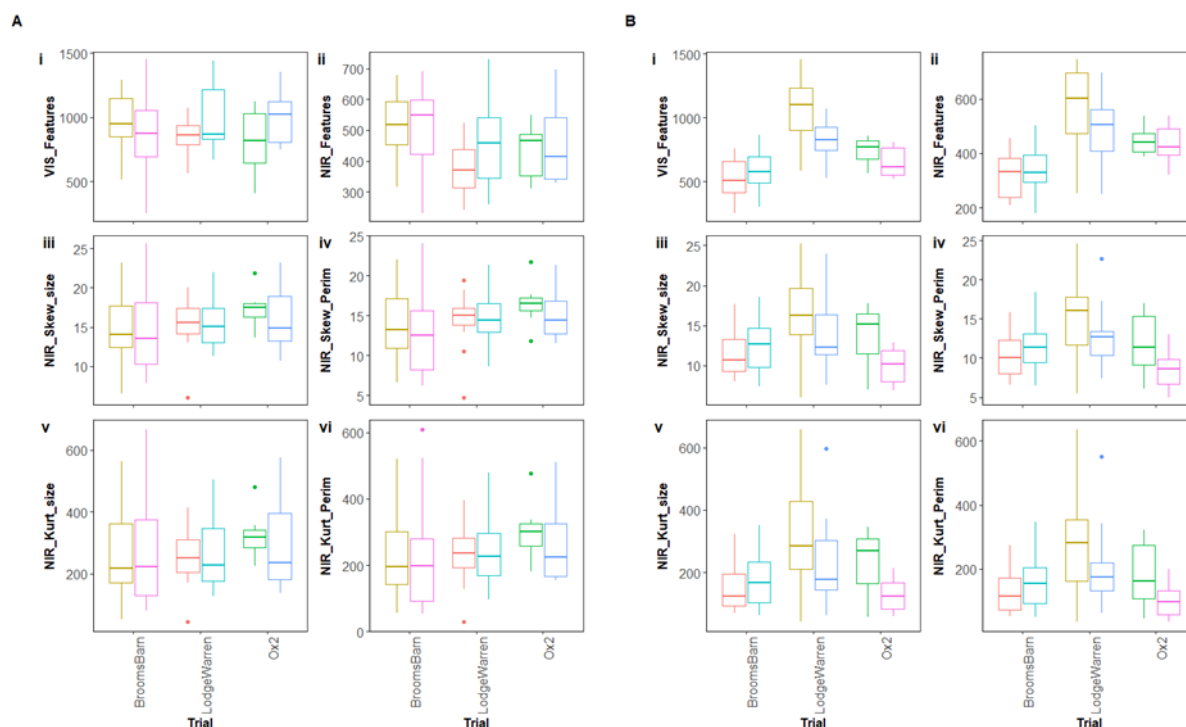
7.4. Discussion

This study aimed to apply an image analysis protocol designed to extract features from soil images using high resolution 2D scanned images, and multispectral images obtained using ximea multispectral cameras. The sampled soils were collected from a range of field trial sites with different managements and rotations. In order, to apply the developed methods to the field samples, streamlining of the methods was undertaken, with improvements in automatically finding the core in the image implemented, and implementation of changes to increase speed from the initial protocols. Within the RGB analysis there were issues at the edge of the soil core image where structures were not assessed due to being in contact with the edge of the core, therefore in the multispectral analysis an edge correction section of the analysis was added.

The adaption of the methods allowed analysis of soil image datasets from two rotational sites for the high-resolution scanning methods (CSC & Grieves House), both of which include crop rotations and reduced tillage methods in comparison with inversion plough cultivation. Within the Grieves House samples, differences were found between the tillage methods in terms of the distribution of the pore space, but no strong correlation to crops within rotation. In the CSC samples there were differences found between tillage methods in some of the crop fields (Potato and WOSR) but not in all fields. The methods were also able to show differences between the tillage methods and the soils in the rows and furrows of the potato fields. Further analysis is ongoing to correlate these results with soil properties such as DBD.

The multispectral method was applied to samples from three field trials (Brooms Barn, Oxnead and Lodge Warren), two of which had organic amendments (Ox, LW) with Brooms Barn having treatments comprising old and new application of manure. Analysis of the distribution of wavelengths was able to separate the soils into site categories and some of the treatment categories within individual field trials, showing the potential to track changes in field

composition. Evaluation of the structural information gained from the images also showed differences between trial treatments. Further study will allow an in-depth analysis of the within feature wavelength variation and correlations between calculated features and other soil measurements (calculations of pore distribution, soil strength and DBD, water content (at time of imaging)). However, the work demonstrated the potential of these two methods in assessing changes in structural composition between soil management within trials.

7.5. Conclusions

- Flatbed scanner imaging, followed by image analysis of the soil structure was sensitive enough to differentiate between structural changes under different tillage / management systems.
- Multispectral imaging with ximea cameras followed by image analysis was faster than the flatbed scanner process due to smaller datasets. This process was also able to demonstrate differences between treatments in terms of soil spectra and in terms of soil, structure.
- Edge correction was possible for the RGB due to the lower resolution, but further development is required to apply this to the higher resolution RGB images.
- The tool offers a protocol for tracking structural changes over time at a scale relevant to root:soil interactions
- Further analysis is needed to assess whether the spectral patterns obtained from the multispectral camera correlates with soil properties.
- Both methods gave an alternative way of tracking structural changes in soils, and as previously experienced with soil structural measure (See WP1 report), differences in soil were found more frequently when comparing across trials or sites, however differences were found with sites across treatments.

8. TRAFFICKING IN ARABLE FIELDS

8.1. Introduction

The purpose of this study was to gather information on the effects of (1) different implement working widths and (2) variation tyre pressure on soil compaction and on crop performance.

8.2. Materials and Methods

8.2.1. Experiment at Greenwell Farms, Orford, Suffolk 2017 (2017-18)

This comparison was done in Poor Walk at Greenwell Farms. There was one strip trial examining bedformer configuration and soil compaction at Greenwell Farms, Orford, Suffolk in the same field as Expt 2017-4 (Table 2). This was conducted on sand soil (91 % S, 6 % Z, 3 % C, 1.6 % OM). Two different width bedformer were used: a 4-bed Grimme bedformer pulled by a tracked Case IH Quadtrac 540 (laden weight 21.7 t) which was standard farm practice and a single bed machine pulled by a Case IH Puma 215 (8.1 t) running on 650/65 R42 + 540/65 R30 tyres at a pressure of 19 PSI. Strips of eight beds were pulled up using both machines in three areas of the field on 15 March following Sumo and Flatlift cultivations on 11 and 14 March, respectively. Measurements of soil resistance were taken immediately after bedforming using an Eijkelkamp Penetrograph with a 60° 2 cm^2 cone tip. The positions corresponding to the centre of each row were located and measured to a depth of 50 cm. On 19 July, duplicate soil cores (55 mm diameter x 40mm cylinders) were taken from four depths (25, 45, 65 and 85 cm from the top of the ridge) under each bed and furrow position under each bedformer. One core was dried at 105 °C for 24 hours to determine dry bulk density and the other was sent to James Hutton Institute for measurements of water release and micro-penetrometer resistance.

8.2.2. Experiment at Farmcare Ltd, Cambridgeshire 2017 (2017-20)

The second trial looked at tyre pressure modifications at Farmcare Ltd, Coldham Estate, Cambridgeshire. This was conducted on a silty clay loam soil (12 % S, 54 % Z, 34 % C, 5.3 % OM). The single-pass cultivation implement was a three-bed Basilier 5.4 m rotoridger pulled by a John Deere 8360R tractor with a combined weight (tractor, rotoridger, fertilizer tank) of 19.9 t. The tyres were Michelin Axiobib (rear 800/70/38 and front 600/70/30). The standard tyre pressure was 17 PSI and two treatments were imposed: low (14.5 PSI) and high (22.5 PSI). Soil strength was measured using the Eijkelkamp Penetrograph (as described above), in 12 equally- spaced positions across a full three-bed module immediately after the bedforming was completed (19 April). On 26 September, duplicate soil cores (55 mm diameter x 40 mm cylinders) were taken from four depths (17, 37, 57 and 77 cm from the top of the ridge) under each bed and furrow position under each tyre pressure treatment. One core was dried at 105 °C for 24 hours to determine dry bulk density and the other was sent to James Hutton Institute for measurements of water release and micro-penetrometer resistance.

8.2.3. Experiment at Greenwell Farms, Orford, Suffolk 2018 (2018-40)

Expt 2018-40 was done in Orford walk at Greenwell Farms, Orford, Suffolk. It tested the effect of compost amendment on trafficking compaction from the bedformer was examined. The soil was a sand (88 % S, 6 % Z, 6 % C, 1.6 % OM). At planting on 11 April, the four-bed Grimme bedformer was pulled by a tracked Case IH Quadtrac 540 (laden weight 21.7 t). Measurements of soil resistance were taken at harvest on 24 July using an Eijkelkamp Penetrograph with a 60°

2 cm^2 cone tip. The positions corresponding to the centre of each row were located and measured to a depth of 50 cm. On the same date, duplicate soil cores (55 mm diameter x 40 mm cylinders) were taken from four depths (20, 30, 40 and 50 cm from the top of the ridge) under each bed and furrow position under each bedformer. One core was cold stored at 3 °C to examine root length density at a later date and the other was sent to the James Hutton Institute for measurements of water release and micro-penetrometer resistance. A final harvest of 3 m length of single row was taken on 24 July from each of the four rows formed by one half of the bedformer to assess the effect of trafficking on yield.

8.2.4.   Experiment at Stevenson Brother, Essex 2018 (2018-41)

Experiment 2018-41 The second trial looked at trafficking compaction on two contrasting areas of a heavy clay field near Hatfield Broad Oak, farmed by Stevenson Bros. The position of the centre of two bedformer runs was located on two contrasting soil types planted with a crop of King Edward on 9 May. One area was conducted on a clay loam soil (25 % S, 44 % Z, 32 % C, 3.2 % OM) with moderate water holding capacity and the other was on a silty clay loam soil (12 % S, 54 % Z, 34 % C, 2.8 % OM) with high water holding capacity. The bedforming operations were carried out with a Caterpillar Challenger MT775E running on 75 cm tracks (gross weight 15.6 t) and three-bed Grimme bedformer. Soil strength was measured using the Eijkelkamp Penetrograph (as described above) on 21 September under each of the three rows of one half of a bedformer module. On the same date, duplicate soil cores (55 mm diameter x 40 mm cylinders) were taken from four depths (15, 25, 35 and 45 cm from the top of the ridge) in each of the three rows. One core was cold stored at 3 °C to assess root length density at a later date and the other was sent to the James Hutton Institute for measurements of water release and micro-penetrometer resistance. A final harvest of 3 m length of single row was taken from each of the three rows on 28 September to assess the effect of trafficking on yield on the two different soil types. Three replicate areas were sampled in each soil type for soil strength, rooting and yield.

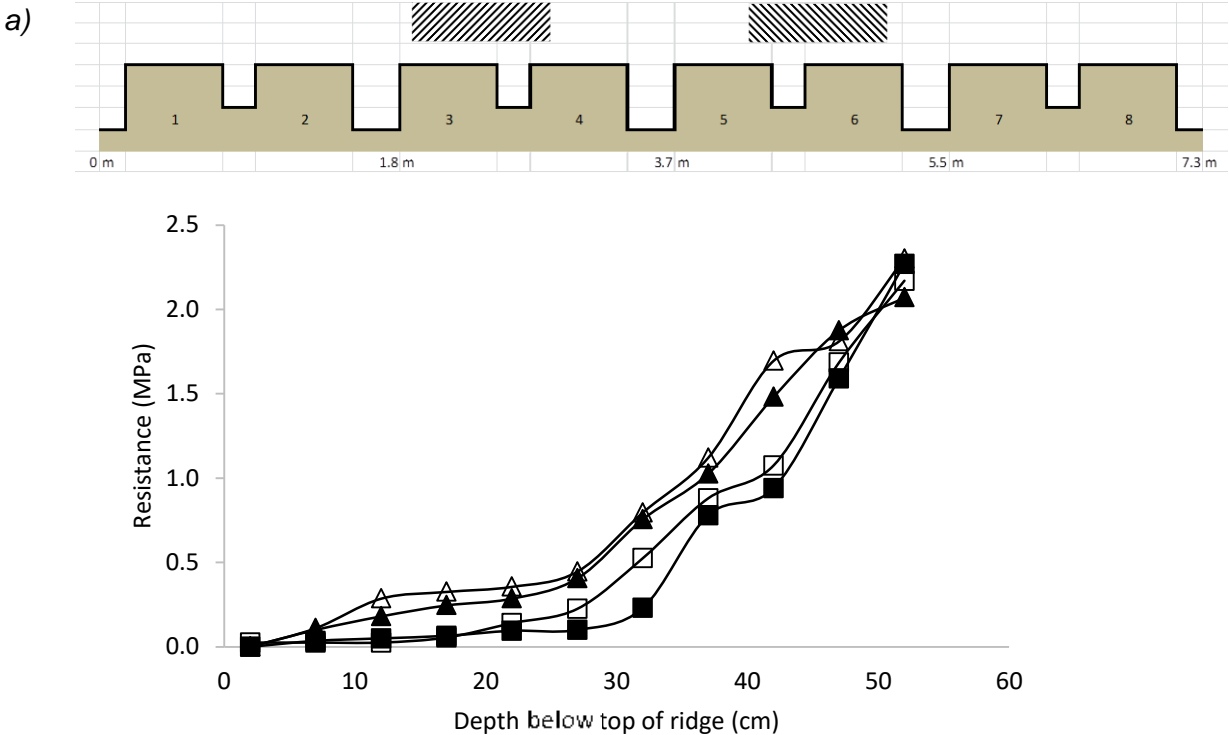## 8.3. Results and discussion of wheeling management studies

8.3.1.   Experiment at Greenwell Farms (Expt 2017-18)

At Greenwell Farms, with the standard four-bed bedformer and Quadtrac combination, there were effects of compaction measured down to 45 cm depth and there was greater compaction within beds (both in row and furrow positions) under the tracks than in untracked areas. The further away from tracks, the lower the compaction and the inside of each track created more compaction than the outer edges (Figure 45*a*). With the single-bed bedformer and wheeled tractor, compaction was still evident down to 45 cm depth and compaction under the rows was worse than outer rows of the four-bed system, but not as severe as under the tracks in the four-bed system (Figure 45*b*). Overall, the effects between extra loading and wider tracks of the four-bed system compared with the single-bed system probably cancelled out any benefits of more untrafficked rows in the four-bed system.

8.3.2.   Experiment at Farmcare Ltd (2017-20)

On the heavier soil at Farmcare Coldham Estate, with low tyre pressure outside beds were slightly more compacted than the middle bed at 20-25 cm depth and wheeled areas were slightly more compacted than unwheeled at 20-40 cm depth. The outside of the tyre created more compaction at 20-30 cm depth than inside. Wheeled furrows were slightly more compacted than where wheels were absent. The effects of increasing the tyre pressure from 14 to 22 PSI were restricted to depths shallower than 40 cm (most effects were observed between 20 and 40 cm deep). Outside beds were more compacted than the middle bed at 22 PSI than at 14 PSI, but there was limited overall effect of tyre pressure in unwheeled beds, wheeled beds or wheeled furrows (Figure 46).

Figure 45.   **Soil resistance at planting in different positions *a)* 4-row bedformer; *b)* single row bedformer. *a)* Rows 1 and 8, ■; Rows 2 and 7, □; Rows 3 and 6, ▲; Rows 4 and 5, △; *b)* Rows 1 and 2, ■. Hatched areas represent the position and width of tracks or wheels.**
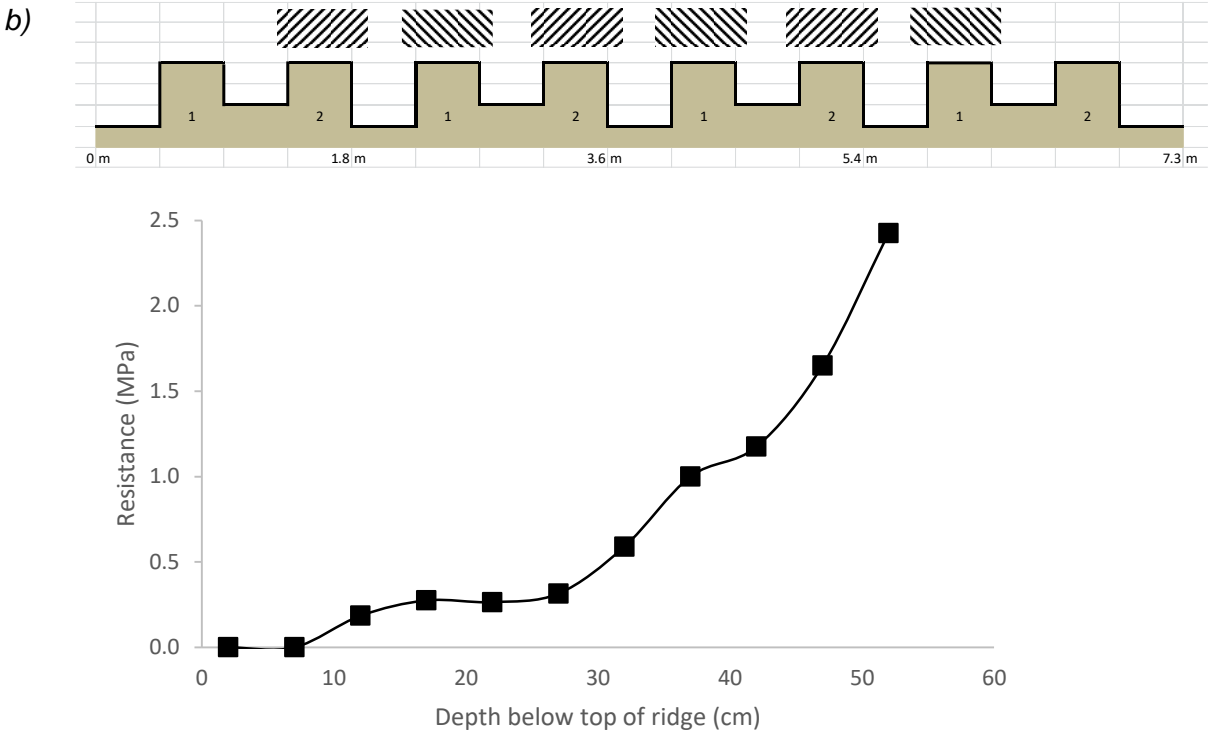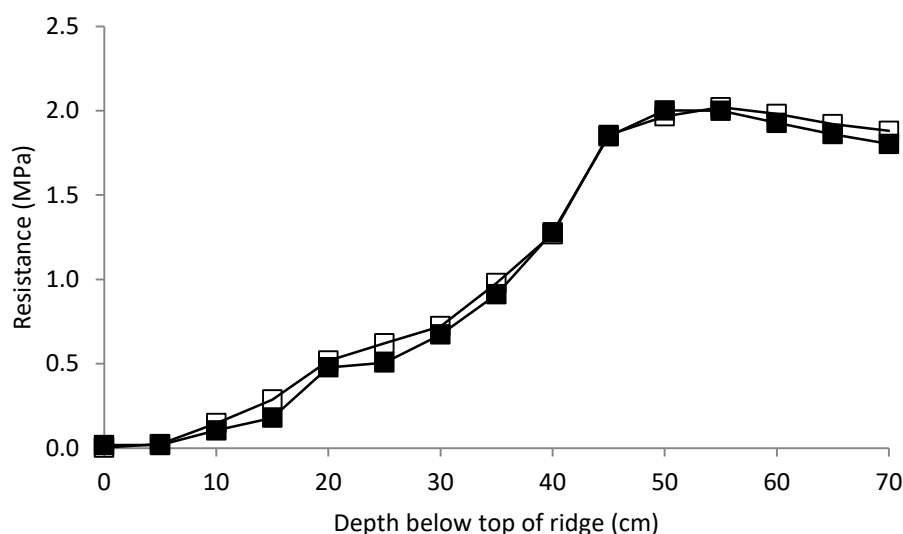
a)

4

b)

Figure 46. Soil resistance at planting for different tyre pressures. Data are means of 12 positions across a three-bed module. 14 PSI, ■; 22 PSI, □.


8.3.3. Experiment at Greenwell Farms Orford (Expt 2018-40)

At Greenwell Farms, with the standard four-bed bedformer and Quadtrac combination, there were effects of compaction measured down to 45 cm depth and using the whole four-bed cultivated module, there was greater compaction under the four rows trafficked by the tracks of the bedformer than in the four rows in untracked areas. The further away from tracks, the lower the compaction and the inside of each track created more compaction than the outer edges (Figure 45*a; b*). Averaged over all eight rows, compost amendment seemed to slightly reduce soil strength by *c.* 0.5 MPa between 30 and 40 cm depth below the top of the ridge compared with no compost amendment (Figure 45*c*). When comparing the whole eight-row module width, there was a consistent trend for the four rows trafficked by the bedformer to have a lower yield than the four untrafficked rows, but there was no effect of compost amendment on reducing the effects of trafficking on yield (Table 12).

Table 12. Effect of row position and compost amendment on yield (t/ha) at Orford Walk, Greenwell Farms (Expt 2018-40)

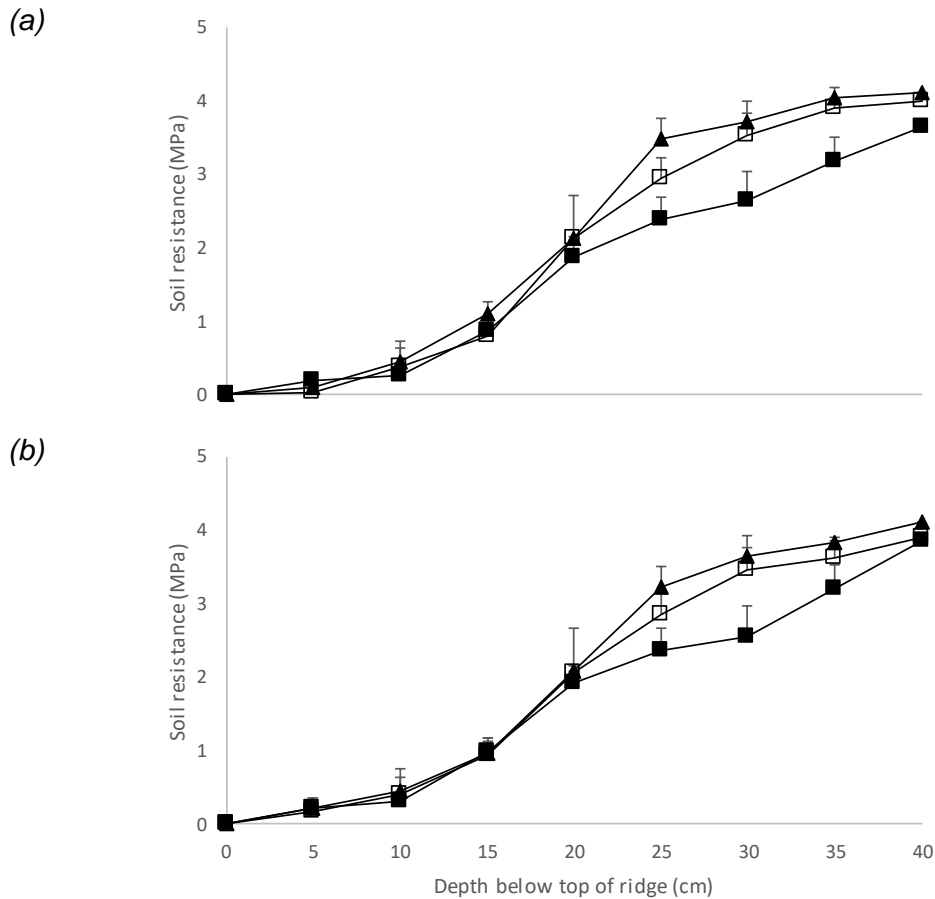|	Position			
	Untrafficked		Trafficked	
Amendment	Row 1/8	Row 2/7	Row 3/6	Row 4/5
None	36.1	37.9	34.8	31.8
Compost	33.5	33.6	29.5	31.2
Mean	34.8	35.7	32.2	31.5
S.E.	1.45	1.89	1.49	1.91

Figure 47. **Soil resistance in different positions under 8-row bedforme at Orford Walk, Greenwell Farm (Expt 2018-40).** *(a)* **No compost;** *(b)* **compost;** *(c)* **mean effect of compost treatment averaged over all rows.** *(a)* **and** *(b)* **Rows 1/8, ■; Rows 2/7, □; Rows 3/6, ▲; Rows 4/5, △.** *(c)* **No compost, ■; compost, □.**
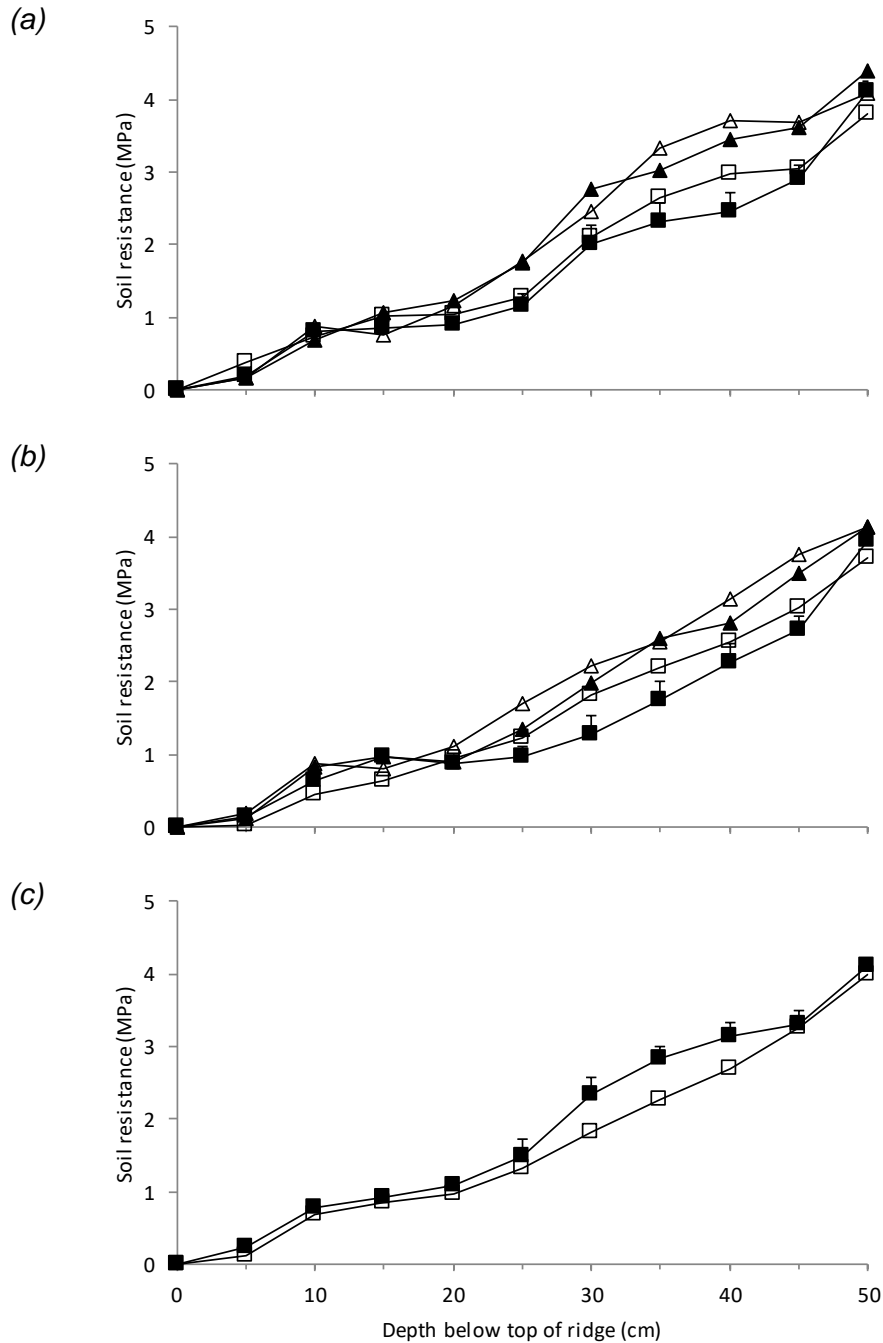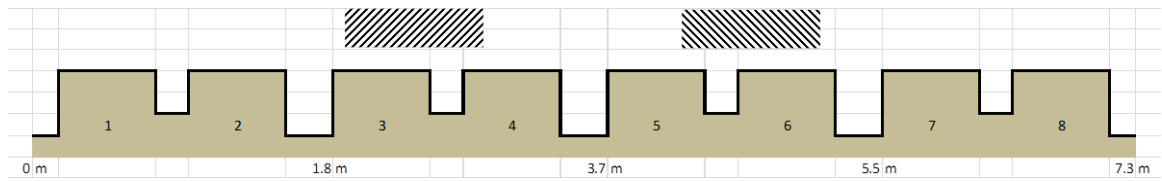
8.3.4. Experiment at Stevenson Brother, Essex 2018 (2018-41)

On the heavier soil at Stevenson Bros in Essex, there was a similar effect of row position on soil resistance to that found in Suffolk. The untrafficked Row 1 had lower resistance between 30 and 40 cm below the top of the ridge than Rows 2 and 3 where the bedformer wheels had run, but there was little effect of soil type on the resistance measured (Figure 48).

Figure 48. **Effect of row position and soil type on soil resistance at Missens, Stevenson Bros (Expt 2018-41) in one half of a six-row bedformer configuration.** *(a)* **clay loam;** *(b)* **silty clay loam. Row 1, ■; Row 2, □; Row 3, ▲.**

Tuber yield appeared to be reduced in rows previously trafficked by the bedformer tractor than in untrafficked rows and there was a larger effect of row position on the wetter silty clay loam soil than the drier clay loam soil (Table 13).

Table 13. **Effect of row position and soil type on yield (t/ha) at Missens, Stevenson Bros (Expt 2018-41)**

Soil type	Sample position	
(water content at cultivation)	Untrafficked Row 1	Trafficked Row 2/3
Silty clay loam (31 %)	46.6	41.7
S.E.	1.45	1.76
Clay loam (26 %)	51.6	48.2
S.E.	1.66	1.72

8.4. Conclusions

There appears to be a clear effect of trafficking reducing yield as a consequence of increased soil strength under areas of the bed where wheels have run during the bedforming operation, and compost may help in increasing the soil's resistance to damage from compaction. Once fully analysed, the soil data will help determine to what the extent the treatment differences are explicable in terms of soil-physical properties or are due to increased nutrient availability. In some experiments, the residual effects of the treatment will be followed in subsequent crops and these data will also provide valuable insights into the relative benefits of cover crops and amendments

9. REFERENCES

AITCHISON, J. (1982). The statistical analysis of compositional data. *Journal of the Royal Statistical Society (Series B)* **139**-177.

BLANCHY, G., WATTS, C., RICHARDS, J., BUSSELL, J., HUNTENBURG, K., SPARKES, D., STALHAM, M., HAWKESFORD, M., WHALLEY, W. & BINLEY, A. (2020). Time-lapse geophysical assessment of agricultural practices on soil moisture dynamics, *Vadose Zone Journal*, **19,** .20080

BOYDELL, B. & MCBRATNEY, A. (2002). Identifying potential within field management zones from cotton-yield estimates. Precision Agriculture 3, 9-23.

DUNN J. (1977). *Fuzzy Automata and Decision Processes*. Chapter on Indices of partition fuzziness and the detection of clusters in large data sets, Elsevier, New York.

GUASTAFERRO F., CASTRIGNANÒ, A., DE BENEDETTO, D., SOLLITTO, D., TROCCOLI, A. & CAFARELLI B. (2010) A comparison of different algorithms for the delineation of management zones. *Precision Agriculture* **11**, 600-620.

HAGHI, R.K., PEREZ-FERNANDEZ, E. & ROBERTSON, A.H.J. (2021). Prediction of various soil properties for a national spatial dataset of Scottish soils based on four different chemometric approaches: A comparison of near infrared and mid-infrared spectroscopy. *Geoderma* **396** 115071

HASSALL, K.L., WHITMORE, A.P. AND MILNE, A.E. (2019). Accounting for data sparsity when forming spatially coherent zones. *Applied Mathematical Modelling.* **72**, 537-552.

HATHAWAY, R.J. & BEZDEK, J.C. (2001). Fuzzy c-means clustering of incomplete data, *IEEE Transaction on Systems, Man, and Cybernetics* **31**, 735-744.

HEDLEY, C., YULE, I., EASTWOOD, C., SHEPHERD, T. & ARNOLD, G. (2004). Rapid identification of soil textural and management zones using electromagnetic induction sensing of soils. *Soil. Research* **42**, 389-400.

HOLLAND J, BROWN, J L, MACKENZIE, K, NEILSON, R, PIRAS, S, & MCKENZIE, B M. (2021). Over winter cover crops provide yield benefits for spring barley and maintain soil health in northern Europe. *European Journal of Agronomy* **130**, 126363

LARK, R.M. (1998). Forming spatially coherent regions by classifiation of multi-variate data: an example from the analysis of maps of crop yield. *International Journal of Geographic Information Science* **12**, 83-98.

MCKENZIE, B.M., STOBART, R., BROWN, J.L., GEORGE, T.S., MORRIS, N., NEWTON, A.C., VALENTINE, T.A. & HALLETT P.D. (2017). Platforms to test and demonstrate sustainable soil management: integration of major UK field experiments. *AHDB Final Report RD-2012-3786.* AHDB, Stoneleigh.

MILNE, A., WEBSTER, R., GINSBURG, D. & KINDRED, D. (2012). Spatial multivariate classification of an arable field into compact management zones based on past crop yields. *Computers and Electronics in Agriculture* **80** 17-30.

ROBERTSON, A.H.J., HILLIER, S.J., DONALD, C. & HILL HR. (2013). A Robust FTIR Database for Scotland. In: *Proceedings of the 3rd Global Workshop on Proximal Soil Sensing, 26-29 May 2013*, Potsdam, Germany, pp182- 185

ROUBENS, M. (1982). Fuzzy clustering algorithms and their cluster validity. *European Journal of Operational Research* **10**, 294-301.

SONG, X., WANG, J., HUANG, W., LIU, L. YAN, G., & PU, R. (2009). The delineation of agricultural management zones with high resolution remotely sensed data. *Precision Agriculture* **10**, 471-487.

VALENTINE, T.A., HALLETT, P.D., BINNIE, K., YOUNG, M.W., SQUIRE, G.R., HAWES, C. & BENGOUGH, A.G. (2012). Soil strength and macropore volume limit root elongation rates in many UK agricultural soils. *Annals of Botany*. **110**, 259–270.

WEBSTER, R. & BURROUGH, P.A. (1972). Computer-based soil mapping of small areas from sample data: II. Classification smoothing. *Journal of Soil Science* **23**, 222-234.

WEBSTER, R. & OLIVER, M.A. (2007). *Geostatistics for environmental scientists*, John Wiley & Sons, 2007

10. APPENDIX – ZONING OF POTATO YIELDS

This section describes the results from an extensive empirical study, designed to investigate how the zoning methods detailed in Section 3.2.3 address the issues created by different types of data sparsity. Specifically, there were three fields with wheat yield measurements obtained from multiple years at a reasonable spatial density. The effects of variable sparsity were studied by restricting data to different subsets of years, and the effects of spatial sparsity, by considering different grid sizes, on clustering and smoothing. In combination, these enabled us to investigate the effect of colocation sparsity. To each data scenario 2 cluster options were implemented,

- Original fuzzy c-means, requiring complete observations
- Fuzzy c-means with optimal completion strategy

and two smoothing options,

- Over a neighbourhood defined using the underlying grid alignment
- Over a neighbourhood defined using the Voronoi tessellation.

For these data, explicit information, such as soil maps, which designate a definitive clustering are not available. As such, no true validation datasets exist that can be used to calculate algorithm error. Thus, to assess algorithm performance, a subjective assessment of the clustering and smoothing was made for each data scenario. The clustering was categorised as "good" if a classification could be clearly identified from the calculated cluster entropy, "moderate" if a classification could be identified, albeit with some scepticism or "bad" if no clear classification could be identified. The smoothing was categorised as "good" if a clear maximum could be identified from the coherence index, "moderate" if a maximum existed but was not clearly identified, e.g. through discontinuities in the coherence index and "bad" if no clear maximum could be identified. Examples of these categorisations are shown in Figure 49.

Figure 49. (A) – (C) The relationship between the cluster entropy and number of clusters. These are illustrative examples of a "bad" (no distinct change point in the gradient of entropy can be identified), "moderate" and "good" (a distinctive change in gradient can be identified) cluster assessment, respectively. (D) – (F) The coherence index plotted as a function of the smoothing radius. These are illustrative examples of a "bad" (jagged, ill-behaved curve), "moderate" and "good" (smooth, with clear maximum identifiable) smoothing assessments, respectively.
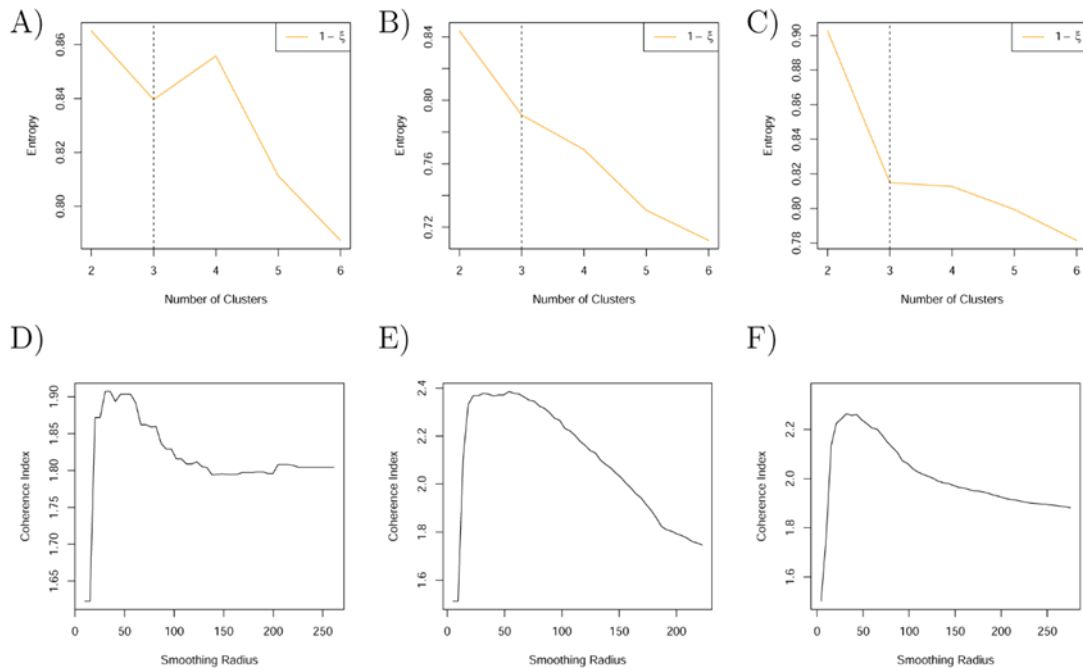
The results of this assessment are shown in Figure 50. From here, a tendency for improved clustering with the inclusion of more variables can be identified (Figure 50A)). Furthermore, at the smallest grid sizes, cluster identification appears to worsen as there is a greatly reduced set of locations which are fully observed (Figure 50C)). It is interesting to note, that at the smaller grid sizes, the cluster assessment becomes more dichotomous when using the original fuzzy c-means algorithm compared to the two alternative clustering methods. This reflects the fact that the fuzzy c-means relies upon having a sufficient number of completely observed locations to make an effective assessment. In comparison, the alternative approaches incorporate partially observed locations which could both increase available information but also dilute information if there is little overlap in the partially observed subset (e.g. many locations for which only a single variable is observed).

Figure 50(D) shows a tendency for improved smoothing with a finer grid size, particularly when the clustering algorithm allows the inclusion of partially observed locations. In addition, in scenarios of poorly identified clusters, this coincides with a poorer performance of the coherence index, where peaks are difficult to identify, and the coherence index exhibits jagged behaviour. This may be due to the relatively little information that distinguishes one location from another, regardless of its position in the field.

Figure 50. Figure 16 Results from an empirical study of three fields through an assessment of clustering (A and C) and smoothing (B and D). A)-B) The frequency of data scenarios that were considered to have "bad," "moderate" or "good" assessment for differing numbers of variables (years of data) under each of the three clustering options. C)-D) The frequency of data scenarios that were considered to have "bad," "moderate" or "good" assessment for data aligned to different grid sizes under each of the three clustering options. Frequency refers to the number of data scenarios of each type. Cluster option 1, refers to the original fuzzy c-means, option 2 includes the post-hoc allocation of partially observed locations and option 3 refers to the fuzzy c-means with optimal completion strategy.